Preconditioning unified mixed discretizations of coupled Darcy–Stokes flow

by

Ada Johanne Ellingsrud

THESIS
for the degree of

MASTER OF SCIENCE

Master in applied mathematics and mechanics

Faculty of Mathematics and Natural Sciences
University of Oslo

May 2015

Acknowledgements

First, I would like to thank my supervisors Kent–Andre Mardal and Marie Rognes. They have provided invaluable insight and expertise, and this thesis would not have been possible without their guidance and help. They have always taken their time to answer my questions and engage in discussions. For that I am truly grateful. I also wish to express my gratitude to Rainer Helmig and Timo Koch, who supervised me during my stay at the University of Stuttgart. Martin Alnæs, Johannes Ring and Miroslav Kuchta have provided highly appreciated support when it comes to installation and usage of FEniCS. A special thanks goes to my father who inspired me to study mathematics, and for the academic support he has provided during my time at the University of Oslo. Finally, I would like to thank the rest of my family, friends and Lars for their love and support.

Contents

Chapter 1

Introduction

The coupling of viscous and porous flow is of fundamental importance in many geophysical processes and industrial applications, such as water flowing across soil, oil filtering through sand or rocks and groundwater flow. Within medical research this model can be used to simulate the blood flow in our circulatory system and the surrounding tissue. As blood transports oxygen and nutrients through the body, phenomenas such as sugar transportation to a tumor, drug delivery to arteries and passage of oxygen in the brain can be modeled. The mathematical simulations are often easier to conduct and less expensive than finding exact measures through e.g. advanced digital image processing or experiments, hence they provide an opportunity to obtain a better understanding of complicated natural processes. This can potentially lead to improvement of diagnosis and treatment of diseases or new and better engineering techniques. However, robust and efficient numerical algorithms for this type of flow are challenging because viscous and porous flow require different numerical strategies.

The flow is governed by the Stokes equations in the viscous domain and by Darcy's law in the porous domain, and is therefore commonly referred to as Darcy–Stokes flow. Darcy–Stokes flow is coupled at the interface Γ between the two domains, introducing coupling conditions. The system is, as earlier stated, difficult to approximate because the Stokes and the Darcy solutions have different regularity properties. The Stokes equations require that the fluid velocities are approximated in H^1, which is more restrictive than the requirements on the Darcy velocities, namely that they are approximated in $H(\mathrm{div})$. Hence, the Darcy equations only require the weak continuity of normal velocity components, whereas the Stokes equations require both normal and tangential velocity components to be weakly continuous.

In this thesis, the Darcy–Stokes problem is solved using a mixed finite element method, resulting in a coupled, indefinite and ill-conditioned saddle

point system. We will look at so called unified discretizations of the model, meaning that the same elements are used throughout the entire domain. An advantage with these unified methods is that the Stokes and the Darcy equations can be treated in the same manner, and it often simplifies the numerical implementation. However, finding uniformly stable elements is not trivial [1].

Several researchers [2, 3, 4, 5] have suggested to use unstable element combinations along with stabilization techniques. The primary motivation for such an approach is the advantage of flexibility when it comes to the choice of finite elements. For example, it typically requires less computational power than using uniformly stable elements, as they often have more degrees of freedom. In addition, stabilization techniques enable better approximation of solutions which vary in character from one part of the domain to another. Burman et al. [3] develop a lower order method using $P_1 \times P_1$ elements in combination with an interior penalty technique. Badia et al. [2] follow Burmans approach, and apply the method with $P_1 \times DG_0$ elements. Rui et al. [4] use stabilized Crouzeix–Raviart elements. Karper et al. [6] suggest a discretization where the Taylor–Hood or the Mini element produce a stable scheme for the coupled problem. Mardal et al. [1] propose a new stable $H(\mathrm{div})$ conforming element that gives optimal order estimates in both regions. These relatively new elements have to the author's knowledge not yet been successfully implemented.

We will consider the two formulations suggested by Karper et al. [6] for the Darcy–Stokes problem, that is, the L^2-formulation where the Darcy velocities are assumed to be in L^2 and the $H(\mathrm{div})$-formulation where the Darcy velocities are assumed to be in $H(\mathrm{div})$. The L^2-formulation will be discretized using the uniformly stable Taylor-Hood [7] elements, as suggested in [6]. The $H(\mathrm{div})$-formulation will be discretized using the $H(\mathrm{div})$ conforming Brezzi–Douglas–Marini [8] elements. However, as these elements only have normal continuity and not tangential continuity on the mesh facets, they are not conforming in the Stokes region. The problem is solved by using an interior penalty method to impose the tangential continuity in the Stokes region weakly, as suggested by Kanschat et al. [9]. One problem with both models is that they are ill-conditioned, hence inefficient. In order to solve larger systems, powerful preconditioners are needed.

There has also been active research on preconditioning of unified discretizations of the Darcy–Stokes problem. Angelo et al. [10] suggest a preconditioner based on the Schur complement. Cai et al. [11] propose preconditioners based on well-known preconditioners for Stokes flow, and decouple the problem through the preconditioner. The authors look at Taylor–Hood elements for the fluid region and P_2 elements for porous region. Márquez

et al. [12] further explored this technique on $H(\mathrm{div})$ conforming elements, using the auxiliary space preconditioning technique introduced by Hiptmair et al. [13]. In this thesis, we will develop coupled preconditioners using a similar approach as [11] and [12], that is, to find optimal preconditioners for the Stokes problem and the Darcy problem and combine them.

Cai et al. [11] and Márquez et al. [12] decouple the problem through the preconditioners, and solve the local Darcy and Stokes subproblems separately using different elements. We will apply decoupled preconditioners similar to the ones proposed in [11, 12], and solve the preconditioned problems using the same elements throughout the whole domain. An advantage with this technique, is that the software used does not need support for different elements in different parts of the domain. In addition, we suggest two new preconditioners that preserves the coupling between the Darcy and the Stokes flow.

For practical reasons, it is desirable to create generic preconditioners that are applicable to various employments of the Darcy–Stokes model. As these applications have different parameter values, the preconditioners should ideally be insensitive to variations in the model parameters. This motivates us to run numerical experiments to determine how robust the preconditioners are to changes in the model parameters.

The thesis is organized as follows. In Chapter 2, the mathematical model is introduced. The numerical method used within this work is the finite element method, which is explained in Chapter 3. Chapter 4 presents the two different formulations, namely the L^2-formulation and the $H(\mathrm{div})$-formulation. In addition, *a priori* error estimates for both discretizations are presented. In Chapter 5, preconditioners for both formulations are suggested and analyzed. Chapter 6 contains a presentation of the numerical experiments, along with the numerical results. In Chapter 7, the results are summarized and discussed.

The numerical experiments in this thesis are executed using FEniCS [14], an automated software for solving partial differential equations using the finite element method. The source code can be found at `https://bitbucket.org/adaje/masterthesis`.

1.1 Notation

The convention that a bold face character denotes a vector is adopted within this thesis. Furthermore, the following list of symbols are used.

	General symbols	
Ω	The domain of interest, an open subset of $\mathbb{R}^n$	
Ω_s	Stokes part of the domain	
Ω_d	Darcy part of the domain	
Γ	Interface between Ω_s and Ω_d, i.e $\partial\Omega_s \cap \partial\Omega_d$	
$\Gamma_{\partial\Omega}$	Exterior boundary of Ω, i.e. $\partial\Omega$	
$\Gamma_{\partial\Omega_s}$	Exterior boundary of Ω_s, i.e. $\partial\Omega_s \cap \partial\Omega$	
$\Gamma_{\partial\Omega_d}$	Exterior boundary of Ω_d, i.e. $\partial\Omega_d \cap \partial\Omega$	
$\mathbf{n}_s$	Unit normal vector exterior to $\partial\Omega_s$	
$\mathbf{n}_d$	Unit normal vector exterior to $\partial\Omega_d$	
τ	Unit tangential vector at Γ	
$\mathbf{u}$	Velocity field	
p	Pressure	
$(\cdot)_s$	Physical quantity of Stokes domain	
$(\cdot)_d$	Physical quantity of Darcy domain	
$\nabla \cdot f$	Divergence of f	
∇f	Gradient of f	
$\nabla^2 f$	$:= \nabla \cdot (\nabla f) = \Delta f$	
$C_i, i \in \mathbb{N}$	Generic constant where $C_i \in \mathbb{R}$, $C_i > 0$	
	Model parameters	
$\mathbf{K}, K$	Tensor permeability, scalar permeability	m^2
ρ	Density	$kg\ m^{-3}$
μ	Viscosity	$m^2 s^{-1}$
α	Beavers–Joseph–Saffmann coefficient	
β_n	Penalty parameter, Nitsche's method	
β_s, β_d	Penalty parameters, the IP method	
	Function spaces	
$\mathbb{R}$	Real numbers	
$\mathbb{N}$	Natural numbers	
$C^0(\Omega)$	Set of continuous functions	
$C^\infty(\Omega)$	Set of smooth functions	

$C^k(\Omega)$	Set of functions with continuous derivatives up to order k
$C_0^k(\Omega)$	Subset of C_k of functions with compact support
$L^2(\Omega)$	Space of square-integrable functions
$L_0^2(\Omega)$	Subset of L^2 of functions with compact support
$H^m(\Omega)$	Sobolev space of L^2 functions with square-integrable
$H_0^m(\Omega)$	Subset of H^m of functions with compact support
	derivatives up to order m
$H(\mathrm{div}, \Omega)$	$:= \{\mathbf{v} \in \mathbf{L}^2(\Omega) : \mathrm{div}\, \mathbf{v} \in L^2(\Omega)\}$
$H^{-1}(\Omega)$	Dual space of $H^1(\Omega)$
$H^*(\Omega)$	Dual space of $H(\Omega)$
	The finite element method
$\langle \cdot, \cdot \rangle_\Omega$	L^2-inner product over Ω
$\partial\Omega_D$	Part of the boundary $\partial\Omega$ with Dirichlet boundary conditions
$\partial\Omega_N$	Part of the boundary $\partial\Omega$ with Neumann boundary conditions
$\mathcal{T}_h$	Partition of Ω
T	Element in $\mathcal{T}_h$
$\mathcal{P}_q(T)$	Space of polynomials of total degree $\leq q$ over T
h	Maximum diameter of the elements in $\mathcal{T}_h$
P_q	Lagrange element of degree q
DG_q	Discontinuous Galerkin element of degree q
RT_k	Raviart–Thomas element of degree k
BDM_k	Brezzi–Douglas–Marini element of degree k
Γ_h^I	Interior facets in $\mathcal{T}_h$
Γ_h^s	Interior facets in Stokes part of $\mathcal{T}_h$
Γ_h^d	Interior facets in Darcy part of $\mathcal{T}_h$
	Iterative methods
$\mathcal{K}_k$	Krylov space of order k
$\kappa(A)$	Condition number of A
$N(A)$	Number of iterations it takes to solve $Ax = b$

Chapter 2

Mathematical model

In this chapter a short presentation of the mathematical model for coupled Darcy–Stokes flow is provided. The theory is compiled from the works of [15, 16, 17]. For a comprehensive introduction and complete derivations of the equations presented, we refer to White [15, Chapter 2] for viscous flow, to Neuman [16] for porous flow and to Discacciati et al. [17] for coupled Darcy–Stokes flow.

2.1 Viscous flow

Incompressible Newtonian viscous flow is governed by the Navier–Stokes equations,

$$\frac{\partial \mathbf{u}}{\partial t} + (\mathbf{u} \cdot \nabla)\mathbf{u} = -\frac{1}{\rho}\nabla p + \nu \nabla^2 \mathbf{u} + \mathbf{f} \tag{2.1}$$

$$\nabla \cdot \mathbf{u} = 0 \tag{2.2}$$

where $\mathbf{u}$ represents a velocity field, p the pressure, ρ denotes the density and ν denotes the kinematic viscosity. The body forces are represented by $\mathbf{f}$. Equation (2.1) arises from Newtons second law, which states that the net force is equal to the rate of change of the momentum, while (2.2) arises from conservation of mass within the system. In addition, the fluid is assumed to be Newtonian and incompressible: a Newtonian fluid is an isotropic, viscous fluid in which the strain rates are proportional to the viscous stress, while incompressible means that the fluid density is constant. For real fluids these assumptions are rarely true, but in many cases this gives a fairly good approximation of the fluid [15]. For flows at very low Reynolds numbers ($Re \lll 1$), the convective forces are assumed to be neglectable compared to the viscous forces. If the problem in addition is stationary, we are left with a simplification of the Navier–Stokes equations, namely the linear stationary Stokes equations,

$$\nu\nabla^2\mathbf{u} - \frac{1}{\rho}\nabla p + \mathbf{f} = 0 \tag{2.3}$$

$$\nabla \cdot \mathbf{u} = 0 \tag{2.4}$$

A complete derivation of the Navier–Stokes equations can be found in [15, Chapter 2].

2.2 Porous flow

Incompressible porous media flow is described by Darcy's law,

$$\mathbf{q} = -\frac{\mathbf{K}}{\mu}\nabla p \tag{2.5}$$

The law is a proportional relationship between the volumetric flux $\mathbf{q}$, referred to as the Darcy flux, and the pressure gradient. The permeability is denoted by $\mathbf{K}$, a measure of the ability of a porous material to permit fluids to pass through it, while μ denotes the viscosity of the fluid. For simplicity the porous medium is assumed to be homogeneous and isotropic, which allows the permeability to be represented by a scalar K. However, in reality most porous materials are both heterogeneous and anisotropic. The Darcy flux $\mathbf{q}$ is related to the fluid velocity $\mathbf{u}$ by the porosity ϕ, which is a measure of the void space in a material. As the material only permits flow through the void space, the Darcy flux is divided by the porosity to obtain the actual fluid velocity,

$$\mathbf{u} = \frac{\mathbf{q}}{\phi} \tag{2.6}$$

Darcy's law (2.5) in combination with the porous media analogue of the continuity equation (2.4) gives the Darcy equations,

$$\frac{\mu}{K}\mathbf{u} + \nabla p = \mathbf{f} \tag{2.7}$$

$$\nabla \cdot \mathbf{u} = 0 \tag{2.8}$$

Note that a source term $\mathbf{f}$ has been added to Darcy's law, providing the possibility to take body forces such as gravity into account. A complete derivation of Darcy's law can be found in [16].

2.3 Coupled Darcy–Stokes flow

A domain $\Omega = \Omega_s \cup \Omega_d$ is considered, consisting of a porous region Ω_d where the flow is a Darcy flow, and an open region Ω_s where the flow is governed by the linear stationary Stokes equations. The coupled Darcy–Stokes problem reads: Find $(\mathbf{u}, p) \in \mathbf{V} \times Q$ such that

$$\begin{aligned} -\mu\Delta\mathbf{u} + \nabla p &= \mathbf{f} \quad \text{in } \Omega_s \\ \nabla \cdot \mathbf{u} &= 0 \quad \text{in } \Omega_s \end{aligned} \tag{2.9}$$

$$\begin{aligned} \frac{\mu}{K}\mathbf{u} + \nabla p &= \mathbf{f} \quad \text{in } \Omega_d \\ \nabla \cdot \mathbf{u} &= 0 \quad \text{in } \Omega_d \end{aligned} \tag{2.10}$$

Here K denotes the permeability, $\mu \geq 0$ is the viscosity of the fluid while the body forces are represented by $\mathbf{f}$. The spaces $\mathbf{V}$ and Q are the solution spaces for the velocity $\mathbf{u}$ and the pressure p, respectively. The equations (2.9) and (2.10) are coupled at the interface $\Gamma = \partial\Omega_s \cap \partial\Omega_d$ between the porous and the open region. At the interface the following boundary conditions applies,

$$\mathbf{u_s} \cdot \mathbf{n_s} = \mathbf{u_d} \cdot \mathbf{n_s} \qquad \text{on } \Gamma \tag{2.11}$$

$$\mu\mathbf{n}_s \cdot \nabla\mathbf{u}_s \cdot \mathbf{n_s} = p_s - p_d \qquad \text{on } \Gamma \tag{2.12}$$

$$-\mathbf{n_s} \cdot \nabla\mathbf{u_s} \cdot \tau = \alpha K^{-\frac{1}{2}} \mathbf{u_s} \cdot \tau \qquad \text{on } \Gamma \tag{2.13}$$

Here (2.11) represents mass conservation, (2.12) represents continuity of normal stress and (2.13) represents the Beavers–Joseph–Saffmann condition introduced by Beavers and Joseph [18] in 1967, and later simplified by Saffmann [19] in 1971. The quantity α is a dimensionless coefficient determined by the structure near the interface. The unit tangential vector at Γ is denoted by τ, $\mathbf{n_s}$ is the unit normal vector exterior to Ω_s and $\mathbf{u}_s = \mathbf{u}|_{\Omega_s}$, $\mathbf{u}_d = \mathbf{u}|_{\Omega_d}$, $p_s = p|_{\Omega_s}$ and $p_d = p|_{\Omega_d}$. In addition, Dirichlet and Neumann conditions must be set on the exterior boundaries $\Gamma_{\partial\Omega_s} = \partial\Omega_s \cap \partial\Omega$ and $\Gamma_{\partial\Omega_s} = \partial\Omega_d \cap \partial\Omega$ in order to close the system.

Note that in the Stokes equations (2.9) there is a second-order operator acting on the velocities, whereas in Darcy's equations (2.10) the only operator acting on the velocities is a divergence operator. Consequently, the velocities in the Stokes parts of the domain require higher regularity than the velocities in the Darcy part of the domain.

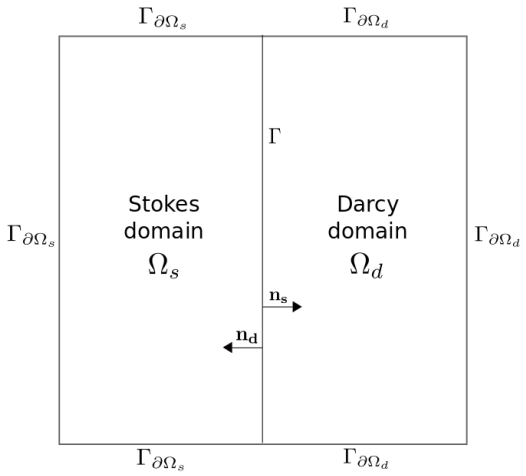

Figure 2.1: The domain is split into a fluid part Ω_s and a porous part Ω_d by the interface $\Gamma = \partial\Omega_s \cap \partial\Omega_d$. The exterior boundaries $\partial\Omega_s \cap \partial\Omega$ and $\partial\Omega_d \cap \partial\Omega$ are denoted by $\Gamma_{\partial\Omega_s}$ and $\Gamma_{\partial\Omega_d}$, respectively.

Chapter 3

Numerical methods

Solving elliptic and parabolic partial differential equations (PDEs) analytically is often challenging, in some cases even impossible [20]. Instead, one has to resort to seeking numerical approximations to the unknown analytical solution. The finite element method is one of the main tools for such a numerical treatment of PDEs [20], and is the numerical method used within this work. In this chapter, an explanation of the finite element method is given. Most of the theory presented in this chapter is compiled from the works of Braess [20], Mardal et al. [14] and Elman et al. [21]. The exceptions being the theory in Section 3.3.1 and 3.3.2, which is collected from Juntunen [22], Douglas et al. [23] and Rivière [24].

3.1 The finite element method

The finite element method is a numerical method for finding approximate solutions to partial differential equations. The first step in the finite element method is to define a weak form of the PDE. Then the domain is discretized and a finite dimensional function space in which to search for the solution is chosen. A Galerkin method is used to approximate the weak form in the finite element space, and the problem reduces to solving a system of algebraic equations. An advantage with the finite element method compared to other numerical methods for solving partial differential equations, is that it easily adapts to more complicated domains and geometries. In order to give a detailed explanation of the finite element method, we need some preliminaries.

Definition 3.1 (L^p-spaces [25, Appendix D])**.** *Let Ω be an open subset of $\mathbb{R}^n$. For $1 \leq p \leq \infty$, $L^p(\Omega)$ is defined as*

$$L^p(\Omega) = \{u \in \Omega : (\int_\Omega |u|^p \, \mathrm{d}x)^{\frac{1}{p}} < \infty\}$$

with the corresponding norm $\|u\|_{L^p(\Omega)} = (\int_\Omega |u|^p \,\mathrm{d}x)^{\frac{1}{p}}$

Definition 3.2 (Weak derivative [25, Section 5.2])**.** *Let* Ω *be an open subset of* $\mathbb{R}^n$*. Assume* $u, v \in L^1_{loc}(\Omega)$*, and let* $\alpha = (\alpha_1, \ldots, \alpha_n)$ *denote a multi-index. Then* v *is referred to as the* α^{th} *weak derivative of* u *if*

$$\int_\Omega u D^\alpha \phi dx = (-1)^{|\alpha|} \int_\Omega v\phi \,\mathrm{d}x$$

For all $\phi \in C_0^\infty(\Omega)$*.*

Definition 3.3 (Sobolev spaces [25, Section 5.2])**.** *Let* Ω *be an open subset of* $\mathbb{R}^n$*. For a nonnegative integer* m *where* $\alpha = (\alpha_1, \ldots, \alpha_n)$ *denotes a multi-index, the Sobolev space* $H^m(\Omega)$ *is defined as*

$$H^m(\Omega) = \{u \in \Omega : (\sum_{|\alpha| \leq m} \int_\Omega |D^\alpha u|^2 \,\mathrm{d}x)^{\frac{1}{2}} < \infty\}$$

with the corresponding norm $\|u\|_{H^m(\Omega)} = (\sum_{|\alpha| \leq m} \int_\Omega |D^\alpha u|^2 \,\mathrm{d}x)^{\frac{1}{2}}$

3.1.1 Strong form

The finite element method is explained through the model problem of PDEs, namely the Poisson problem:

Definition 3.4 (Strong form)**.** *Let* $\Omega \subset \mathbb{R}^n$ *be an open set, find* $u \in C^2(\Omega)$ *such that*

$$-\Delta u = f \qquad \text{in } \Omega \tag{3.1}$$
$$u = g \qquad \text{on } \partial\Omega_D \tag{3.2}$$
$$\nabla u \cdot \mathbf{n} = h \qquad \text{on } \partial\Omega_N \tag{3.3}$$

Here u is the unknown, f is a source term and $\mathbf{n}$ is the outward unit normal on $\partial\Omega$. The solution u will be referred to as the strong solution, while Definition 3.4 will be referred to as the strong form of the problem. The parts of the boundary with Dirichlet conditions and Neumann conditions are denoted by $\partial\Omega_D$ and $\partial\Omega_N$, respectively. A Neumann boundary condition specifies the values the normal derivative of the solution has on the boundary, and is typically of the form (3.3). A boundary condition of the form (3.2) is referred to as a Dirichlet boundary condition, and specifies what values the solution itself has on the boundary.

3.1.2 Weak form

The requirement $u \in C^2(\Omega)$ is quite strict. In cases of non-smooth boundaries or discontinuous source functions, the function u may not be sufficiently smooth to hold the requirements of the strong solution. In order to work with less restrictive problems in terms of admissible data, the weak form is introduced. To derive the weak form, (3.4) is multiplied with an arbitrary test function v from a given function space and integrated over the domain Ω,

$$-\int_\Omega \Delta u v \, \mathrm{d}x = \int_\Omega f v \, \mathrm{d}x \tag{3.4}$$

If v is sufficiently smooth, the smoothness required of u can be reduced by integration by parts of terms involving higher-order derivatives,

$$\int_\Omega \nabla u \cdot \nabla v \, \mathrm{d}x - \int_{\partial\Omega} (\nabla u \cdot \mathbf{n}) v \, \mathrm{d}s = \int_\Omega f v \, \mathrm{d}x \tag{3.5}$$

The next question to be addressed, is where the above formulation makes sense and which requirements to set on v. The integral on the left-hand side of (3.5) is well defined if the first derivatives of u and v are in $L^2(\Omega)$. Hence, the natural space for the weak solution u is $H^1(\Omega)$. This is also the natural space for the test functions v. In addition, the test functions are required to be zero at the Dirichlet boundary. Similarly, the right-hand side is well defined if f is in $L^2(\Omega)$. The strict requirement $u \in C^2(\Omega)$ from the strong form, is now reduced to $u \in H^1(\Omega)$. The last step in obtaining the weak form is the insertion of the Neumann condition, which is typically enforced weakly, along with using the fact that test functions vanish on the Dirichlet boundary. This yields,

$$\int_{\partial\Omega} (\nabla u \cdot \mathbf{n}) v \, \mathrm{d}s = \int_{\partial\Omega_N} h v \, \mathrm{d}s \tag{3.6}$$

The Dirichlet boundary condition is included in the solution space, that is, the solution u lies in $H^1_{g,D}(\Omega)$, where the subscript "g, D" means that $u = g$ on the Dirichlet boundary. The test functions are required to be zero at the Dirichlet boundary, hence the natural space for the test functions is $H^1_{0,D}(\Omega)$. The above deliberations give rise to the weak form, also referred to as the variational formulation of the problem.

Definition 3.5 (Variational formulation)**.** *Find all* $u \in H^1_{g,D}(\Omega)$ *such that*

$$\int_\Omega \nabla u \cdot \nabla v \, \mathrm{d}x = \int_\Omega f v \, \mathrm{d}x + \int_{\partial\Omega_N} h v \, \mathrm{d}s \tag{3.7}$$

for all $v \in H^1_{0,D}(\Omega)$.

3.1.3 Finite elements

The choice of a finite dimensional function space in which to search for the solution, is defined through finite elements. The standard definition [14] of a finite element is the Ciarlet definition [26], and it reads as follows:

Definition 3.6 (Finite Element)**.** *A finite element is defined by a triple* $(T, \mathcal{V}, \mathcal{L})$*, where*

- *the domain* T *is a bounded, closed subset of* $\mathbb{R}^d$ *with nonempty interior and piecewise smooth boundary. For instance, an interval for* $d = 1$*, a triangle for* $d = 2$ *and a tetrahedron for* $d = 3$*,*
- *the space* $\mathcal{V} = \mathcal{V}(T)$ *is a finite-dimensional function space on* T *of dimension* N*,*
- *the set of degrees of freedom (nodes)* $\mathcal{L} = \{L_1, L_2, \ldots, L_N\}$ *is a basis for the dual space* $\mathcal{V}^*$*, that is, the space of bounded linear functionals on* $\mathcal{V}$*.*

Definition 3.7 (Nodal basis)**.** *The nodal basis* $\{\phi_1, \phi_2, \ldots, \phi_N\}$ *for a finite element* $(T, \mathcal{V}, \mathcal{L})$ *is the unique basis satisfying*

$$L_i(\phi_j) = \delta_{i,j} \tag{3.8}$$

There is one basis function associated with each node and its value is one at this node and zero at all other nodes. Each basis function is nonzero only at cells associated with the corresponding node. The diameter of an element T is denoted by h and will from now on be referred to as the discretization parameter. A common choice of elements, are the so called Lagrange elements [14]. Their basis consists of continuous piecewise polynomials of degree q, where $q \geq 1$, and the elements are denoted by P_q. Another popular class of elements are the discontinuous Galerkin elements, denoted by DG_q, where the basis consists of discontinuous piecewise polynomials of degree q, where $q \geq 0$.

After a finite element is chosen, the element domains T are patched together to form a mesh $\mathcal{T}_h$, where $\mathcal{T}_h = \{T_1, T_2, \ldots, T_m\}$ is a partition of the domain

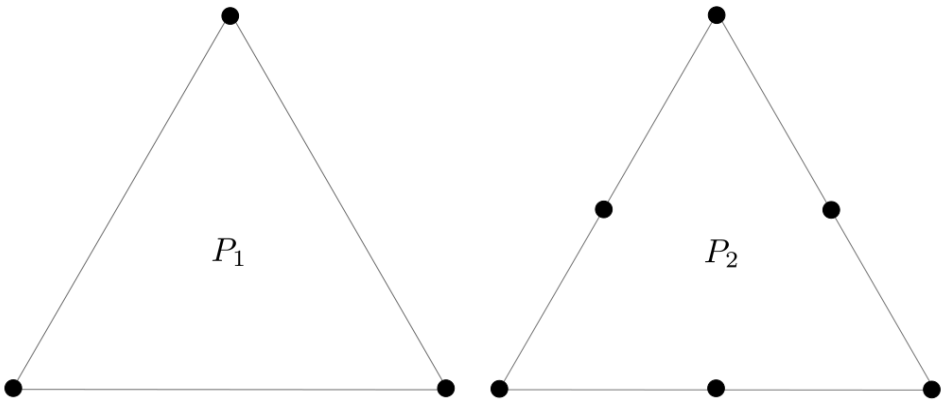

Figure 3.1: An illustration of the degrees of freedom of two Lagrange elements in 2D. On the left-hand side is a Lagrange element with linear approximations, denoted by P_1. On the right-hand side is a Lagrange element with quadratic approximations, referred to as a P_2 element.

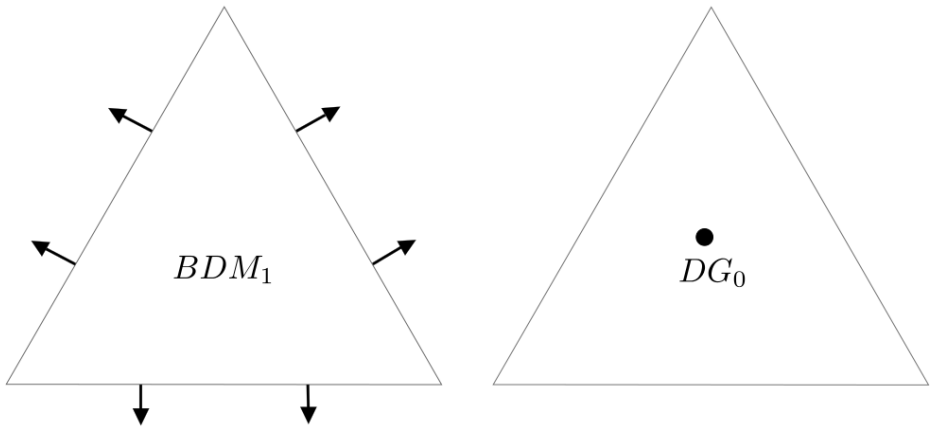

Figure 3.2: On the left-hand side is an illustration of the degrees of freedom of a Brezzi–Douglas–Marini [8] element of lowest order in 2D, referred to as a BDM_1 element. The degrees of freedom are normal components evaluated at the edge of the element. On the right-hand side is a DG_0 element in 2D depicted, which has a constant basis function evaluated at the node in the middle of the element. Hence these elements are discontinuous across the edge of each element.

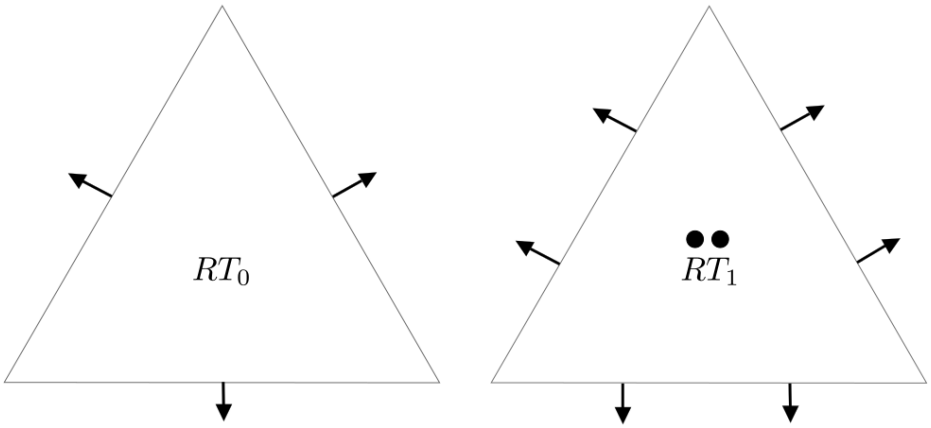

Figure 3.3: On the left-hand side is the degrees of freedom of a Raviart–Thomas [27] element of lowest order in 2D depicted, referred to as a RT_0 element. On the right-hand side is an illustration of the degrees of freedom of an RT_1 element.

Ω, such that $\bar{\Omega} = \cup_{i=1}^{m} T_i$. The global finite element space $V_h = V_h(\mathcal{T}_h)$ for the mesh is made up of the local function spaces $\mathcal{V}_T$ at each element T. We require that the restriction of $v_h \in V_h$ to each cell T lies in the local function space $\mathcal{V}_T$. In addition, if two local degrees of freedom are mapped to the same global degree of freedom, they must agree for each function $v_h \in V_h$. For a comprehensive explanation of the process, see [14, Chapter 2]. If the discrete space V_h is a subset of the space in which to search for a solution to the continuous problem, the elements are said to be conforming.

3.1.4 Reduction to a system of algebraic equations

The final part in the finite element method is to discretize the weak form into the finite element space. Let V_h be the finite dimensional space in which to to search for the approximate solution. The Galerkin projection of u in V_h can be expressed as

$$u_h = \sum_{i=1}^{N} u_i \phi_i \tag{3.9}$$

Replacing u with u_h and v with an arbitrary test function ϕ_j in the variational formulation in Definition 3.5 yields

Definition 3.8 (Discrete variational formulation)**.** *Find all $u_h \in V_h$ such that*

$$\int_\Omega \nabla u_h \cdot \nabla \phi_j \, \mathrm{d}x = \int_\Omega f\phi_j \, \mathrm{d}x + \int_{\partial\Omega_N} h\phi_j \, \mathrm{d}s \tag{3.10}$$

for all $\phi_j \in \hat{V}_h$.

Solving the system of equations (3.10) is equivalent to solving the matrix equation

$$A\mathbf{u} = \mathbf{b}$$

where $\mathbf{u}$ is a vector with components u_i for $i = 1, 2 \ldots, N$ and A is a $N \times N$ matrix

$$A_{ij} = \int_\Omega \nabla \phi_i \cdot \nabla \phi_j \, \mathrm{d}x \tag{3.11}$$

while $\mathbf{b}$ is a vector of length N with components

$$b_i = \int_\Omega f\phi_j \, \mathrm{d}x + \int_{\partial\Omega_N} g\phi_j \, \mathrm{d}s \tag{3.12}$$

The partial differential equation is now transformed into a system of linear equations. As each basis function is nonzero only at cells associated with the corresponding node, the matrix A will be sparse. In addition, solving a physical problem requires a great number of degrees of freedom to get an accurate solution, which leads to a large matrix. Hence, solving the system directly will require infeasible computation resources for linear systems of larger dimensions [21]. Efficient techniques for solving such systems will be discussed in Chapter 5.

3.2 The mixed finite element method

The finite element discretization of a problem where different variables are approximated in different finite element spaces results in a mixed variational formulation. In the Stokes equations (2.3)–(2.4) presented in Chapter 2, the unknowns are the velocity field $\mathbf{u}$ and the pressure p. By letting $\mathbf{V} = \mathbf{V}(\Omega)$ be the solution space for the velocity and $Q = Q(\Omega)$ the solution space for the pressure, the Stokes problem is to find $\mathbf{u}$ in $\mathbf{V}$ and p in Q such that (2.3)–(2.4) hold. The first step in obtaining the variational formulation is to multiply (2.3) with a test function $\mathbf{v} \in \hat{\mathbf{V}}$ and (2.4) with a test function

$q \in \hat{Q}$, where $\hat{\mathbf{V}}$ and $\hat{Q}$ are suitable function spaces for the test functions. The equations are integrated over the domain Ω and the terms involving higher order derivatives are integrated by parts. Assuming zero velocity at the entire boundary and zero average pressure, the above deliberations yield the variational formulation: Find $(\mathbf{u}, p) \in \mathbf{V} \times Q$ such that

$$-\mu \int_\Omega \nabla \mathbf{u} \cdot \nabla \mathbf{v} \, \mathrm{d}x + \int_\Omega p \nabla \cdot \mathbf{v} \, \mathrm{d}x = \int_\Omega \mathbf{f}\mathbf{v} \, \mathrm{d}x \tag{3.13}$$

$$\int_\Omega q \nabla \cdot \mathbf{u} \, \mathrm{d}x = 0 \tag{3.14}$$

for all $(\mathbf{v}, q) \in \hat{\mathbf{V}} \times \hat{Q}$. By introducing the bilinear forms

$$a(\mathbf{u}, \mathbf{v}) = -\mu \langle \nabla \mathbf{u}, \nabla \mathbf{v} \rangle_\Omega \tag{3.15}$$

$$b(\mathbf{v}, p) = \langle p, \nabla \cdot \mathbf{v} \rangle_\Omega \tag{3.16}$$

$$b(\mathbf{u}, q) = \langle q, \nabla \cdot \mathbf{u} \rangle_\Omega \tag{3.17}$$

and the linear form

$$l(\mathbf{v}) = \langle \mathbf{f}, \mathbf{v} \rangle_\Omega \tag{3.18}$$

problem (3.13)–(3.14) can be written as:

Definition 3.9 (Saddle point problem)**.** *Find* $(\mathbf{u}, p) \in \mathbf{V} \times Q$ *such that*

$$a(\mathbf{u}, \mathbf{v}) + b(\mathbf{v}, p) = l(\mathbf{v}) \tag{3.19}$$

$$b(\mathbf{u}, q) = 0 \tag{3.20}$$

for all $(\mathbf{v}, q) \in \hat{\mathbf{V}} \times \hat{Q}$.

Problems that can be written on this form are often referred to as saddle point problems [20]. For a saddle point problem to be well posed, that is, to have a unique solution, some requirements have to be put on the solution spaces $\mathbf{V}$ and Q.

Theorem 3.1 (Brezzi's splitting theorem [20, Chapter 3, Theorem 4.3])**.** *A saddle point problem of the form (3.19)–(3.20) has a unique solution if there exist constants* C_1, C_2, C_3, C_4 *such that*

$$a(\mathbf{u}, \mathbf{v}) \leq C_1 \|\mathbf{u}\|_{\mathbf{V}} \|\mathbf{v}\|_{\mathbf{V}} \qquad \forall \, \mathbf{u} \in \mathbf{V}, \forall \, \mathbf{v} \in \mathbf{V} \tag{3.21}$$

$$b(\mathbf{u}, q) \leq C_2 \|\mathbf{u}\|_{\mathbf{V}} \|q\|_Q \qquad \forall \, \mathbf{u} \in \mathbf{V}, \forall \, q \in Q \tag{3.22}$$

$$a(\mathbf{u}, \mathbf{u}) \geq C_3 \|\mathbf{u}\|_{\mathbf{V}}^2 \qquad \forall \, \mathbf{u} \in \mathbf{K} \tag{3.23}$$

$$\sup_{\mathbf{u} \in \mathbf{V}} \frac{b(\mathbf{u}, q)}{\|\mathbf{u}\|_{\mathbf{V}}} \geq C_4 \|\mathbf{u}\|_{\mathbf{V}}^2 \qquad \forall \, q \in Q \tag{3.24}$$

where $\mathbf{K}$ *is the kernel of* $b(\mathbf{u}, q_h)$.

The first two conditions are continuity, or boundedness, of the forms a and b. The third condition (3.23) states that a has to be coercive, while (3.24) is the inf-sup condition.

The next step is to discretize (3.19)–(3.20). To this end, finite element spaces $\mathbf{V}_h$ and Q_h must be chosen. Discretizing the saddle point problem by the procedure explained in Section 3.1.4, results in the discrete saddle point problem: Find $(\mathbf{u}_h, p_h) \in \mathbf{V}_h \times Q_h$ such that

$$a(\mathbf{u}_h, v) + b(\mathbf{v}, p_h) = l_1(\mathbf{v}) \tag{3.25}$$

$$b(\mathbf{u}_h, q) = 0 \tag{3.26}$$

for all $(\mathbf{v}, q) \in \hat{\mathbf{V}}_h \times \hat{Q}_h$. The approach is called a mixed method, and the difficulty in such methods is to find proper function spaces and finite elements, as not all combinations of elements results in stable schemes. The finite element spaces $\mathbf{V}_h$ and Q_h have to satisfy requirements similar to those on $\mathbf{V}$ and Q in Theorem 3.1. Next, the discrete analog of (3.23)–(3.24), namely the Babuška–Brezzi conditionswill be stated.

Definition 3.10 (Babuška–Brezzi conditions [20, Chapter 3, Definition 4.4])**.** *A family of finite element spaces $\mathbf{V}_h$, Q_h is said to satisfy the Babuška–Brezzi conditions provided there exist constants C_1 and C_2 independent of h such that*

$$a(\mathbf{u}_h, \mathbf{u}_h) \geq C_3 \|\mathbf{u}_h\|^2_{\mathbf{V}_h} \qquad \forall\, \mathbf{u}_h \in \mathbf{K}_h \tag{3.27}$$

$$\sup_{\mathbf{u}_h \in \mathbf{V}_h} \frac{b(\mathbf{u}_h, q)}{\|\mathbf{u}_h\|_{\mathbf{V}_h}} \geq C_4 \|\mathbf{u}_h\|^2_{\mathbf{V}_h} \qquad \forall\, q \in Q_h \tag{3.28}$$

where $\mathbf{K}_h$ is the kernel of $b(\mathbf{u}_h, q)$

If the continuity requirements (3.21)–(3.22) hold for the continuous problem, they will in most cases also hold for the discrete problem. The difficulty is often to find finite element spaces such that the coercivity condition (3.27) and the inf-sup condition (3.28) hold. Numerical experience shows that enforcing the Babuška–Brezzi conditions in Definition 3.10 is of great importance for the stability of the scheme [20, Chapter 4]. A scheme where the Babuška–Brezzi conditions hold, will from now on be referred to as a stable scheme.

3.2.1 *A priori* error estimates

Under the assumption that the Babuška–Brezzi conditions (3.27)– (3.28) are fulfilled, an *a priori* error estimate can be obtained.

Theorem 3.2 (Babuška–Brezzi theorem [20, Chapter 3, Theorem 4.5])**.** *Assume we have a discrete saddle point problem where the conditions (3.27)–(3.28) hold for some function spaces* $\mathbf{V}_h$ *and* Q_h*. Let* $(\mathbf{u}, p) \in \mathbf{V} \times Q$ *solve the continuous saddle point problem, and* $(\mathbf{u}_h, p_h)$ *solve the discrete saddle point problem. Then there exists a constant* C *independent of the mesh size such that*

$$\|\mathbf{u} - \mathbf{u}_h\|_{\mathbf{V}} + \|p - p_h\|_Q \leq C(\inf_{\mathbf{v}_h in \mathbf{V}} \|\mathbf{u} - \mathbf{v}_h\|_{\mathbf{V}} + \inf_{q_h \in Q} \|p - q_h\|_Q)$$

Theorem 3.3 (Approximation by interpolation [28, Theorem 4.7.3])**.** *There exists an interpolation operator* $\pi_h : H^t(\Omega) \to \mathbf{V}_h$*, where* $\mathbf{V}_h$ *is a piecewise polynomial field of order* $t - 1$ *with the property that for any* $\mathbf{u} \in H^t(\Omega)$

$$\|\mathbf{u} - \pi_h \mathbf{u}\|_{H^m} \leq C h^{t-m} \|\mathbf{u}\|_{H^t}$$

3.3 Stabilization techniques

If the Babuška–Brezzi conditions (3.27)–(3.28) are not fulfilled, stabilization techniques can in some cases be applied to circumvent the conditions. The primary motivation for such stabilization techniques is the flexibility when it comes to the choice of finite elements. In this section the IP method [24] will be presented, a stabilization technique that penalizes jumps across interior facets, along with Nitsche's method [29].

3.3.1 Nitsche's method

The method was first proposed by Nitsche [29] in 1971, and it provides the opportunity to impose Dirichlet boundary conditions weakly in the variational formulation, as opposed to including them in the solution space. Nitsche's method will, in the same manner as Juntunen et al. [22], be explained using the Poisson problem (3.4) with the Dirichlet boundary condition $u = g$ on $\partial\Omega$. The variational formulation reads: Find $u \in H^1(\Omega)$ such that

$$\int_\Omega \nabla u \cdot \nabla v \, \mathrm{d}x - \int_{\partial\Omega} (\nabla u \cdot \mathbf{n}) v \, \mathrm{d}s = \int_\Omega f v \, \mathrm{d}x \tag{3.29}$$

for all $v \in H^1(\Omega)$. Note that the solution u belongs to the space $H^1(\Omega)$, i.e. the Dirichlet condition $u = g$ on $\partial\Omega$ has not been included in the solution space. In Nitsche's method the Dirichlet condition is enforced weakly by penalizing $(u_h - g)$, that is, by adding the penalty term

$$\int_{\partial\Omega} \frac{\beta_n}{h}(u_h - g)v \, \mathrm{d}s \tag{3.30}$$

to the discrete variational formulation. Here β_n is the so called penalty parameter, and h is the discretization parameter. Discretizing equation (3.29) and adding the penalty term (3.30) yields

$$\int_{\Omega} \nabla u_h \cdot \nabla v \, \mathrm{d}x - \int_{\partial\Omega} (\nabla u_h \cdot \mathbf{n})v \, \mathrm{d}s + \int_{\partial\Omega} \frac{\beta_n}{h}(u_h - g)v \, \mathrm{d}s = \int_{\Omega} fv \, \mathrm{d}x \tag{3.31}$$

This term is not symmetric. To remedy this, the term

$$-\int_{\partial\Omega} \nabla v \cdot \mathbf{n}(u_h - g) \, \mathrm{d}s \tag{3.32}$$

is added to ensure symmetry of the discrete form in a consistent manner. Adding the symmetrization term (3.32) to (3.31) yields the discrete problem: Find $u_h \in V_h$ such that

$$\begin{aligned} &\int_{\Omega} \nabla u_h \cdot \nabla v \, \mathrm{d}x - \int_{\partial\Omega} (\nabla u_h \cdot \mathbf{n})v \, \mathrm{d}s - \int_{\partial\Omega} (\nabla v \cdot \mathbf{n})u_h \, \mathrm{d}s + \int_{\partial\Omega} \frac{\beta_n}{h} u_h v \, \mathrm{d}s \\ &= \int_{\Omega} fv \, \mathrm{d}x - \int_{\Omega} (\nabla v \cdot \mathbf{n})g \, \mathrm{d}s + \int_{\partial\Omega} \frac{\beta_n}{h} gv \, \mathrm{d}s \end{aligned} \tag{3.33}$$

for all $v \in \hat{V}_h$. The method is consistent [20, Chapter 1, Definition 4.1], in the sense that the solution u to the continuous problem (3.29) also satifsty the discrete problem (3.33).

3.3.2 An interior penalty method for discontinuous Galerkin elements (The IP method)

The IP method was first introduced in 1973 by Reed and Hill [30] for hyperbolic equations, and has later been extended to elliptic equations, cf. [31, 32, 33]. The method arouse from the observation that, just as Dirichlet boundary conditions could be imposed weakly through Nitsche's method, interelement continuity could be attained in a similar fashion [34]. This makes it possible to use spaces of discontinuous piecewise polynomials for solving second-order problems. As a consequence, the IP method is similar to Nitsche's method, in the sense that a penalty term is added, along with a term that ensures symmetry of the discrete problem. The IP method will

be explained using the same approach as Rivière [24], namely through the Poisson equation (3.4) with the Dirichlet condition $u = 0$ on $\partial\Omega$. Multiplying equation (3.4) with a test function v, integrating over a subset E of Ω and integrating the terms involving higher order derivatives by parts yields,

$$\int_E \nabla u \cdot \nabla v \, \mathrm{d}x - \int_{\partial E} (\nabla u \cdot \mathbf{n}_E) v \, \mathrm{d}s = \int_E f v \, \mathrm{d}x \tag{3.34}$$

where $\mathbf{n}_E$ denotes the outward normal unit vector to ∂E. Now, let E denote a finite element in the triangulation $\mathcal{T}_h = \{E_1, E_2, \ldots, E_m\}$ of the domain Ω. Let $V_h = V_h(\mathcal{T}_h)$ be the finite element space in which to search for a solution, consisting of discontinuous piecewise polynomials. Summing over the elements $E \in \mathcal{T}_h$ in (3.34) yields,

$$\sum_{E \in \mathcal{T}_h} \int_E \nabla u \cdot \nabla v \, \mathrm{d}x - \sum_{E \in \mathcal{T}_h} \int_{\partial E} (\nabla u \cdot \mathbf{n}_E) v \, \mathrm{d}s = \sum_{E \in \mathcal{T}_h} \int_E f v \, \mathrm{d}x \tag{3.35}$$

Note that integrals over interior facets no longer vanish. In order to deal with the sum of boundary integrals over ∂E, it is useful to introduce the average $\{u\}$ and the jump $[\![u]\!]$ of a function u. To this end, let E^+ and E^- be two elements sharing an interior facet, and denote the restriction of a function u to E^+ and E^- by u^+ and u_-, respectively. In a similar manner, the unit normals exterior to ∂E^+ and ∂E^- are denoted by $\mathbf{n}_+$ and $\mathbf{n}_-$, respectively.

$$\{u\} = \frac{1}{2}(u^+ + u^-) \ , \ [\![u]\!] = u^+ - u^- \tag{3.36}$$

Some simple calculations using the definition of the average and the jump in (3.36), give rise to the identity

$$[\![u \cdot v]\!] = [\![u]\!] \cdot \{v\} + \{u\} \cdot [\![v]\!] \tag{3.37}$$

Observe that the integrals over ∂E in (3.35) reduce to integrals over the interior facets, as the Dirichlet condition $u = 0$ on $\partial\Omega$ will cause the terms integrated over the exterior facets to vanish. Thus,

$$\sum_{E \in \mathcal{T}_h} \int_{\partial E} (\nabla u \cdot \mathbf{n}_E) v \, \mathrm{d}s = \sum_{e \in \Gamma_h^I} \int_e (\nabla u^+ v^+ - \nabla u^- v^-) \cdot \mathbf{n}_+ \, \mathrm{d}s \tag{3.38}$$

where Γ_h^I is the collection of interior facets. Note that there is a sign " $-$ " in the integral on the right-hand side, since $\mathbf{n}_+ = -\mathbf{n}_-$. Under the assumption that u is sufficiently regular [24], we have

$$[\![u]\!] = [\![\nabla u]\!] = 0 \tag{3.39}$$

$$\nabla u^+ = \nabla u^- = \{\nabla u\} \tag{3.40}$$

Thus, by applying the identity (3.37), the integrand on the right-hand side in (3.38) can be written on the form

$$(\nabla u^+ v^+ - \nabla u^- v^-) \cdot \mathbf{n}_+ = \{\nabla u\}[\![v]\!] \cdot \mathbf{n}_+ \tag{3.41}$$

Insertion of the identities (3.38) and (3.41) in (3.35), along with discretization of the form yields

$$\sum_{E \in \mathcal{T}_h} \int_E \nabla u_h \cdot \nabla v \, \mathrm{d}x - \sum_{e \in \Gamma_h^I} \int_e \{\nabla u_h\}[\![v]\!] \cdot \mathbf{n}_+ \, \mathrm{d}s = \sum_{E \in \mathcal{T}_h} \int_E f v \, \mathrm{d}x \tag{3.42}$$

To remedy that (3.42) is not symmetric, the term

$$- \sum_{E \in \mathcal{T}_h} \int_{\partial E} (\nabla v \cdot \mathbf{n}_E) u \, \mathrm{d}s \tag{3.43}$$

is added. Note that this term is handled in the same manner as the sum of boundary integrals over ∂E in (3.35), that is, by applying the identities (3.38) and (3.41). To mimic the continuity of the approximate solution, the jumps over interior facets are penalized by adding the term

$$\sum_{e \in \Gamma_h^I} \int_e \frac{\beta}{h} [\![u_h]\!][\![v]\!] \, \mathrm{d}s \tag{3.44}$$

to equation (3.42), yielding the discrete variational formulation: Find $u_h \in V_h(\mathcal{T}_h)$ such that

$$\begin{aligned} &\sum_{E \in \mathcal{T}_h} \int_E \nabla u_h \cdot \nabla v dv - \sum_{e \in \Gamma_h^I} \int_e \{\nabla u_h\}[\![v]\!] \cdot \mathbf{n}_+ \, \mathrm{d}s - \sum_{e \in \Gamma_h^I} \int_e \{\nabla v\}[\![u]\!] \cdot \mathbf{n}_+ \, \mathrm{d}s \\ &+ \sum_{e \in \Gamma_h^I} \int_e \frac{\beta}{h} [\![u_h]\!][\![v]\!] \, \mathrm{d}s = \sum_{E \in \mathcal{T}_h} \int_E f v dv \end{aligned}$$

for all $v \in \hat{V}_h(\mathcal{T}_h)$.

The penalty parameter β should be chosen large enough to ensure stability. However, a large β will have a negative impact on the condition number, in the sense that it will increase as β increases [24]. Theoretical estimates of the lower bound can be obtained, cf. [35].

Chapter 4

Unified mixed discretizations of coupled Darcy–Stokes flow

In this chapter the Darcy–Stokes problem (2.9)–(2.10) will be discretized using the finite element method. We will derive the two formulations suggested by Karper et al. [6], namely the L^2-formulation and the $H(\mathrm{div})$-formulation. In addition, *a priori* error estimates for both formulations will be presented.

4.1 Numerical scheme I: The L^2-formulation

A natural solution space for the Darcy velocities is $\mathbf{L}^2(\Omega_d)$, while $H^1(\Omega_d)$ constitutes a natural space for the Darcy pressure. They are natural in the sense that the Darcy problem is well posed in these spaces [36]. The L^2-formulation of the coupled Darcy–Stokes problem presented in this section is posed using the space $\mathbf{V}^2$ for the velocities and Q^2 for the pressure.

$$\mathbf{V}^2 = \mathbf{V}^2(\Omega) = \{\mathbf{v} \in \mathbf{L}^2(\Omega) : \mathbf{v}_s \in \mathbf{H}^1(\Omega_s)\} \tag{4.1}$$

$$Q^2 = Q^2(\Omega) = \{q \in L_0^2(\Omega) : q_d \in H^1(\Omega_d)\} \tag{4.2}$$

with the corresponding norms,

$$\|\mathbf{u}\|^2_{\mathbf{V}^2(\Omega)} := \|\mathbf{u}\|^2_{L^2(\Omega)} + \|\nabla \mathbf{u}\|^2_{L^2(\Omega_s)} \tag{4.3}$$

$$\|p\|^2_{Q^2(\Omega)} := \|p\|^2_{L^2(\Omega)} + \|\nabla p\|^2_{L^2(\Omega_d)} \tag{4.4}$$

We follow the nomenclature from [6], and denote the spaces with the superscript 2. The L^2-formulation will be discretized using Taylor–Hood [7] elements, which results in a mixed problem that is stable [6]. The Taylor–Hood elements consist of P_2 elements for the velocity and P_1 elements for the pressure. Using Taylor–Hood elements also results in discrete function

spaces $\mathbf{V}_h$ and Q_h with the property that $\mathbf{V}_h \subset \mathbf{V}^2$ and $Q_h \subset Q^2$, that is, the elements are conforming. In addition to a derivation of the variational formulation, *a priori* error estimates will be presented.

4.1.1 Variational formulation

The first step in obtaining a variational formulation is to multiply the momentum equation and Darcy's law in the Darcy–Stokes problem (2.9)–(2.10) with test functions $\mathbf{v} \in \hat{\mathbf{V}}^2$, and multiply the continuity equations with test functions $q \in \hat{Q}^2$. Here, $\hat{\mathbf{V}}^2$ and $\hat{Q}^2$ are suitable function spaces for the test functions. Then next step is to integrate the equations over the entire domain Ω, which results in the equations

$$\begin{aligned} -\mu\langle\Delta\mathbf{u},\mathbf{v}\rangle_{\Omega_s} + \mu K^{-1}\langle\mathbf{u},\mathbf{v}\rangle_{\Omega_d} + \langle\nabla p,\mathbf{v}\rangle_{\Omega} &= \langle\mathbf{f},\mathbf{v}\rangle_{\Omega} \\ -\langle\nabla\cdot\mathbf{u},q\rangle_{\Omega} &= 0 \end{aligned} \tag{4.5}$$

where $\langle\cdot,\cdot\rangle_{\Omega}$ denotes the L^2-inner product over Ω. Integrating the term involving the Laplace operator by parts yields

$$\begin{aligned} -\mu\langle\Delta\mathbf{u},\mathbf{v}\rangle_{\Omega_s} &= \mu\langle\nabla\mathbf{u},\nabla\mathbf{v}\rangle_{\Omega_s} - \mu\langle\nabla\mathbf{u}\cdot\mathbf{n}_s,\mathbf{v}\rangle_{\Gamma_{\partial\Omega_s}} - \mu\langle\nabla\mathbf{u}_s\cdot\mathbf{n}_s,\mathbf{v}_s\rangle_{\Gamma} \\ &= \mu\langle\nabla\mathbf{u},\nabla\mathbf{v}\rangle_{\Omega_s} - \mu\langle\nabla\mathbf{u}\cdot\mathbf{n}_s,\mathbf{v}\rangle_{\Gamma_{\partial\Omega_s}} \\ &\quad - \mu\langle(\nabla\mathbf{u}_s\cdot\mathbf{n}_s\cdot\mathbf{n}_s)\mathbf{n}_s,\mathbf{v}_s\rangle_{\Gamma} - \mu\langle(\nabla\mathbf{u}_s\cdot\mathbf{n}_s\cdot\tau)\tau,\mathbf{v}_s\rangle_{\Gamma} \\ &= \mu\langle\nabla\mathbf{u},\nabla\mathbf{v}\rangle_{\Omega_s} - \mu\langle\nabla\mathbf{u}\cdot\mathbf{n}_s,\mathbf{v}\rangle_{\Gamma_{\partial\Omega_s}} \\ &\quad + \langle(p_d - p_s),\mathbf{v}_s\cdot\mathbf{n}_s\rangle_{\Gamma} + \mu\alpha K^{-\frac{1}{2}}\langle\mathbf{u}_s\cdot\tau,\mathbf{v}_s\cdot\tau\rangle_{\Gamma} \end{aligned}$$

Here $\mathbf{n}_s$ denotes the unit outward normal vector on $\partial\Omega_s$. The first equality results from integration by parts, while the second step is decomposition of $\nabla\mathbf{u}_s\cdot\mathbf{n}_s = (\nabla\mathbf{u}_s\cdot\mathbf{n}_s\cdot\tau)\tau + (\nabla\mathbf{u}_s\cdot\mathbf{n}_s\cdot\mathbf{n}_s)\mathbf{n}_s$ in tangential and normal direction, respectively. In the third step the interface conditions (2.12) and (2.13) are inserted. Integration by parts of the term involving the pressure gradient yields,

$$\begin{aligned} \langle\nabla p,\mathbf{v}\rangle_{\Omega} &= \langle\nabla p,\mathbf{v}\rangle_{\Omega_s} + \langle\nabla p,\mathbf{v}\rangle_{\Omega_d} \\ &= -\langle p,\nabla\cdot\mathbf{v}\rangle_{\Omega_s} + \langle\nabla p,\mathbf{v}\rangle_{\Omega_d} + \langle p,\mathbf{v}\cdot\mathbf{n}_s\rangle_{\Gamma_{\partial\Omega_s}} + \langle p_s,\mathbf{v}_s\cdot\mathbf{n}_s\rangle_{\Gamma} \end{aligned}$$

The first equality results from splitting the domain Ω into the Stokes domain Ω_s and the Darcy domain Ω_d. The second step is integration by parts of the term integrated over the Stokes domain. The last term integrated by parts is the term involving the divergence of $\mathbf{u}$, yielding,

$$\begin{aligned} -\langle\nabla\cdot\mathbf{u},q\rangle_{\Omega} &= -\langle\nabla\cdot\mathbf{u},q\rangle_{\Omega_s} - \langle\nabla\cdot\mathbf{u},q\rangle_{\Omega_d} \\ &= -\langle q,\nabla\cdot\mathbf{u}\rangle_{\Omega_s} + \langle\nabla q,\mathbf{u}\rangle_{\Omega_d} - \langle q,\mathbf{u}\cdot\mathbf{n}_d\rangle_{\Gamma_{\partial\Omega_d}} - \langle q_d,\mathbf{u_d}\cdot\mathbf{n}_d\rangle_{\Gamma} \\ &= -\langle q,\nabla\cdot\mathbf{u}\rangle_{\Omega_s} + \langle\nabla q,\mathbf{u}\rangle_{\Omega_d} - \langle q,\mathbf{u}\cdot\mathbf{n_d}\rangle_{\Gamma_{\partial\Omega_d}} + \langle q_d,\mathbf{u}_s\cdot\mathbf{n}_s\rangle_{\Gamma} \end{aligned}$$

Here $\mathbf{n}_d$ denotes the unit outward normal vector on $\partial\Omega_d$. The first step is splitting the domain Ω into the Stokes domain Ω_s and the Darcy domain Ω_d. The second step is integration by parts of the term integrated over the Darcy domain, while in the third step the fact that $\mathbf{n}_s = -\mathbf{n}_d$ is used, in addition to insertion of the interface condition (2.11). The above deliberations give rise to the variational formulation: Find $(\mathbf{u}, p) \in \mathbf{V}^2 \times Q^2$ such that

$$\begin{aligned} a(\mathbf{u}, \mathbf{v}) + b(p, \mathbf{v}) &= l_1(\mathbf{v}) \\ b(q, \mathbf{u}) &= l_2(q) \end{aligned} \tag{4.6}$$

for all $(\mathbf{v}, q) \in \hat{\mathbf{V}}^2 \times \hat{Q}^2$. Here, the bilinear forms $a(\mathbf{u}, \mathbf{v})$ and $b(p, \mathbf{v})$ are given as

$$a(\mathbf{u}, \mathbf{v}) = \mu K^{-1} \langle \mathbf{u}, \mathbf{v} \rangle_{\Omega_d} + \mu \langle \nabla \mathbf{u}, \nabla \mathbf{v} \rangle_{\Omega_s} + \mu \alpha K^{-\frac{1}{2}} \langle \mathbf{u}_s \cdot \tau, \mathbf{v} \cdot \tau \rangle_{\Gamma} \tag{4.7}$$

$$b(p, \mathbf{v}) = -\langle p, \nabla \cdot \mathbf{v} \rangle_{\Omega_s} + \langle \nabla p, \mathbf{v} \rangle_{\Omega_d} + \langle p_d, \mathbf{v}_s \cdot \mathbf{n}_s \rangle_{\Gamma} \tag{4.8}$$

and the linear forms $l_1(\mathbf{v})$ and $l_2(q)$ are given as

$$l_1(\mathbf{v}) = \mu \langle \nabla \mathbf{u} \cdot \mathbf{n}_s, \mathbf{v} \rangle_{\Gamma_{\partial\Omega_s}} - \langle p, \mathbf{v} \cdot \mathbf{n}_s \rangle_{\Gamma_{\partial\Omega_s}} + \langle \mathbf{f}, \mathbf{v} \rangle_{\Omega} \tag{4.9}$$

$$l_2(q) = -\langle q, \mathbf{u} \cdot \mathbf{n}_d \rangle_{\Gamma_{\partial\Omega_d}} \tag{4.10}$$

To obtain the discrete variational formulation, finite element spaces $\mathbf{V}_h$ and Q_h must be chosen. As earlier stated, discretizing (4.6) with Taylor–Hood elements will result in a stable scheme [6]. The discrete variational formulation reads: Find $(\mathbf{u}_h, p_h) \in \mathbf{V}_h \times Q_h$ such that

$$\begin{aligned} a(\mathbf{u}_h, \mathbf{v}) + b(p_h, \mathbf{v}) &= l_1(\mathbf{v}) \\ b(q, \mathbf{u}_h) &= 0 \end{aligned} \tag{4.11}$$

for all $(\mathbf{v}, q) \in \hat{\mathbf{V}}_h \times \hat{Q}_h$. Here, the forms $a(\mathbf{u}_h, \mathbf{v})$, $b(p_h, \mathbf{v})$ and $l_1(\mathbf{v})$ are given as,

$$\begin{aligned} a(\mathbf{u}_h, \mathbf{v}) = {} & \mu K^{-1} \langle \mathbf{u}_h, \mathbf{v} \rangle_{\Omega_d} + \mu \langle \nabla \mathbf{u}_h, \nabla \mathbf{v} \rangle_{\Omega_s} \\ & + \mu \alpha K^{-\frac{1}{2}} \langle \mathbf{u}_{s,h} \cdot \tau, \mathbf{v} \cdot \tau \rangle_{\Gamma} \end{aligned} \tag{4.12}$$

$$b(p_h, \mathbf{v}) = -\langle p_h, \nabla \cdot \mathbf{v} \rangle_{\Omega_s} + \langle \nabla p_h, \mathbf{v} \rangle_{\Omega_d} + \langle p_{d,h}, \mathbf{v}_s \cdot \mathbf{n}_s \rangle_{\Gamma} \tag{4.13}$$

$$l_1(\mathbf{v}) = -\langle p_{in}, \mathbf{v} \cdot \mathbf{n}_s \rangle_{\Gamma_{\partial\Omega_{in}}} + \langle \mathbf{f}, \mathbf{v} \rangle_{\Omega} \tag{4.14}$$

Note that boundary conditions on the exterior boundaries $\Gamma_{\partial\Omega_s}$ and $\Gamma_{\partial\Omega_d}$ have to be imposed to close the problem.

4.1.2 *A priori* error estimates

In this section, *a priori* error estimates for the Stokes problem and the Darcy problem posed using the space $\mathbf{V}^2 \times Q^2$ and discretized with Taylor–Hood elements will be derived. We could not find an *a priori* error estimate for the coupled Darcy–Stokes problem discretized with Taylor–Hood elements. Instead, we state the *a priori* error estimate for the coupled Darcy–Stokes problem discretized with the Mini element, presented by Karper et al. [6]. The Mini element [37, Chapter VI, Example 3.7] consists of continuous piecewise linears plus a bubble function for the velocity, and continuous piecewise linears for the pressure. When using Taylor–Hood elements, the velocities are approximated by continuous piecewise second order polynomials and the pressure is approximated by continuous piecewise linears.

***A priori* estimate 4.1** (Coupled Darcy–Stokes [6])**.** *Let $(\mathbf{u}, p) \in \mathbf{V}^2(\Omega) \times Q^2(\Omega)$ be the solution of problem (4.6). Let $(\mathbf{u}_h, p_h)$ be the discrete solution of (4.11), discretized with the Mini elements. Then, the following estimate hold*

$$\|\mathbf{u} - \mathbf{u}_h\|_{\mathbf{V}^2} + \|p - p_h\|_{Q^2} \leq C\Big(\inf_{\mathbf{v}_h \in \mathbf{V}^2} \|\mathbf{u} - \mathbf{v}_h\|_{\mathbf{V}^2} + \inf_{q_h \in Q^2} \|p - q_h\|_{Q^2}\Big)$$

In particular, a linear convergence estimate of the form

$$\begin{aligned} &\|\mathbf{u} - \mathbf{u}_h\|_{\mathbf{V}^2} + \|p - p_h\|_{Q^2} \\ &\leq Ch(\|\mathbf{u}_d\|_{H^1} + \|\mathbf{u}_s\|_{H^2} + \|p_d\|_{H^2} + \|p_d\|_{H^1}) \end{aligned} \tag{4.15}$$

is obtained. In this estimate, the velocity is approximated using piecewise linears. Using Taylor Hood elements, the velocities are approximated with piecewise second-order polynomials. Therefore, we make the assumption that the velocity error is of one order higher when discretizing with Taylor–Hood elements.

***A priori* estimate 4.2** (Stokes)**.** *Let $(\mathbf{u}, p) \in \mathbf{V}^2(\Omega_s) \times Q^2(\Omega_s)$ be the solution of the problem (4.6) with $\Omega = \Omega_s$. Let $(\mathbf{u}_h, p_h)$ be the discrete solution of (4.11). Then, it follows from Theorem 3.2 that the following estimate holds,*

$$\|\mathbf{u} - \mathbf{u}_h\|_{H^1} + \|p - p_h\|_{L^2} \leq C\Big(\inf_{\mathbf{v}_h \in \mathbf{V}^2} \|\mathbf{u} - \mathbf{v}_h\|_{H^1} + \inf_{q_h \in Q^2} \|p - q_h\|_{L^2}\Big)$$

Using the interpolation approximation from Theorem 3.3 on $\inf_{\mathbf{v}_h \in \mathbf{V}^2} \|\mathbf{u} - \mathbf{v}_h\|_{H^1}$ with $m = 1$ and $t = 3$, and on $\inf_{q_h \in Q^2} \|p - q_h\|_{L^2}$ with $m = 0$ and $t = 2$, yields

$$\|\mathbf{u}-\mathbf{u}_h\|_{H^1}+\|p-p_h\|_{L^2}\leq Ch^2(\|\mathbf{u}\|_{H^3}+\|p\|_{H^2}) \tag{4.16}$$

for sufficiently smooth solutions. The estimate (4.16) states that the H^1-error for the velocity is expected to be of at least second order, while the expected convergence rate of the L^2-error for the pressure is of at least second order. If the domain is convex, the L^2-error of the velocity is expected to be of third order, cf. Langtangen et al. [38].

***A priori* estimate 4.3** (Darcy)**.** *Let $(\mathbf{u},p)\in\mathbf{V}^2(\Omega_d)\times Q^2(\Omega_d)$ be the solution of the problem (4.6) with $\Omega=\Omega_d$. Let $(\mathbf{u}_h,p_h)$ be the discrete solution of (4.11). Then, it follows from Theorem 3.2 that the following estimate holds,*

$$\|\mathbf{u}-\mathbf{u}_h\|_{L^2}+\|p-p_h\|_{H^1}\leq C(\inf_{\mathbf{v}_h\in\mathbf{V}^2}\|\mathbf{u}-\mathbf{v}_h\|_{L^2}+\inf_{q_h\in Q^2}\|p-q_h\|_{H^1})$$

Using the interpolation approximation from Theorem 3.3 on $\inf_{v_h\in\mathbf{V}^2}\|\mathbf{u}_h-\mathbf{u}\|_{L^2}$ with $m=0$ and $t=3$, and on $\inf_{q_h\in Q^2}\|p_h-p\|_{H^1}$ with $m=1$ and $t=2$, gives

$$\|\mathbf{u}-\mathbf{u}_h\|_{L^2}+\|p-p_h\|_{H^1}\leq Ch^3\|\mathbf{u}\|_{H^3}+Ch\|p\|_{H^2} \tag{4.17}$$

for sufficiently smooth solutions. Under the assumption that $\|\mathbf{u}\|_H^3$ and $\|p\|_{H^2}$ are of the same magnitude, the L^2-error for the velocity is expected to be of at least first order and the H^1-error for the pressure is expected to be of at least first order as h tends to zero.

4.2 Numerical Scheme II: The $H(\mathrm{div})$-formulation

In this section, the $H(\mathrm{div})$-formulation of the coupled Darcy–Stokes problem proposed by Karper et al. [6] is derived, posed using spaces with higher regularity for the velocities as follows

$$\begin{aligned}\mathbf{V}^1(\Omega)&=\{\mathbf{v}\in\mathbf{H}_0(\mathrm{div},\Omega):\mathbf{v}_s\in\mathbf{H}^1(\Omega_s)\}\\ Q^1(\Omega)&=L^2_0(\Omega)\end{aligned}$$

Again, we follow the nomenclature from [6], and denote the spaces with the superscript 1. Discretizing the $H(\mathrm{div})$-formulation results in a mixed problem, and several finite element combinations will be considered. For the velocity, lower order Brezzi–Douglas–Marini [8] or Raviart–Thomas [27] elements will be used. The elements are $H(\mathrm{div})$ conforming, in the sense that

the discrete function spaces will be subsets of $H(\text{div})$. However, discretizing the velocities with these $H(\text{div})$ conforming elements will not result in a stable scheme [9]. The elements are not in $H^1(\Omega)$, hence the gradients arising from integration by parts of the second-order term in (4.5) will not be well-defined. To obtain a stable scheme, the IP method will be used to penalize the jumps of the velocity at the interior facets in the Stokes part of the domain, as suggested by Kanschat et al. [9]. For the pressure, DG_q elements will be used. In addition, *a priori* error estimates will be presented.

4.2.1 Variational formulation

The first step in obtaining a variational formulation is to multiply the momentum equation and Darcy's law in the Darcy–Stokes problem (2.9)–(2.10) with test functions $\mathbf{v} \in \hat{\mathbf{V}}^1$, and multiply the continuity equations with test functions $q \in \hat{Q}^1$. Here, $\hat{\mathbf{V}}^1$ and $\hat{Q}^1$ are suitable function spaces for the test functions. Then next step is to integrate the equations over the entire domain Ω, which results in (4.5). Integration by parts of the term involving the Laplace operator yields,

$$\begin{aligned} -\mu\langle\Delta\mathbf{u},\mathbf{v}\rangle_{\Omega_s} = \mu\langle\nabla\mathbf{u},\nabla\mathbf{v}\rangle_{\Omega_s} - \mu\langle\nabla\mathbf{u},\mathbf{v}\cdot\mathbf{n}_s\rangle_{\Gamma_{\partial\Omega_s}} \\ - \mu\langle\nabla\mathbf{u}_s,\mathbf{v}_s\cdot\mathbf{n}_s\rangle_{\Gamma} \end{aligned} \tag{4.18}$$

where $\mathbf{n}_s$ denotes the unit outward normal vector on $\partial\Omega_s$. Integrating the term involving the pressure gradient by parts yields,

$$\begin{aligned} \langle\nabla p,\mathbf{v}\rangle_{\Omega} = -\langle p,\nabla\cdot\mathbf{v}\rangle_{\Omega} + \langle p,\mathbf{v}\cdot\mathbf{n}_s\rangle_{\Gamma_{\partial\Omega_s}} + \langle p,\mathbf{v}\cdot\mathbf{n}_d\rangle_{\Gamma_{\partial\Omega_d}} \\ +\langle p_s,\mathbf{v}_s\cdot\mathbf{n}_s\rangle_{\Gamma} + \langle p_d,\mathbf{v}_d\cdot\mathbf{n}_d\rangle_{\Gamma} \end{aligned} \tag{4.19}$$

Here $\mathbf{n}_d$ denotes the unit outward normal vector on $\partial\Omega_d$. We take a closer look at the terms in (4.18)–(4.19) integrated over the interface Γ. Decomposition of the vector $\nabla\mathbf{u}_s = (\nabla\mathbf{u}_s\cdot\tau)\tau + (\nabla\mathbf{u}_s\cdot\mathbf{n}_s)\mathbf{n}_s$ in tangential and normal direction, respectively, in addition to insertion of the interface conditions (2.12) and (2.13) yields,

$$\begin{aligned} -\mu\langle\nabla\mathbf{u}_s,\mathbf{v}_s\cdot\mathbf{n}_s\rangle_{\Gamma} &= -\mu\langle(\nabla\mathbf{u}_s\cdot\mathbf{n}_s)\mathbf{n}_s,\mathbf{v}_s\cdot\mathbf{n}_s\rangle_{\Gamma} \\ &\quad - \mu\langle(\nabla\mathbf{u}_s\cdot\tau)\tau,\mathbf{v}_s\cdot\mathbf{n}_s\rangle_{\Gamma} \\ &= \langle p_d - p_s,\mathbf{v}_s\cdot\mathbf{n_s}\rangle_{\Gamma} + \mu\alpha K^{-\frac{1}{2}}\langle\mathbf{u}_s\cdot\tau,\mathbf{v}_s\cdot\tau\rangle_{\Gamma} \end{aligned}$$

Using the fact that $\mathbf{n}_s = -\mathbf{n}_d$, along with insertion of the interface condition (2.11) yields,

$$\begin{aligned}\langle p_s, \mathbf{v}_s \cdot \mathbf{n}_s\rangle_\Gamma + \langle p_d, \mathbf{v}_d \cdot \mathbf{n}_d\rangle_\Gamma &= \langle p_s, \mathbf{v}_s \cdot \mathbf{n}_s\rangle_\Gamma - \langle p_d, \mathbf{v}_d \cdot \mathbf{n}_s\rangle_\Gamma \\ &= \langle p_s, \mathbf{v}_s \cdot \mathbf{n}_s\rangle_\Gamma - \langle p_d, \mathbf{v}_s \cdot \mathbf{n}_s\rangle_\Gamma \\ &= \langle p_s - p_d, \mathbf{v}_s \cdot \mathbf{n}_s\rangle_\Gamma\end{aligned}$$

The above deliberations give rise to the variational formulation: Find $(\mathbf{u}, p) \in \mathbf{V}^1 \times Q^1$ such that

$$\begin{aligned}a(\mathbf{u}, \mathbf{v}) + b(p, \mathbf{v}) &= l(\mathbf{v}) \\ b(q, \mathbf{u}) &= 0\end{aligned} \tag{4.20}$$

for all $(\mathbf{v}, q) \in \hat{\mathbf{V}}^1 \times \hat{Q}^1$. Here, the bilinear forms $a(\mathbf{u}, \mathbf{v})$ and $b(p, \mathbf{v})$ are given as,

$$a(\mathbf{u}, \mathbf{v}) = \mu\langle\nabla\mathbf{u}, \nabla\mathbf{v}\rangle_{\Omega_s} + \mu K^{-1}\langle\mathbf{u}, \mathbf{v}\rangle_{\Omega_d} + \mu\alpha K^{-\frac{1}{2}}\langle\mathbf{u}_s \cdot \tau, \mathbf{v_s} \cdot \tau\rangle_\Gamma \tag{4.21}$$

$$b(p, \mathbf{v}) = -\langle p, \nabla \cdot \mathbf{v}\rangle_\Omega \tag{4.22}$$

and the linear form $l(\mathbf{v})$ is given as,

$$l(\mathbf{v}) = \mu\langle\nabla\mathbf{u} \cdot \mathbf{n}_s, \mathbf{v}\rangle_{\Gamma_{\partial\Omega_s}} - \langle p, \mathbf{v} \cdot \mathbf{n}_s\rangle_{\Gamma_{\partial\Omega_s}} - \langle p, \mathbf{v} \cdot \mathbf{n}_d\rangle_{\Gamma_{\partial\Omega_d}} + \langle\mathbf{f}, \mathbf{v}\rangle_\Omega \tag{4.23}$$

To obtain the discrete variational formulation, finite element spaces $\mathbf{V}_h$ and Q_h must be chosen. Discretizing (4.20) using Brezzi–Douglas–Marini [8] elements or Raviart–Thomas [27] elements for the velocity space results in an unstable scheme [9], as the gradients in (4.21) will not be well-defined. To remedy this, we follow Kanschat et al. [9] and apply the IP method to discretize the second-order term in (4.5). The procedure is explained in Section 3.3.2, and results in the stabilization term $\gamma(\mathbf{u}_h, \mathbf{v})$.

$$\begin{aligned}\gamma(\mathbf{u}_h, \mathbf{v}) = \mu &\sum_{e\in\Gamma_h^s} \frac{\beta_s}{h} \int_e [\![\mathbf{u}_h]\!][\![\mathbf{v}]\!]\,\mathrm{d}S \\ - \mu &\sum_{e\in\Gamma_h^s} \int_e \{\nabla\mathbf{u}_h\} \cdot [\![\mathbf{v}]\!] \cdot \mathbf{n}_+\,\mathrm{d}S \\ - \mu &\sum_{e\in\Gamma_h^s} \int_e \{\nabla\mathbf{v}\} \cdot [\![\mathbf{u}_h]\!] \cdot \mathbf{n}_+\,\mathrm{d}S\end{aligned} \tag{4.24}$$

where Γ_h^s denotes the interior facets in the Stokes region and $\mathbf{n}_+$ denotes the unit normal at the e. A lower bound for the penalty parameter β_s will be found numerically in Section 6.1.3. Discretizing the variational formulation (4.20) and adding the term (4.24) results in the discrete variational formulation: Find $(\mathbf{u}_h, p_h) \in \mathbf{V}_h \times Q_h$ such that

$$\begin{aligned} a(\mathbf{u}_h, \mathbf{v}) + \gamma(\mathbf{u}_h, \mathbf{v}) + b(p_h, \mathbf{v}) &= l(\mathbf{v}) \\ b(q, \mathbf{u_h}) &= 0 \end{aligned} \tag{4.25}$$

for all $(\mathbf{v}, q) \in \hat{\mathbf{V}}_h \times \hat{Q}_h$. Here, the forms a, b, γ and l are given by (4.21), (4.22), (4.24), and (4.23), respectively. Boundary conditions on the exterior boundaries $\Gamma_{\partial\Omega_s}$ and $\Gamma_{\partial\Omega_d}$ have to be imposed to close the problem. Note that Dirichlet conditions on the velocity have to be enforced through Nitsche's method in tangential direction, as the degrees of freedom at the edge consist solely of normal components.

4.2.2 *A priori* error estimates

In this section *a priori* error estimates for the Stokes problem and the Darcy problem posed using the space $\mathbf{V}^1 \times Q^1$ and discretized with $BDM_1 \times DG_0$ elements will be derived. We could not find an *a priori* error estimate for the coupled Darcy–Stokes problem discretized with $BDM_1 \times DG_0$ elements. Kanschat et al. [9] and Girault et al. [39] prove *a priori* error estimates for the coupled Darcy–Stokes problem discretized with Raviart–Thomas elements.

***A priori* estimate 4.4** (Stokes)**.** *Let $(\mathbf{u}, p) \in \mathbf{V}^1(\Omega_s) \times Q^1(\Omega_s)$ be the solution of the problem (4.20) with $\Omega = \Omega_s$. Let $(\mathbf{u}_h, p_h)$ be the discrete solution of (4.25). Then, it follows from Theorem (3.2) that the following estimate holds*

$$\|\mathbf{u} - \mathbf{u}_h\|_{H^1} + \|p - p_h\|_{L^2} \leq C(\inf_{\mathbf{v}_h \in \mathbf{V}^1} \|\mathbf{u} - \mathbf{v}_h\|_{H^1} + \inf_{q_h \in Q^1} \|p - q_h\|_{L^2})$$

Using the interpolation approximation in Theorem 3.3 on $\inf_{\mathbf{v}_h \in \mathbf{V}^1} \|\mathbf{u} - \mathbf{v}_h\|_{H^1}$ with $m = 1$ and $t = 2$, and on $\inf_{q_h \in Q^1} \|p - q_h\|_{L^2}$ with $m = 0$ and $t = 1$, yields

$$\|\mathbf{u} - \mathbf{u}_h\|_{H^1} + \|p - p_h\|_{L^2} \leq Ch(\|\mathbf{u}\|_{H^2} + \|p\|_{H^1}) \tag{4.26}$$

for sufficiently smooth solutions. The estimate (4.26) states that the expected convergence rate of the L^2-error for the pressure is of at least first order. The H^1-error for the velocity is expected to be of at least first order.

***A priori* estimate 4.5** (Darcy)**.** *Let $(\mathbf{u}, p) \in \mathbf{V}^1(\Omega_d) \times Q^1(\Omega_d)$ be the solution of the problem (4.20) with $\Omega = \Omega_d$. Let $(\mathbf{u}_h, p_h)$ be the discrete solution of (4.25). Then, it follows from Theorem (3.2) that the following estimate holds*

$$\|\mathbf{u} - \mathbf{u}_h\|_{H(\mathrm{div})} + \|p - p_h\|_{L^2} \leq C(\inf_{\mathbf{v}_h in \mathbf{V}^1} \|\mathbf{u} - \mathbf{u}_h\|_{H(\mathrm{div})} + \inf_{q_h \in Q^1} \|p - q_h\|_{L^2})$$

Using the interpolation approximation in Theorem 3.3 on $\inf_{\mathbf{v}_h in \mathbf{V}^1} \|\mathbf{u}_h - \mathbf{u}\|_{H(\mathrm{div})}$ *with* $m = 0$ *and* $t = 2$*, and on* $\inf_{q_h \in Q^1} \|p_h - p\|_{L^2}$ *with* $m = 0$ *and* $t = 1$*, yields*

$$\|\mathbf{u} - \mathbf{u}_h\|_{H(\mathrm{div})} + \|p - p_h\|_{L^2} \leq Ch^2 \|\mathbf{u}\|_{H^2} + Ch\|p\|_{H^1} \tag{4.27}$$

for sufficiently smooth solutions. The estimate (4.27) states that the $H(\mathrm{div})$*-error for the velocity is expected to be of at least first order and that the expected* L^2*-rate of the pressure-error is of at least first order when* h *tends to zero.*

Chapter 5

Preconditioning

In this chapter, a presentation of Krylov space methods and the preconditioned minimal residual method is provided. For a complementary introduction to Krylov space methods and a detailed explanation of the minimal residual method, the reader is referred to Elman et al. [21]. The theory in Section 5.1 is compiled from the works of Elman et al. [21], Saad [40] and Mardal et al. [41]. The rest of the chapter is dedicated to proposing and analyzing possible preconditioners for the coupled Darcy–Stokes problem, both discretized with the L^2-formulation and the $H(\mathrm{div})$-formulation.

5.1 Iterative methods

The finite element method results in a system of algebraic equations,

$$A\mathbf{u} = \mathbf{b} \tag{5.1}$$

that has to be solved. The matrix A is usually sparse, that is, only a very small proportion of the entries are nonzero. In addition, solving a physical problem requires a great number of degrees of freedom to get an accurate solution, which leads to a large matrix. Hence, solving the system directly is not an option, as inverting A will require infeasible computation resources for linear systems of larger dimensions [21]. A Krylov space method is typically used to solve problems of the form (5.1), as they take advantage of the sparsity of the coefficient matrix. Their storage requirements depend only on the number of nonzero entries in the matrix [21]. The most celebrated Krylov method [40] is the conjugate gradient method, which requires A to be symmetric and positive-definite. Discretizing the Darcy–Stokes equations using the finite element method results in a system that is symmetric, but not positive-definite. A robust Krylov space method for such systems is the minimal residual method (MinRes), as it takes advantage of the symmetry, but does not require positivity [21].

5.1.1 The minimal residual method

The theory presented in this section is compiled from the works of Elman et al. [21, Chapter 2] and Mardal et al. [41]. Krylov space methods aims to approximate the solution $\mathbf{u} = A^{-1}\mathbf{b}$ of a linear system of the form (5.1) in a Krylov space $\mathcal{K}_k$, by an iterative procedure. The sparsity of the coefficient matrix A enables the product with any vector $\mathbf{x}$ to be computed cheaply. Hence, it is easy to compute the members of the The Krylov space of order k given as

$$\mathcal{K}_k = \mathcal{K}_k(A, \mathbf{x}) = \text{span}\{\mathbf{x}, A\mathbf{x}, \ldots, A^{k-1}\mathbf{x}\}$$

by taking linear combinations of these vectors. Note that $\mathcal{K}_k$ is a linear span of k vectors, hence it is a k-dimensional subspace of $\mathbb{R}^n$ if the vectors are linearly independent. More precisely, by letting $\mathbf{u}_0$ be the initial guess and $\mathbf{r}_0 = \mathbf{b} - A\mathbf{u}_0$ denote the initial residual, the methods generate a sequence $\mathbf{u}_k \in \mathbf{u}_0 + \mathcal{K}_k(A, \mathbf{r}_0)$ that is successively closer to the true solution $\mathbf{u}$. When the norm of the residual $\|\mathbf{r}_k\| = \|\mathbf{b} - A\mathbf{u}_k\|$ is smaller than some given tolerance, we say that the method has converged.

Observe that a function $\mathbf{y} \in \mathcal{K}_k(A, \mathbf{r}_0)$ can be written of the form $\mathbf{y} = q_{k-1}(A)\mathbf{r}_0$, where $q_{k-1}(A)$ is a real polynomial of degree at most $k-1$. This observation, the fact that A is nonsingular and the Cayley–Hamilton theorem [21, Section 2.1] gives that for $k = n$,

$$\mathbf{u} - \mathbf{u}_0 = A^{-1}\mathbf{r}_0 = q_{n-1}(A)\mathbf{r}_0 \tag{5.2}$$

To generate a sequence of solutions $\mathbf{u}_k$, the correction to $\mathbf{u} - \mathbf{u}_0$ is computed. It remains to decide how to choose the sequence of polynomials q_k such that

$$\mathbf{u}_k = \mathbf{u}_0 + q_{k-1}(A)\mathbf{r}_0 \tag{5.3}$$

are successively closer to the true solution $\mathbf{u}$. Different choices of the polynomials q_k gives rise to different Krylov space methods. In the minimal residual method, the Lanczos method [21, Chapter 2, Section 2.4] is used to create an orthonormal basis for the Krylov space $\mathcal{K}_k(A, \mathbf{r}_0)$. Then, the euclidean norm of the residual $\|\mathbf{r}_k\| = \|\mathbf{b} - A\mathbf{u}_k\|$ is minimized using the least squares method. The minimal residual method has the convergence estimate [21, Chapter 2, (2.40)],

$$\|\mathbf{r}_k\| \leq \min_{p_k \in \Pi_k, p_k(0)=1} \max_j |p_k(\lambda_j)| \|\mathbf{r}_0\| \tag{5.4}$$

where Π_k is the set of real polynomials with degree less than or equal to k and the max is taken over the eigenvalues λ of A. Symmetry of the matrix

A ensures orthogonality of the eigenvectors, consequently the convergence depends solely on the eigenvalues [21, Chapter 2]. As A is not positive-definite, the eigenvalues are however, not necessarily positive. Mardal et al. [41] point out that consequently, it is in general not straightforward to obtain a sharp estimate for $\min_{p_k \in \Pi_k, p_k(0)=1} \max_j |p_k(\lambda_j)|$. However, restricting the admissible polynomials in Π_k to even polynomials leads to the convergence estimate [41, Remark 2.2],

$$\|\mathbf{r}_{2k}\| \leq (\frac{\kappa(A)-1}{\kappa(A)+1})^k \|\mathbf{r}_0\| \tag{5.5}$$

where $\kappa(A)$ is the condition number of A.

Definition 5.1 (Condition number [42, Proposition 5.3.2])**.** *The condition number of a symmetric matrix A is defined as*

$$\kappa(A) = \frac{|\lambda_{max}(A)|}{|\lambda_{min}(A)|} \tag{5.6}$$

where $|\lambda_{min}(A)|$ and $|\lambda_{max}(A)|$ are respectively the modulus of the smallest and largest eigenvalues of A.

From the convergence estimate (5.5), it is clear that how fast the minimal residual method converges, depends critically on the condition number $\kappa(A)$. A low condition number results in fast convergence, whereas a high condition number results in slow convergence. The matrix A in system (5.1) typically has a condition number that grows as $1/h^2$, hence the condition number will grow rapidly as h decreases. To obtain fast convergence, MinRes should therefore be used with a preconditioner. Applying a preconditioner P^{-1} on system (5.1) results in the preconditioned system,

$$P^{-1}A\mathbf{u} = P^{-1}\mathbf{b} \tag{5.7}$$

The preconditioner P^{-1} must be positive-definite [21]. To conserve the symmetry of system (5.1), the preconditioner should in addition be symmetric. Arguments similar to those that were used to obtain (5.5) gives a convergence estimate for the preconditioned minimal residual method [41] that depends on the condition number of the preconditioned system $P^{-1}A$. The minimal residual method will convergence faster if the condition number of the preconditioned system $\kappa(P^{-1}A)$ is smaller than the condition number of the original system $\kappa(A)$. For practical reasons, it is important that the preconditioner is relatively cheap to compute and store. Therefore, it is required that P^{-1} uses $\mathcal{O}(N)$ flops for evaluation and storage. The last requirement on the preconditioner is that the condition number $\kappa(P^{-1}A)$

is bounded independently of the discretization parameter h. This ensures robustness to refinement of the mesh. A preconditioner with this desired property will from now on be referred to as an optimal preconditioner.

In the construction of discrete preconditioners, it is important that we can replace a computationally costly preconditioner B_1 by a more efficient preconditioner B_2. Assume B_1 is an optimal preconditioner. If the new preconditioner B_2 is spectrally equivalent to B_1, then B_2 is also optimal [41, Remark 2.6].

Definition 5.2 (Spectral equivalence [21, Chapter 2, Remark 2.5])**.** *Two linear operators B_1 and B_2 are spectrally equivalent if there exist constants $C_1, C_2 > 0$ independent of the matrix size such that:*

$$C_1\langle B_1\mathbf{u}, \mathbf{u}\rangle \leq \langle B_2\mathbf{u}, \mathbf{u}\rangle \leq C_2\langle B_1\mathbf{u}, \mathbf{u}\rangle$$

Moreover, if B_1 and B_2 are spectrally equivalent, we have that $\kappa(B_1B_2) \leq \frac{C_2}{C_1}$.

5.2 Preconditioning coupled Darcy–Stokes flow

The coupled Darcy–Stokes equations (2.9)–(2.10) can be written on block form as

$$\mathcal{A} \times \begin{bmatrix} \mathbf{u} \\ p \end{bmatrix} = \begin{bmatrix} \mathbf{f} \\ 0 \end{bmatrix} \tag{5.8}$$

where

$$\mathcal{A} = \begin{bmatrix} -\Delta_s + I_d & \text{grad} \\ \text{div} & 0 \end{bmatrix} \tag{5.9}$$

The subscripts "s" and "d" have been added to indicate the operators specific to Stokes flow and Darcy flow, respectively. The Darcy problem is well posed in both $\mathbf{L}^2(\Omega) \times H^1(\Omega)$ and $\mathbf{H}(\text{div}, \Omega) \times L_0^2(\Omega)$, cf. [36]. Therefore, the coupled Darcy–Stokes equations have at least two possible solutions spaces X and Y,

$$X = \mathbf{V}^2 \times Q^2 = (\mathbf{L}^2(\Omega) \cap \mathbf{H}^1(\Omega_s)) \times (L_0^2(\Omega) \cap H^1(\Omega_d)) \tag{5.10}$$

$$Y = \mathbf{V}^1 \times Q^1 = (\mathbf{H}_0(\text{div}, \Omega) \cap \mathbf{H}^1(\Omega_s)) \times L_0^2(\Omega) \tag{5.11}$$

with the corresponding dual spaces with respect to the L^2-inner product

$$X^* = (\mathbf{L}^2(\Omega) \cap \mathbf{H}^{-1}(\Omega_s)) \times (L_0^2(\Omega) \cap H^{-1}(\Omega_d)) \tag{5.12}$$

$$Y^* = (\mathbf{H}_0(\mathrm{div}, \Omega)^* \cap \mathbf{H}^{-1}(\Omega_s)) \times L_0^2(\Omega) \tag{5.13}$$

Karper et al. [6] show that $\mathcal{A}$ is an isomorphism mapping both X onto X^* and Y onto Y^*, hence the problem is well posed both in X and Y. The approach taken here for finding good preconditioners is to use well known preconditioners for the Stokes problem and the Darcy problem and combine them. Next, we will present the Stokes preconditioners and the Darcy preconditioners used for this purpose.

5.2.1 Stokes

By letting $\Omega = \Omega_s$ the Darcy–Stokes equations are equivalent with the Stokes equations which can be written on the form (5.8) with $\mathcal{A} = \mathcal{A}_s$ where,

$$\mathcal{A}_s = \begin{bmatrix} -\Delta & \mathrm{grad} \\ \mathrm{div} & 0 \end{bmatrix} \tag{5.14}$$

It is well known that with proper boundary conditions, $\mathcal{A}_s$ is an isomorphism mapping $X_s = \mathbf{H}^1(\Omega_s) \times L^2(\Omega_s)$ onto its dual space $X_s^* = \mathbf{H}^{-1}(\Omega_s) \times L^2(\Omega_s)$, cf. [36]. A widely used preconditioner for the Stokes system (5.14) is $\mathcal{B}_s^{-1}$ where,

$$\mathcal{B}_s = \begin{bmatrix} -\Delta & 0 \\ 0 & I \end{bmatrix} \tag{5.15}$$

The preconditioner $\mathcal{B}_s^{-1}$ is the identity Riesz operator mapping X_s^* onto X_s, cf. [36]. Moreover, the condition number of $\mathcal{B}_s^{-1}\mathcal{A}_s$ posed in X_s is bounded. Note that $Y_s = \mathbf{H}^1(\Omega_s) \times L^2(\Omega_s)$ is equal to X_s, consequently, $\mathcal{A}_s$ and $\mathcal{B}_s^{-1}$ have the same properties when the Stokes problem is posed in Y_s.

The operator $\mathcal{B}_s$ will be used to construct preconditioners for both the L^2-formulation and the $H(\mathrm{div})$-formulation. Consequently, the operator must be discretized using Taylor–Hood elements and Brezzi–Douglas–Marini elements. Discretizing $\mathcal{B}_s$ using Taylor Hood elements is straightforward. The discretization with BDM elements, is however not obvious. The discrete velocity space consisting of these elements will not be in $H^1(\Omega)$, consequently, the gradients arising from integration by parts of the second-order operator in the upper left corner of $\mathcal{B}_s$ will not be well-defined. The IP method is used to weakly penalize the jumps of the approximate velocities across interior facets. The procedure is explained in detail in Section 3.3.2, and reults in the term $\eta(\mathbf{u}_h, \mathbf{v})$.

$$\begin{aligned}\eta(\mathbf{u}_h, \mathbf{v}) = \mu &\sum_{E \in \mathcal{T}_h} \langle \nabla \mathbf{u}_h, \nabla \mathbf{v} \rangle_E \\ &+ \mu \sum_{e \in \Gamma_h^s} \frac{\beta_s}{h} \langle [\![\mathbf{u}_h]\!], [\![\mathbf{v}]\!] \rangle_e \\ &+ \mu \sum_{e \in \Gamma_{\partial\Omega_{s,h}}} \frac{\beta_s}{h} \langle \mathbf{u}_h, \mathbf{v} \rangle_e\end{aligned} \tag{5.16}$$

Here $\mathcal{T}_h$ is a partition of the Stokes domian Ω_s, Γ_h^s is the set of interior facets in the Stokes region, while $\Gamma_{\partial\Omega_{s,h}}$ is the set of exterior facets at the Stokes region. Note that the boundary conditions of the problem to which the preconditioner is applied on affects which parts of the exterior boundary $\Gamma_{\partial\Omega_s}$ that should be included in the latter sum in (5.16). The discrete operator $B_{s,h}$ then becomes,

$$\mathcal{B}_{s,h} = \begin{bmatrix} \eta(\mathbf{u}_h, \mathbf{v}) & 0 \\ 0 & \frac{1}{\mu} \langle p_h, q \rangle_{\Omega_s} \end{bmatrix} \tag{5.17}$$

Note that relevant conditions on the exterior boundary of the problem to which the preconditioner is applied, also have to be imposed.

5.2.2 Darcy

By letting $\Omega = \Omega_d$, system (5.8) is equivalent to the Darcy equations with $\mathcal{A} = \mathcal{A}_d$ where,

$$\mathcal{A}_d = \begin{bmatrix} I & \text{grad} \\ \text{div} & \mathbf{0} \end{bmatrix} \tag{5.18}$$

The operator $\mathcal{A}_d$ is an isomorphism mapping both $X_d = \mathbf{L}^2(\Omega_d) \times H^1(\Omega_d)$ onto its dual space $X_d^* = \mathbf{L}^2(\Omega_d) \times H^{-1}(\Omega_d)$, and $Y_d = \mathbf{H}(\text{div}, \Omega_d) \times L^2(\Omega_d)$ onto its dual space $Y_d^* = \mathbf{H}(\text{div}, \Omega_d)^* \times L^2(\Omega_d)$, cf. [36]. Hence, the Darcy problem is well posed in both spaces. Two preconditioners will be explored, namely $\mathcal{B}_{d,I}^{-1}$ and $\mathcal{B}_{d,II}^{-1}$ where,

$$\mathcal{B}_{d,I} = \begin{bmatrix} I & 0 \\ 0 & -\Delta \end{bmatrix}, \; \mathcal{B}_{d,II} = \begin{bmatrix} I - \text{grad}\,\text{div} & 0 \\ 0 & I \end{bmatrix} \tag{5.19}$$

The preconditioner $\mathcal{B}_{d,I}^{-1}$ is the identity Riesz operator mapping X_d^* onto X_d, cf. [36]. Furthermore, the preconditioned system $\mathcal{B}_{d,I}^{-1}\mathcal{A}_d$ has a bounded condition number. In a similar manner, the preconditioner $\mathcal{B}_{d,II}^{-1}$ is the identity Riesz operator mapping Y_d^* onto Y_d, cf. [36]. Moreover, the preconditioned

system $\mathcal{B}_{d,II}^{-1}\mathcal{A}_d$ has a bounded condition number.

The preconditioner $\mathcal{B}_{d,I}^{-1}$ will be used to construct preconditioners for both the L^2-formulation and the $H(\text{div})$-formulation. To this end, $\mathcal{B}_{d,I}$ has to be discretized with Taylor–Hood elements and with Brezzi–Douglas–Marini elements. Discretizing the operator using Taylor–Hood elements is straightforward. The discretization using BDM elements is however, not as obvious. The corresponding pressure space consists of DG_q elements, which are not in H^1. Hence, the gradients arising from integration by parts of the second-order operator in the lower right corner of $\mathcal{B}_{d,I}$ will not be well defined. Winther et al. [43] suggest to remedy this by applying the IP method. The procedure is explained in Section 3.3.2, and results in the term

$$\begin{aligned}\zeta(p_h, q) = &\sum_{E\in\mathcal{T}_h} \langle \nabla p_h, \nabla q\rangle_E \\ &+ \sum_{e\in\Gamma_h^d} \frac{\beta_d}{h}\langle [\![p_h]\!], [\![q]\!]\rangle_e \\ &+ \sum_{e\in\Gamma_{\partial\Omega_{d,h}}} \frac{\beta_d}{h}\langle p_h, q\rangle_e\end{aligned} \tag{5.20}$$

Here $\mathcal{T}_h$ is a partition of the Darcy domian Ω_d, Γ_h^d is the set of interior facets in the Darcy region, while $\Gamma_{\partial\Omega_{d,h}}$ is the set of exterior facets at the Darcy region. Note that the boundary conditions of the problem to which the preconditioner is applied on affects which parts of the exterior boundary $\Gamma_{\partial\Omega_d}$ that should be included in the latter sum in (5.20). The discrete operator $\mathcal{B}_{d,I,h}$ then becomes,

$$\mathcal{B}_{d,I,h} = \begin{bmatrix} \frac{K}{\mu}\langle \mathbf{u}_h, \mathbf{v}\rangle_{\Omega_d} & 0 \\ 0 & +\frac{\mu}{K}\zeta(p_h, q)) \end{bmatrix} \tag{5.21}$$

The preconditioner $\mathcal{B}_{d,II,h}^{-1}$ will only be applied on the $H(\text{div})$-formulation, and the discretization using BDM elements is obvious.

5.2.3 Coupled Darcy–Stokes

As earlier stated, we will create preconditioners for the coupled Darcy–Stokes problem based on the previously presented preconditioners for the Stokes and the Darcy problem. The technique has been suggested by Cai et al. [11] and Márquez et al. [12]. However, they decoupled the problem through the preconditioners, and solves the local Darcy and Stokes subproblems separately using different elements. We will in addition to applying decoupled preconditioners similar to the ones proposed in [11, 12], suggest

two preconditioners that preserves the coupling between the Darcy and the Stokes flow.

When posing the coupled Darcy–Stokes problem in (5.10), the preconditioner should be an operator $\mathcal{P}^{-1}$ mapping X^* onto X. An operator with this property is $\mathcal{P}_I^{-1}$, where

$$\mathcal{P}_I = \mathcal{B}_s + \mathcal{B}_{d,I} = \begin{bmatrix} -\Delta_s + I_d & 0 \\ 0 & I_s - \Delta_d \end{bmatrix} \tag{5.22}$$

When posing the coupled Darcy–Stokes problem in (5.11), the preconditioner should be an operator $\mathcal{Q}^{-1}$ mapping Y^* onto Y. An operator with this property is $\mathcal{Q}_I^{-1}$, where

$$\mathcal{Q}_I = \mathcal{B}_s + \mathcal{B}_{d,II} = \begin{bmatrix} -\Delta_s + I_d - \operatorname{grad}\operatorname{div}_d & 0 \\ 0 & I_s + I_d \end{bmatrix} \tag{5.23}$$

Note that $\mathcal{P}_I^{-1}$ and $\mathcal{Q}_I^{-1}$ are fully decoupled preconditioners, where the coupling conditions at the interface are not taken into consideration. As we aim to find preconditioners that are similar to the inverse of $\mathcal{A}$, preconditioners where the coupling conditions are included are also proposed. The coupling conditions at the interface introduces an additional operator O_Γ given as,

$$\langle O_\Gamma \mathbf{u}, \mathbf{v} \rangle = \mu\alpha K^{-\frac{1}{2}} \langle \mathbf{u_s} \cdot \tau, \mathbf{v_s} \cdot \tau \rangle_\Gamma \tag{5.24}$$

Preconditioners including the coupling conditions are the modified preconditioners $\mathcal{P}_{II}^{-1}$ and $\mathcal{Q}_{II}^{-1}$ where,

$$\mathcal{P}_{II} = \begin{bmatrix} -\Delta_s + I_d + O_\Gamma & 0 \\ 0 & I_s - \Delta_d \end{bmatrix} \tag{5.25}$$

$$\mathcal{Q}_{II} = \begin{bmatrix} -\Delta_s + I_d - \operatorname{grad}\operatorname{div}_d + O_\Gamma & 0 \\ 0 & I_s + I_d \end{bmatrix} \tag{5.26}$$

We will apply the preconditioners $\mathcal{P}_I^{-1}$ and $\mathcal{P}_{II}^{-1}$ to the Darcy–Stokes system arising from the L^2-formulation. The Darcy–Stokes system arising from the $H(\text{div})$-formulation will be preconditioned with both $\mathcal{P}_I^{-1}$, $\mathcal{P}_{II}^{-1}$, $\mathcal{Q}_I^{-1}$ and $\mathcal{Q}_{II}^{-1}$. Within this work, we do not show that these preconditioners are isomorphism mapping Y^* onto Y. Instead, we check how well they preform through numerical experiments. Next, we will show that the preconditioners $\mathcal{P}_I^{-1}$ and $\mathcal{P}_{II}^{-1}$ are isomorphism mapping $X^* = \mathbf{V}^{2^*} \times Q^{2^*}$ onto $X = \mathbf{V}^2 \times Q^2$. In order to do this, we need some well-known results.

5.2.4 Preliminaries

All the theorems and lemmas in these preliminaries are collected from Evans [25], the exceptions being Lemma 2 which is collected from Arbogast et al. [44] and Lemma 3.

Theorem 5.1 (Lax–Milgram [25, Section 6.2, Theorem 1]). *Let H be a Hilbert space. Assume that*

$$a : H \times H \to \mathbb{R}$$

is a bilinear mapping, for which there exist constants $C_1, C_2 > 0$ such that

$$a(u, v) \leq C_1 \|u\| \|v\|_H \qquad \text{for all } u, v \in H \tag{5.27}$$

$$a(u, u) \geq C_2 \|u\|_H^2 \qquad \text{for all } u \in H \tag{5.28}$$

Finally, let $l : H \to \mathbb{R}$ be a bounded linear functional on H. Then there exists a unique element $u \in H$ such that

$$a(u, v) = l(v)$$

for all $v \in H$.

Theorem 5.2 (Poincarè's inequality [25, Section 5.8, Theorem 1]). *Let U be a bounded, open subset of $\mathbb{R}^n$ with C^1 boundary ∂U. Assume $1 \leq p \leq \infty$. Then for every $u \in H_0^p(U)$, there exists a constant C such that*

$$\|u\|_{L^p(U)} \leq C \|\nabla u\|_{L^p(U)}$$

for each $u \in H_0^p(\Omega)$.

Theorem 5.3 (Trace theorem [25, Section 5.5, Theorem 1]). *Let U be a bounded, open subset of $\mathbb{R}^n$ with C^1 boundary ∂U. The there exist a bounded linear operator*

$$T : H^p(U) \to L^p(\partial U)$$

such that

$$\|Tu\|_{L^p(\partial U)} \leq C \|u\|_{H^p(U)}$$

for each $u \in H^p(U)$, with the constant C depending only on p and U.

Lemma 1 (Hölder's inequality [25, Appendix B]). *Assume* $1 \leq p, q \leq \infty$, $\frac{1}{p} + \frac{1}{q} = 1$. *Then if* $u \in L^p(U)$, $v \in L^q(U)$, *we have*

$$\int_U |uv| \, \mathrm{d}x \leq \|u\|_{L^p(U)} \|v\|_{L^q(U)}$$

Lemma 2 ([44, Lemma 5.2]). *If* U *is a Lipschitz domain and* $u \in H^1(U)$, *then there exists a constant* C *such that*

$$\|u\|_{H^1(U)} \leq C(\|\nabla u\|_{L^2(U)} + \|u \cdot \tau\|_{L^2(\partial U)}) \tag{5.29}$$

Lemma 3. *Let* $a, b, c, d \geq 0$ *be reals. Then*

$$\sqrt{(a^2 + b^2)(c^2 + d^2)} \geq ac + bd \tag{5.30}$$

Proof: Squaring both sides of (5.30) shows it is equivalent to $\frac{bc}{ad} + \frac{ad}{bc} \geq 2$. Letting $x = \frac{bc}{ad}$, this is equivalent to $x + x^{-1} \geq 2$, which is obviously true.

5.2.5 Analysis of preconditioners

We are now ready to show that the operators $\mathcal{P}_I^{-1}$ and $\mathcal{P}_{II}^{-1}$ are isomorphism mapping $X^* = \mathbf{V}^{2^*} \times Q^{2^*}$ onto $X = \mathbf{V}^2 \times Q^2$. Note that similar proofs can be found in [6, 11, 44]. Recall the solution spaces,

$$\mathbf{V}^2(\Omega) = \{\mathbf{v} \in \mathbf{L}^2(\Omega) : \mathbf{v}_s \in \mathbf{H}^1(\Omega_s)\}$$
$$Q^2(\Omega) = \{q \in L_0^2(\Omega) : q_d \in H^1(\Omega_d)\}$$

with the corresponding norms,

$$\|\mathbf{u}\|^2_{\mathbf{V}^2(\Omega)} := \|\mathbf{u}\|^2_{L^2(\Omega)} + \|\nabla \mathbf{u}\|^2_{L^2(\Omega_s)}$$
$$\|p\|^2_{Q^2(\Omega)} := \|p\|^2_{L^2(\Omega)} + \|\nabla p\|^2_{L^2(\Omega_d)}$$

and the operators,

$$\mathcal{P}_I = \begin{bmatrix} -\Delta_s + I_d & 0 \\ 0 & I_s - \Delta_d \end{bmatrix} = \begin{bmatrix} A & 0 \\ 0 & B \end{bmatrix}$$

$$\mathcal{P}_{II} = \begin{bmatrix} -\Delta_s + I_d + O_\Gamma & 0 \\ 0 & I_s - \Delta_d \end{bmatrix} = \begin{bmatrix} A + O_\Gamma & 0 \\ 0 & B \end{bmatrix}$$

where the linear mappings are associated with the bilinear forms in the following manner,

$$A : \mathbf{V}^2 \to \mathbf{V}^{2^*}, \langle A\mathbf{u}, \mathbf{v}\rangle = a_s(\mathbf{u}, \mathbf{v}) + a_d(\mathbf{u}, \mathbf{v}) \quad \text{for all } \mathbf{u}, \mathbf{v} \in \mathbf{V}^2 \tag{5.31}$$

$$O_\Gamma : \mathbf{V}^2 \to \mathbf{V}^{2^*}, \langle O_\Gamma \mathbf{u}, \mathbf{v}\rangle = a_\Gamma(\mathbf{u}, \mathbf{v}) \quad \text{for all } \mathbf{u}, \mathbf{v} \in \mathbf{V}^2 \tag{5.32}$$

$$B : Q^2 \to Q^{2^*}, \langle Bp, q\rangle = b_s(p, q) + b_d(p, q) \quad \text{for all } p, q \in Q^2 \tag{5.33}$$

where,

$$a_s(\mathbf{u}, \mathbf{v}) + a_d(\mathbf{u}, \mathbf{v}) = \int_{\Omega_s} \nabla\mathbf{u} \cdot \nabla\mathbf{v} \, \mathrm{d}x + \int_{\Omega_d} \mathbf{u} \cdot \mathbf{v} \, \mathrm{d}x \tag{5.34}$$

$$a_\Gamma(\mathbf{u}, \mathbf{v}) = \int_\Gamma (\mathbf{u}_s \cdot \tau)(\mathbf{v}_s \cdot \tau) \, \mathrm{d}S \tag{5.35}$$

$$b_s(p, q) + b_d(p, q) = \int_{\Omega_s} pq \, \mathrm{d}x + \int_{\Omega_d} \nabla p \cdot \nabla q \, \mathrm{d}x \tag{5.36}$$

It follows that $\mathcal{P}_I$ and $\mathcal{P}_{II}$ are mappings from X onto X^*. We assume that $\mathbf{u} = 0$ on $\Gamma_{\partial\Omega_s}$ and that $\mathbf{u} \cdot \mathbf{n} = 0$ on $\Gamma_{\partial\Omega_d}$.

Proposition 1. *Assume $\Omega \subset \mathbb{R}^2$ is a bounded set with C^1-boundary. Then $\mathcal{P}_I$ is invertible, hence $\mathcal{P}_I^{-1}$ is an isomorphism mapping $X^* = \mathbf{V}^{2^*} \times Q^{2^*}$ onto $X = \mathbf{V}^2 \times Q^2$.*

Proof: First, it is shown that the conditions (5.27)–(5.28) of the Lax–Milgram Theorem 5.1 hold for (5.34) and (5.36). Assume $\mathbf{u}, \mathbf{v} \in \mathbf{V}^2$ and $p, q \in Q^2$,

$$\begin{aligned}
|a(\mathbf{u}, \mathbf{v})_s + a(\mathbf{u}, \mathbf{v})_d| &\le \int_{\Omega_s} |\nabla\mathbf{u} \cdot \nabla\mathbf{v}| \, \mathrm{d}x + \int_{\Omega_d} |\mathbf{u} \cdot \mathbf{v}| \, \mathrm{d}x \\
&\le \|\nabla\mathbf{u}\|_{L^2(\Omega_s)} \|\nabla\mathbf{v}\|_{L^2(\Omega_s)} + \|\mathbf{u}\|_{L^2(\Omega_d)} \|\mathbf{v}\|_{L^2(\Omega_d)} \\
&\le \|\nabla\mathbf{u}\|_{L^2(\Omega_s)} \|\nabla\mathbf{v}\|_{L^2(\Omega_s)} + \|\mathbf{u}\|_{L^2(\Omega)} \|\mathbf{v}\|_{L^2(\Omega)} \\
&\le C_1 \|\mathbf{u}\|_{\mathbf{V}^2(\Omega)} \|\mathbf{v}\|_{\mathbf{V}^2(\Omega)}
\end{aligned}$$

Where Hölder's inequality (Lemma 1) with $p = q = 2$, and that $\Omega_d \subset \Omega$ implies $\|\cdot\|_{L^2(\Omega_d)} \le \|\cdot\|_{L^2(\Omega)}$ is used. In the last inequality, Lemma 3 is used.

$$\begin{aligned}
|a(\mathbf{u}, \mathbf{u})_s + a(\mathbf{u}, \mathbf{u})_d| &= |\int_{\Omega_s} (\nabla\mathbf{u})^2 \, \mathrm{d}x + \int_{\Omega_d} \mathbf{u}^2 \, \mathrm{d}x| \\
&= \frac{1}{2}\|\nabla\mathbf{u}\|^2_{L^2(\Omega_s)} + \frac{1}{2}\|\nabla\mathbf{u}\|^2_{L^2(\Omega_s)} + \|\mathbf{u}\|^2_{L^2(\Omega_d)} \\
&\ge \frac{1}{2}\|\nabla\mathbf{u}\|^2_{L^2(\Omega_s)} + \frac{C}{2}\|\mathbf{u}\|^2_{L^2(\Omega_s)} + \|\mathbf{u}\|^2_{L^2(\Omega_d)} \\
&\ge C_2 \|\mathbf{u}\|^2_{\mathbf{V}^2(\Omega)}
\end{aligned}$$

Where Poincaré's inequality (Theorem 5.2) and that $\Omega_s \cup \Omega_d = \Omega$ implies $\|\cdot\|_{L^2(\Omega_s)} + \|\cdot\|_{L^2(\Omega_d)} = \|\cdot\|_{L^2(\Omega)}$ is used.

$$\begin{aligned}
|b(p,q)_\Omega| &\leq \int_{\Omega_d} |\nabla p \cdot \nabla q| \,\mathrm{d}x + \int_{\Omega_s} |pq| \,\mathrm{d}x \\
&\leq \|\nabla p\|_{L^2(\Omega_d)} \|\nabla q\|_{L^2(\Omega_d)} + \|p\|_{L^2(\Omega_s)} \|q\|_{L^2(\Omega_s)} \\
&\leq \|\nabla p\|_{L^2(\Omega_d)} \|\nabla q\|_{L^2(\Omega_d)} + \|p\|_{L^2(\Omega)} \|q\|_{L^2(\Omega)} \\
&\leq C_3 \|p\|_{Q^2(\Omega)} \|q\|_{Q^2(\Omega)}
\end{aligned}$$

Where Hölder's inequality (Lemma 1) with $p = q = 2$, and that $\Omega_s \subset \Omega$ implies $\|\cdot\|_{L^2(\Omega_s)} \leq \|\cdot\|_{L^2(\Omega)}$ is used. In the last inequality, Lemma 3 is used.

$$\begin{aligned}
|b(p,p)_\Omega| &= |\int_{\Omega_d} (\nabla p)^2 \,\mathrm{d}x + \int_{\Omega_s} p^2 \,\mathrm{d}x| \\
&= \frac{1}{2}\|\nabla p\|^2_{L^2(\Omega_d)} + \frac{1}{2}\|\nabla p\|^2_{L^2(\Omega_d)} + \|p\|^2_{L^2(\Omega_s)} \\
&\geq \frac{1}{2}\|\nabla p\|^2_{L^2(\Omega_d)} + \frac{C}{2}\|p\|^2_{L^2(\Omega_d)} + \|p\|^2_{L^2(\Omega_s)} \\
&\geq C_4 \|p\|^2_{Q^2(\Omega)}
\end{aligned}$$

Where Poincaré's inequality (Theorem 5.2) and $\Omega = \Omega_s \cup \Omega_d$ is used. The conditions of the Lax–Milgram Theorem 5.1 then hold for $a_s(\mathbf{u},\mathbf{v}) + a_d(\mathbf{u},\mathbf{v})$ and $b_s(p,q) + b_d(p,q)$, hence $A : \mathbf{V}^2 \to \mathbf{V}^{2^*}$ and $B : Q^2 \to Q^{2^*}$ are isomorphism. Consequently, $\mathcal{P}_I$ is an isomorphism mapping $X = \mathbf{V}^2 \times Q^2$ onto $X^* = \mathbf{V}^{2^*} \times Q^{2^*}$.

Note that if $Q_h \subset Q^2$ and $\mathbf{V}_h \subset \mathbf{V}^2$, it follows that the conditions of the Lax–Milgram Theorem 5.1 hold for $a_s(\mathbf{u}_h,\mathbf{v}_h) + a_d(\mathbf{u}_h,\mathbf{v}_h)$ and $b_s(p_h,q_h) + b_d(p_h,q_h)$ for $\mathbf{u}_h, \mathbf{v}_h \in \mathbf{V}_h$ and $p_h, q_h \in Q_h$. This gives that $\mathcal{P}^{-1}_{I,h}$ is an isomorphism mapping $\mathbf{V}^*_h \times Q^*_h$ onto $\mathbf{V}_h \times Q_h$.

Proposition 2. *Assume $\Omega \subset \mathbb{R}^2$ is a bounded set with C^1 boundary. Then $\mathcal{P}_{II}$ is invertible, hence $\mathcal{P}^{-1}_{II}$ is an isomorphism mapping $X^* = \mathbf{V}^{2^*} \times Q^{2^*}$ onto $X = \mathbf{V}^2 \times Q^2$.*

Proof:

$$
\begin{aligned}
|a(\mathbf{u},\mathbf{v})_\Gamma + a(\mathbf{u},\mathbf{v})_s + a(\mathbf{u},\mathbf{v})_d| &\leq \int_\Gamma |(\mathbf{u}_s\cdot\tau)(\mathbf{v}\cdot\tau)|\,\mathrm{d}S + \int_{\Omega_s} |\nabla\mathbf{u}\cdot\nabla\mathbf{v}|\,\mathrm{d}x \\
&\quad + \int_{\Omega_d} |\mathbf{u}\cdot\mathbf{v}|\,\mathrm{d}x \\
&\leq \|\mathbf{u}_s\|_{L^2(\Gamma)}\|\mathbf{v}\|_{L^2(\Gamma)} + \|\nabla\mathbf{u}\|_{L^2(\Omega_s)}\|\nabla\mathbf{v}\|_{L^2(\Omega_s)} \\
&\quad + \|\mathbf{u}\|_{L^2(\Omega_d)}\|\mathbf{v}\|_{L^2(\Omega_d)} \\
&\leq C_1\|\mathbf{u}_s\|_{H^1(\Omega_s)}\|\mathbf{v}\|_{H^1(\Omega)} + \|\nabla\mathbf{u}\|_{L^2(\Omega_s)}\|\nabla\mathbf{v}\|_{L^2(\Omega_s)} \\
&\quad + \|\mathbf{u}\|_{L^2(\Omega_d)}\|\mathbf{v}\|_{L^2(\Omega_d)} \\
&\leq C_2(\|\nabla\mathbf{u}\|_{L^2(\Omega_s)}\|\nabla\mathbf{v}\|_{L^2(\Omega_s)} + \|\mathbf{u}\|_{L^2(\Omega)}\|\mathbf{v}\|_{L^2(\Omega)}) \\
&\leq C_3\|\mathbf{u}\|_{V^2(\Omega)}\|\mathbf{v}\|_{V^2(\Omega)}
\end{aligned}
$$

Where Hölder's inequality (Lemma 1) with $p = q = 2$ and with $p = 1, q = \infty$, in addition to that $\|\tau\|_{L^\infty} = \sup_{x\in\Gamma}|\tau(x)| = 1$, and the Trace inequality (Theorem 5.3) is used. In the last inequality, Lemma 3 is used.

$$
\begin{aligned}
|a(\mathbf{u},\mathbf{u})_\Gamma + a(\mathbf{u},\mathbf{u})_s + a(\mathbf{u},\mathbf{u})_d| &= |\int_\Gamma (\mathbf{u}_s\cdot\tau)^2\,\mathrm{d}S + \int_{\Omega_s}(\nabla\mathbf{u})^2\,\mathrm{d}x + \int_{\Omega_d}\mathbf{u}^2\,\mathrm{d}x| \\
&\geq \|\mathbf{u}_s\cdot\tau\|^2_{L^2(\Gamma)} + \|\nabla\mathbf{u}\|^2_{L^2(\Omega_s)} + \|\mathbf{u}\|^2_{L^2(\Omega_d)} \\
&\geq \|\mathbf{u}_s\cdot\tau\|^2_{L^2(\Gamma)} + \frac{1}{2}\|\nabla\mathbf{u}\|^2_{L^2(\Omega_s)} + \frac{1}{2}\|\nabla\mathbf{u}\|^2_{L^2(\Omega_s)} \\
&\quad + \|\mathbf{u}\|^2_{L^2(\Omega_d)} \\
&\geq \frac{C_1}{2}\|\mathbf{u}\|^2_{L^2(\Omega_s)} + \frac{1}{2}\|\nabla\mathbf{u}\|^2_{L^2(\Omega_s)} + \|\mathbf{u}\|^2_{L^2(\Omega_d)} \\
&\geq C_2\|\mathbf{u}\|^2_{V^2(\Omega)}
\end{aligned}
$$

In the third inequality, Lemma 2 is used with $U = \Omega_s$. From Proposition 1 the conditions of the Lax–Milgram Theorem 5.1 hold for $b_s(p,q)$ and $b_d(p,q)$. This gives that $\mathcal{P}_{II}$ is invertible, hence $\mathcal{P}_{II}^{-1}$ is an isomorphism mapping X^* onto X.

Note that if $Q_h \subset Q^2$ and $\mathbf{V}_h \subset \mathbf{V}^2$, it follows that the conditions of the Lax–Milgram Theorem 5.1 hold for $a_s(\mathbf{u}_h,\mathbf{v}_h) + a_d(\mathbf{u}_h,\mathbf{v}_h)$ and $b_s(p_h,q_h) + b_d(p_h,q_h)$ for $\mathbf{u}_h,\mathbf{v}_h \in \mathbf{V}_h$ and $p_h,q_h \in Q_h$. This gives that $\mathcal{P}_{II,h}^{-1}$ is an isomorphism mapping $\mathbf{V}_h^* \times Q_h^*$ onto $\mathbf{V}_h \times Q_h$.

Chapter 6

Numerical experiments

The numerical experiments are executed using FEniCS [14], an automated software for solving partial differential equations using the finite element method. In the numerical results presented in this chapter, the condition numbers are calculated directly using Matlab [45] for $n = 8, 16, 32$, while for larger values of n the condition numbers are estimated using the SLEPcEigenSolver [14, Chapter 10]. The minimal residual method used is the PETSc implementation [14, Chapter 1], while the preconditioners are approximated using "*hypre_amg*". For the stop criteria we use $\frac{\|\mathbf{r}_k\|}{\|\mathbf{r}_0\|} <$ tolerance, were $\mathbf{r}_k = \mathbf{b} - A\mathbf{u}_k$ is the k'th residual. The tolerance is set to 10^{-7} and the initial guess is random.

The resolution of the mesh in the numerical experiments is defined through an integer n or a scalar h. For the sake of clarity, we will shortly state the relation between the two parameters for a square domain. The domain Ω is divided into $n \times n$ rectangles, and each rectangle is split in two by the diagonal from the bottom left corner to the top right corner. That is, the domain is split into $2n^2$ elements. The discretization parameter h is the diameter of an element, defined as two times the circumradius of an element.

6.1 The test problem

In this section, the test problem used for the numerical experiments in this chapter will be presented. The boundary conditions will correspond to pressure driven flow, which occur in many physical applications, cf. [46, 47, 48, 49, 50]. For simplicity, the domain is the square $(-1, 1) \times (-1, 1)$. The domain is split into a fluid region and a porous region, separated by the interface Γ located along the y-axis. At the interface Γ the coupling conditions (2.11)–(2.13) apply. We assume that the fluid walls are rigid and impermeable, and apply the noslip condition,

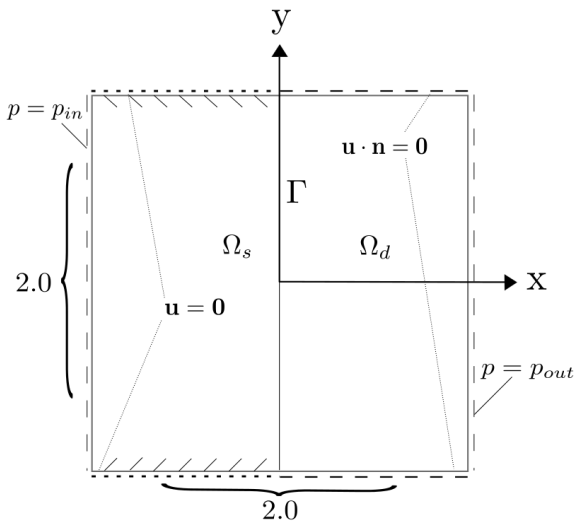

Figure 6.1: The figure shows the domain with boundary conditions corresponding to pressure driven flow. The domain is the square $(-1, 1) \times (-1, 1)$ and the interface Γ is located along the y-axis.

$$\mathbf{u} = \mathbf{0} \tag{6.1}$$

at the walls exterior to the fluid part of the domain. At the porous walls a no-penetration condition is enforced,

$$\mathbf{u} \cdot \mathbf{n} = \mathbf{0} \tag{6.2}$$

At the inlet and outlet Dirichlet conditions are set for the pressure,

$$p = p_{in} \tag{6.3}$$
$$p = p_{out} \tag{6.4}$$

The domain and the corresponding boundary conditions can be seen in Figure 6.1. The physical parameters suggested are a representative selection of viscosities and permeabilities from different physical applications of the coupled Darcy–Stokes model. The viscosity is set to $\mu = 10^{-3} \frac{m^2}{s}$ or $\mu = 10^{-6} \frac{m^2}{s}$, which can model fluids such as blood [51] or groundwater [52]. The permeability values are $K = 10^{-12} m^2$ or $K = 10^{-6} m^2$, which can represent different rocks types or sand [53, 54, 55]. The Beavers–Joseph–Saffmann coefficient is set to $\alpha = 1.0$.

6.1.1 Imposing boundary conditions, L^2-formulation

The boundary conditions from the test problem in Section 6.1 have to be imposed in the L^2-formulation (4.11), presented in Section 4.1. The noslip condition (6.1) for the velocity at the fluid wall is enforced in the function space $\mathbf{V}^2$, while the Dirichlet condition at the outlet for the pressure (6.4) is enforced in the function space Q^2. The no-penetration condition (6.2) at the porous wall and the Dirichlet condition at the inlet (6.3) are enforced through the linear forms $l_1(\mathbf{v})$ and $l_2(q)$ in the following manner,

$$l_1(\mathbf{v}) = -\langle p_{in}, \mathbf{v} \cdot \mathbf{n}_s \rangle_{\Gamma_{\partial\Omega_{in}}} + \langle \mathbf{f}, \mathbf{v} \rangle_{\Omega} \tag{6.5}$$

$$l_2(q) = 0 \tag{6.6}$$

6.1.2 Imposing boundary conditions, $H(\mathrm{div})$-formulation

The boundary conditions must also be imposed in the $H(\mathrm{div})$-formulation (4.25), presented in Section 4.2. At the fluid wall the noslip condition (6.1) applies. As the lower order BDM and RT element's degrees of freedom at the edges consist solely of normal components, the tangential part of (6.1) must be imposed weakly through Nitsche's method. For simplicity, we will impose both the normal and the tangential part of (6.1) using Nitsche's method. In Nitsche's method, the noslip condition is enforced by adding a penalty term. To remedy that the form is not symmetric, a symmetrization term is added. The procedure is explained in detail in Section 3.3.1, and results in adding the term $\xi(\mathbf{u}_h, \mathbf{v})$ to the weak form (4.25).

$$\begin{aligned} \xi(\mathbf{u}_h, \mathbf{v}) = \mu \frac{\beta_n}{h} & \int_{\Gamma_{\partial\Omega_{s,wall}}} [\![\mathbf{u}_h]\!][\![\mathbf{v}]\!] \, \mathrm{d}S \\ - \mu & \int_{\Gamma_{\partial\Omega_{s,wall}}} \{\nabla \mathbf{u}_h\}[\![\mathbf{v}]\!] \cdot \mathbf{n}_s \, \mathrm{d}S \\ - \mu & \int_{\Gamma_{\partial\Omega_{s,wall,h}}} \{\nabla \mathbf{v}\}[\![\mathbf{u}_h]\!] \cdot \mathbf{n}_s \, \mathrm{d}S \end{aligned} \tag{6.7}$$

Here $\Gamma_{\partial\Omega_{s,wall,h}}$ denotes the wall in the Stokes region, and $\mathbf{n}_s$ denotes the unit normal exterior to $\partial\Omega_s$. The no-penetration condition (6.2) at the porous wall and the Dirichlet conditions at the inlet (6.3) and the outlet (6.4) are imposed through the linear form $l(\mathbf{v})$ in the following manner,

$$l(\mathbf{v}) = -\langle p_{in}, \mathbf{v} \cdot \mathbf{n}_s \rangle_{\Gamma_{\partial\Omega_{in}}} - \langle p_{out}, \mathbf{v} \cdot \mathbf{n}_d \rangle_{\Gamma_{\partial\Omega_{out}}} + \langle \mathbf{f}, \mathbf{v} \rangle_{\Omega} \tag{6.8}$$

6.1.3 Penalty parameters

The IP method is used to discretize the second-order terms acting on the Stokes velocities in the $H(\text{div})$-formulation in Section 4.2.1 and the preconditioner $\mathcal{B}_{s,h}$ in Section 5.2.1. The penalty terms arising from the IP method has a parameter β_s that has to be determined. Similarly, the IP method is used to discretize the second-order operator acting on the pressure in the Darcy preconditioner $\mathcal{B}_{d,I,h}$ in Section 5.2.2, giving rise to a penalty parameter β_d. In this section, we will find optimal values for the parameters β_s and β_d through numerical experiments.

The penalty parameter β_s must be chosen large enough to ensure stability. However, a large β_s will have a negative impact on the condition number, in the sense that the condition number will increase as β_s increases [9]. The behaviour is illustrated in Figure 6.2. Consequently, finding a lower bound for β_s is of interest. To obtain the lower bound numerically, the velocity-error is calculated for a range of β_s's. In order to measure the error the method of manufactured solutions, which is explained in detail in Section 6.2, is used. The results are displayed in Figure 6.2. We observe a large velocity error oscillating rapidly for $\beta_s \leq 1.6$. The error stabilizes at approximately $6.0 \cdot 10^{-3}$ for $\beta_s \geq 1.6$.

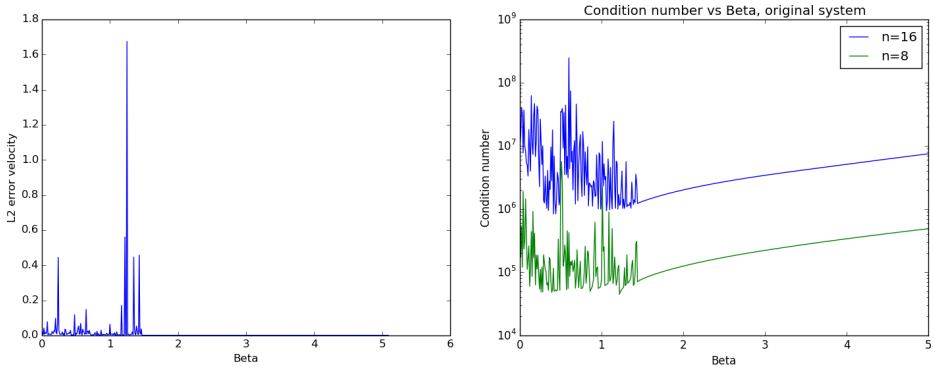

(a) Velocity error, n=80

(b) $\kappa(\mathcal{A}_{s,h})$

Figure 6.2: Plot (a) and plot (b) display respectively the L^2-error for the velocity and the condition number κ of the stabilized Stokes system $\mathcal{A}_{s,h}$ with $\mu = 1.0$ for different penalty parameters β_s. Discretized with $BDM_1 \times DG_0$ elements.

To explore what effect the value of β_s has on the condition number of the preconditioned Stokes system $\mathcal{B}_{s,h}^{-1}\mathcal{A}_{s,h}$, the condition number is calculated

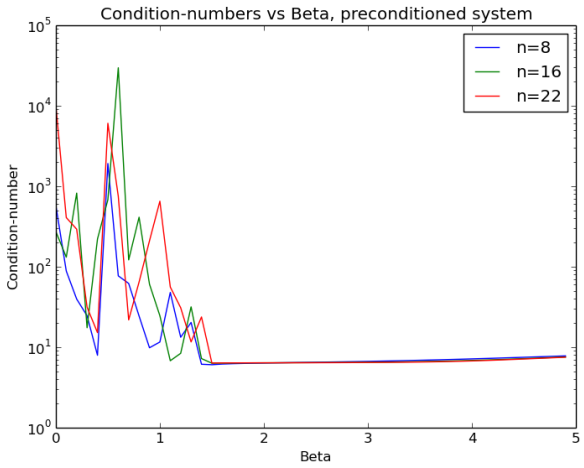

Figure 6.3: Condition number of the preconditioned Stokes system $\mathcal{B}_{s,h}^{-1}\mathcal{A}_{s,h}$ for different penalty parameters β_s.

for different penalty parameters β_s. The results can be seen in Figure 6.3. It seems as if the condition number stabilizes for $\beta_s \geq 1.6$, in contrast to $\kappa(\mathcal{A}_{s,h})$, which increases as β_s increases for $\beta_s \geq 1.6$, cf. Table 6.2.

We are also interested in what effect the value of the penalty parameter β_d has on the condition number of the preconditioned Darcy system $\mathcal{B}_{d,I,h}^{-1}\mathcal{A}_{d,h}$. To this end, the condition number is calculated for different penalty parameters β_d. The results are displayed in Figure 6.4. The condition number is bounded independently of h for approximately $\beta_d \leq 3.8$, but as the condition number grows larger as β_d tends to zero, the value of β_d should not be "too small". The figure only displays the condition numbers for $n = 4, 8, 16$. However, it is reason to believe that when n increases, the condition number will not be bounded independently of an arbitrary mesh parameter h, unless β_d is set to a "small value". Winther et al. [43] set the penalty parameter $\beta_d = 1.0$, with no further discussion.

In the subsequent numerical experiments, we will set $\beta_s = 2.0$ and $\beta_d = 1.0$. For simplicity, the penalty parameter β_n arising from imposing the noslip condition in the $H(\text{div})$-formulation using Nitsche's method, is set to the same value as β_s, i.e. $\beta_n = \beta_s$.

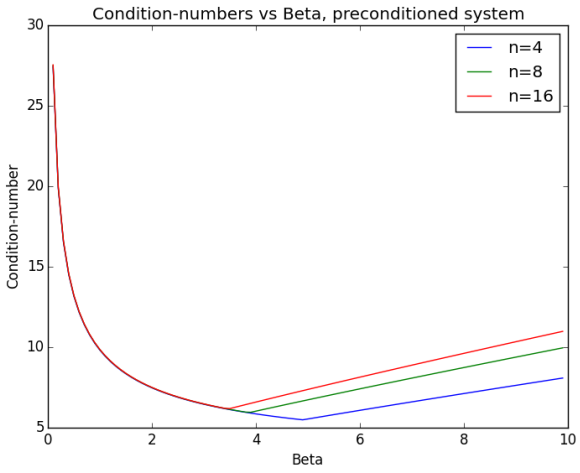

Figure 6.4: Condition number of the preconditioned Darcy system $\mathcal{B}_{d,I,h}^{-1}\mathcal{A}_{d,h}$ for different penalty parameters β_d. The model parameter are set to $\mu = 1.0$ and $K = 1.0$.

6.2 The method of manufactured solutions

The method of manufactured solutions provides an opportunity to check that the code correctly solves its governing mathematical equations, and has been described in several papers, cf. [56, 57, 58, 59]. The basic idea behind the method is to manufacture a solution by fitting the boundary conditions and the source terms according to a chosen solution. The solver is then expected to reproduce the chosen solution as the discretization parameter h tends to zero. Consequently, a measure of the error can be obtained. As the original problem has divergence free velocities, the chosen solution should share this feature. The manufactured solution, which from now on will be referred to as the exact solution, chosen for verification is

$$\begin{aligned} \mathbf{u}_e &= (\sin(\pi y), \cos(\pi x)) \\ p_e &= e^y \sin(\pi x) \end{aligned}$$

The next step is to adjust the source terms to the exact solutions. The term $\mathbf{f}_f$ represents the source term in the momentum equation in the fluid region, while $\mathbf{f}_p$ represents the source term in Darcy's law in the porous region. As the exact velocities are divergence free, the source terms in the continuity equations are zero. The exact solution obviously fulfils interface condition (2.11), but not necessarily the interface conditions (2.12) and (2.13). Therefore, a source term h_1 is added to (2.12), and a source term h_2 is added (2.13). The source terms are calculated by insertion of the exact solutions $\mathbf{u}_e$ and p_e in (2.9), (2.10), (2.12) and (2.13).

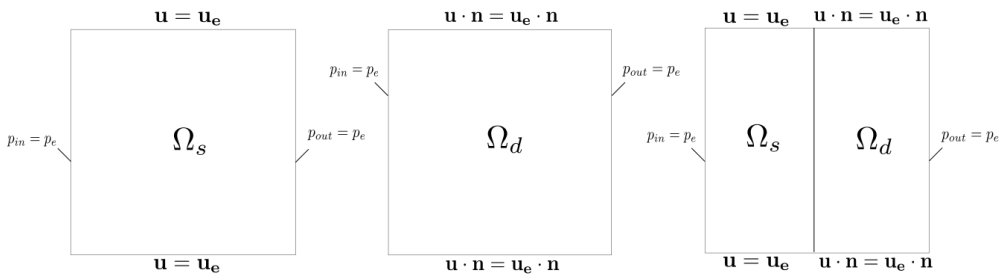

Figure 6.5: Test domains with boundary conditions. From the left, the test domains for pure Stokes flow, pure Darcy flow and for coupled Darcy–Stokes flow are depicted.

$$\mathbf{f}_f = -\mu\Delta\mathbf{u}_e + \nabla p_e = (\mu\pi^2 \sin(\pi y) + \pi\cos(\pi x)e^y, \mu\pi^2\cos(\pi x)) + \sin(\pi x)e^y)$$
$$\mathbf{f}_p = \mu\mathbf{K}^{-1}\mathbf{u}_e + \nabla p_e = (\mu K^{-1}\sin(\pi y) + \pi\cos(\pi x)e^y, \mu K^{-1}\cos(\pi x)) + \sin(\pi x)e^y)$$
$$h_1 = \mu\mathbf{n}_s\Delta\mathbf{u}_e \cdot \mathbf{n}_s - p_e + p_e = 0$$
$$h_2 = -\mathbf{n}_s\Delta\mathbf{u}_s \cdot \tau - \alpha K^{\frac{1}{2}}\mathbf{u}_s \cdot \tau = -\alpha K^{-\frac{1}{2}}\cos(\pi x)$$

The boundary conditions are set to be $p = p_e$ at the inlet, $p = p_e$ at the outlet, $\mathbf{u} = \mathbf{u}_e$ at the fluid wall and $\mathbf{u} \cdot \mathbf{n} = \mathbf{u}_e \cdot \mathbf{n}$ at the porous wall. The test is being performed at the square $(-1, 1) \times (-1, 1)$ and the interface Γ is located at the y-axis with the fluid domain Ω_s on the left, and the porous domain Ω_d on the right. We will calculate the errors when the domain is restricted to a pure Stokes domain, a pure Darcy domain and a coupled Darcy–Stokes domain. In addition to running the tests with unity parameters, we will use some of the more physical model parameters presented in Section 6.1. The test domains and the corresponding boundary conditions can be seen in Figure 6.5.

6.3 Convergence rates

The method of manufactured solutions is used to obtain the errors in the numerical approximations of the solutions. The error is measured in some norm, i.e. $e = \|\mathbf{u}_h - \mathbf{u}_e\|$ or $e = \|p_h - p_e\|$. Here, $\mathbf{u}_h$ and p_h are the numerical approximations of the solutions to the discretized Darcy–Stokes equations, while $\mathbf{u}_e$ and p_e are the exact solutions. The convergence rates are calculated to see if the error obtained by the method of manufactured solutions is of the same order as expected from the *a priori* estimates. The solver is run

with decreasing discretization parameters h and the error is measured. The convergence rates are calculated by

$$
\begin{aligned}
r(p_{L^2}) &= \frac{\ln(e^{i+1}) - \ln(e^i)}{\ln(h^{i+1}) - \ln(h^i)} \ , \ e = \|p_h - p_e\|_{L^2} \\
r(p_{H^1}) &= \frac{\ln(e^{i+1}) - \ln(e^i)}{\ln(h^{i+1}) - \ln(h^i)} \ , \ e = \|p_h - p_e\|_{H^1} \\
r(\mathbf{u}_{L^2}) &= \frac{\ln(e^{i+1}) - \ln(e^i)}{\ln(h^{i+1}) - \ln(h^i)} \ , \ e = \|\mathbf{u}_h - \mathbf{u}_e\|_{L^2} \\
r(\mathbf{u}_{H^1}) &= \frac{\ln(e^{i+1}) - \ln(e^i)}{\ln(h^{i+1}) - \ln(h^i)} \ , \ e = \|\mathbf{u}_h - \mathbf{u}_e\|_{H^1} \\
r(\mathbf{u}_{H(\mathrm{div})}) &= \frac{\ln(e^{i+1}) - \ln(e^i)}{\ln(h^{i+1}) - \ln(h^i)} \ , \ e = \|\mathbf{u}_h - \mathbf{u}_e\|_{H(\mathrm{div})}
\end{aligned}
$$

where i is the refinement step and h is the element diameter of the uniform mesh.

6.3.1 L^2-formulation

In this section the errors and the convergence rates for the Stokes, the Darcy and the coupled Darcy–Stokes equations discretized with the L^2-formulation are presented. The errors are measured in the norms corresponding to the *a priori* error estimates 4.2 and 4.3.

Stokes equations, Taylor–Hood elements

Table 6.2 and Table 6.1 display the error in pressure and velocity for pure Stokes flow, with unity and physical parameters, respectively. In both cases the velocity errors and the pressure errors decrease as the mesh in refined. In addition to the errors, the tables display the convergence rates. Using unity parameters yields the convergence rates we expected from *a priori* estimate 4.2, that is, an L^2-rate of third order for the velocity, an H^1-rate of second order for the velocity and an L^2-rate of second order for the pressure. When using physical parameter values for pure Stokes flow, tendencies to super convergence is observed for the velocity, that is, the H^1-rate and the L^2-rate of the velocity converges with about half an order higher than expected, cf. Table 6.2.

Darcy equations, Taylor–Hood elements

Table 6.3 and 6.4 display the errors in pressure and velocity for pure Darcy flow, with unity and physical parameters, respectively. In both cases the

n	$\|\mathbf{u}_h - \mathbf{u}_e\|_{L^2}$	$\|\mathbf{u}_h - \mathbf{u}_e\|_{H^1}$	$\|p_h - p_e\|_{L^2}$	Convergence rates		
				r($\mathbf{u}_{L^2}$)	r($\mathbf{u}_{H^1}$)	r(p_{L^2})
8	5.5e-03	2.3e-01	5.3e-02			
16	6.0e-04	3.5e-02	1.2e-02	2.99	1.99	2.06
32	8.7e-05	9.0e-03	3.1e-03	2.99	1.99	2.01
64	1.0e-05	2.2e-03	7.0e-04	2.99	1.99	2.00
128	1.3e-06	5.0e-04	1.0e-04	2.99	1.99	2.00
256	1.6e-07	1.0e-04	4.9e-05	2.99	1.99	2.00

Table 6.1: Convergence rates and errors for the velocity $\mathbf{u}$ and the pressure p for Stokes flow with $\mu = 1.0$. Discretized with Taylor–Hood elements.

velocity errors and the pressure errors decrease as the mesh in refined. The tables also present the convergence rates. For pure Darcy flow with both unity and physical parameter values, the L^2-error in the velocity convergences a bit more rapidly than expected. From the *a priori* estimate 4.3, we expected an L^2-rate of at least first order for the velocity, and the numerical results indicate that the scheme converges at an L^2-rate of an order of one and a half. Using both unity and physical model parameters, the H^1-pressure rate is of first order, just as expected from the *a priori* estimate 4.3. We also observe that the L^2-pressure rate is of second order, both using unity and physical model parameters.

Coupled Darcy–Stokes equations, Taylor–Hood elements

Table 6.5 and 6.6 display the errors in the pressure and the velocity for coupled Darcy–Stokes flow, with unity and physical model parameters, respectively. In both cases the velocity errors and the pressure errors decrease as the mesh in refined. In the *a priori* estimate 4.1, we have assumed that the expected rate for the L^2-velocity error is of second order and that the L^2-pressure rate is of first order. Note that these assumptions are solely based on the *a priori* estimate for the Mini element presented in [6], and have not been proved. However, we observe an L^2-rate for the velocity of one and a half order and an L^2-pressure rate of second order when using both unity and physical model parameters, cf. Table 6.5 and 6.6.

n	$\|\mathbf{u}_h - \mathbf{u}_e\|_{L^2}$	$\|\mathbf{u}_h - \mathbf{u}_e\|_{H^1}$	$\|p_h - p_e\|_{L^2}$	Convergence rates		
				r($\mathbf{u}_{L^2}$)	r($\mathbf{u}_{H^1}$)	r(p_{L^2})
8	7.1e-01	17.8	5.5e-02			
16	4.5e-02	2.52	1.2e-02	3.96	2.81	2.05
32	3.0e-03	3.5e-01	3.1e-03	3.88	2.82	2.01
64	2.0e-04	5.1e-02	7.0e-04	3.80	2.77	2.00
128	1.6e-05	7.9e-03	1.0e-04	3.72	2.70	2.00
256	1.3e-06	1.1e-03	4.9e-05	3.64	2.62	2.00

Table 6.2: Convergence rates and errors for the velocity $\mathbf{u}$ and the pressure p for Stokes flow with $\mu = 10^{-3}$. Discretized with Taylor–Hood elements.

n	$\|\mathbf{u}_h - \mathbf{u}_e\|_{L^2}$	$\|p_h - p\|_{H^1}$	$\|p_h - p_e\|_{L^2}$	Convergence rates		
				r($\mathbf{u}_{L^2}$)	r(p_{H^1})	r(p_{L^2})
4	7.7e-01	5.3e-01	6.1e-02			
8	2.5e-01	2.6e-01	1.3e-02	1.59	0.99	2.20
16	8.4e-02	1.3e-01	3.2e-03	1.59	1.00	2.05
32	2.8e-02	6.8e-01	7.9e-04	1.56	1.00	2.01
64	9.8e-03	3.3e-02	1.9e-04	1.53	1.00	2.00
128	3.4e-03	8.7e-03	4.9e-05	1.52	1.00	2.00

Table 6.3: Convergence rates and errors for the velocity $\mathbf{u}$ and the pressure p for Darcy flow with $\mu = K = 1.0$. Discretized with Taylor–Hood elements.

n	$\|\mathbf{u}_h - \mathbf{u}_e\|_{L^2}$	$\|p_h - p_e\|_{H^1}$	$\|p_h - p_e\|_{L^2}$	Convergence rates		
				r($\mathbf{u}_{L^2}$)	r(p_{H^1})	r(p_{L^2})
8	4.7e-03	5.4e-01	6.2e-02			
16	6.9e-04	2.7e-01	1.3e-02	2.77	1.01	2.21
32	1.1e-04	1.3e-01	3.2e-03	2.54	1.00	2.05
64	3.0e-05	6.7e-02	7.9e-04	1.97	1.00	2.01
128	9.9e-06	3.3e-02	1.9e-04	1.62	1.00	2.00
256	3.2e-06	7.7e-03	4.9e-05	1.53	1.00	2.00

Table 6.4: Convergence rates and errors for the velocity $\mathbf{u}$ and the pressure p for Darcy flow with $\mu = 10^{-3}, K = 10^{-6}$. Discretized with Taylor–Hood elements.

n	$\|\mathbf{u}_h - \mathbf{u}_e\|_{L^2}$	$\|p_h - p_e\|_{L^2}$	Convergence rates	
			r($\mathbf{u}_{L^2}$)	r(p_{L^2})
8	5.4e-01	6.2e-02		
16	1.8e-01	1.3e-02	1.56	2.22
32	1.6e-01	3.2e-03	1.60	2.07
64	6.1e-02	7.9e-04	1.57	2.02
128	9.6e-01	1.9e-04	1.54	2.00
256	2.0e-02	4.9e-05	1.52	2.00

Table 6.5: Convergence rates and errors for the velocity $\mathbf{u}$ and the pressure p for coupled Darcy–Stokes flow with $\mu = K = 1.0$. Discretized with Taylor–Hood elements.

n	$\|\mathbf{u}_h - \mathbf{u}_e\|_{L^2}$	$\|p_h - p_e\|_{L^2}$	Convergence rates	
			r($\mathbf{u}_{L^2}$)	r(p_{L^2})
8	5.1e-01	6.0e-02		
16	1.8e-01	1.3e-02	1.56	2.52
32	6.1e-02	3.1e-03	1.60	2.20
64	2.0e-02	7.8e-04	1.57	2.04
128	6.9e-03	1.9e-04	1.54	2.01
256	2.4e-03	3.4e-05	1.52	2.00

Table 6.6: Convergence rates and errors for the velocity $\mathbf{u}$ and the pressure p for coupled Darcy–Stokes flow with $\mu = 10^{-3}, K = 10^{-6}$. Discretized with Taylor–Hood elements.

6.3.2 $H(\text{div})$-formulation

In this section the errors and the convergence rates for the Stokes, the Darcy and the coupled Darcy–Stokes equations discretized with the $H(\text{div})$-formulation are presented. The errors are measured in the norms corresponding to the *a priori* error estimates 4.4 and 4.5.

Stokes equations, $BDM_1 \times DG_0$ elements

Table 6.8 and Table 6.7 display the error in pressure and velocity for pure Stokes flow, with unity and physical parameters, respectively. In both cases the velocity errors and the pressure errors decrease as the mesh in refined. In addition, the tables display the convergence rates. Using both unity and physical model parameters yields the convergence rates we expected from *a priori* estimate 4.4, that is, fist order convergence for both the H^1-error in velocity and the L^2-error in the pressure. In addition, we observe an L^2-rate of second order for the velocity.

Darcy equations, $BDM_1 \times DG_0$ elements

Table 6.9 and 6.10 display the errors in pressure and velocity for pure Darcy flow, when using unity and physical parameters, respectively. The velocity error and the pressure error decrease as the mesh is refined, in both cases. In addition to the errors, the convergence rates are presented in the tables. For pure Darcy flow with unity parameter values, the L^2-error in the pressure has first order convergence, just as expected from the *a priori* estimate 4.5. Using physical parameter values, we observe that the L^2-rate for the pressure converges at a rate just above first order. The $H(\text{div})$-error for the velocity has an rate of second order, and we expected a rate of at least first

order. The L^2-rate for the velocity is observed to be of second order.

Coupled Darcy–Stokes equations, $BDM_1 \times DG_0$ elements

Table 6.11 and 6.12 display the errors in pressure and velocity for coupled Darcy–Stokes flow, for unity and physical parameters, respectively. The velocity error and the pressure error decrease as the mesh is refined, in both cases. In addition to the errors, the convergence rates are presented in the tables. We have not presented an *a priori* error estimate for the coupled Darcy–Stokes problem discretized with BDM elements. However, we observe that using both unity and physical model parameters yields an L^2-rate and a $H(\text{div})$-rate for the velocity of second order. The pressure L^2-rate is observed to be of first order.

Coupled Darcy–Stokes equations, $RT_0 \times DG_0$ elements

Table 6.13 displays the velocity error and the pressure error when the Darcy–Stokes equations are discretized with the lowest order Raviart–Thomas elements RT_0 for the velocity and DG_0 elements for the pressure. Within this work we have not presented an *a priori* error estimate for the Darcy–Stokes equations discretized with these elements. However, we observe that the errors does not decrease when the mesh is refined, but is approximately 0.9 for the velocity and 5.8 for the pressure for all mesh parameters h.

Coupled Darcy–Stokes equations, $RT_1 \times DG_1$ elements

Table 6.14 displays the velocity error and the pressure error when the Darcy–Stokes equations are discretized with the Raviart–Thomas elements RT_1 for the velocity and DG_1 elements for the pressure. The errors in both velocity and pressure decrease as the mesh is refined. Within this work we have not presented an *a priori* error estimate for the Darcy–Stokes equations discretized with these elements. However, we observe that the L^2-rate and the $H(\text{div})$-rate of the velocity error is of second order, while the L^2-rate of the pressure is of first order.

n	$\|\mathbf{u}_h - \mathbf{u}_e\|_{L^2}$	$\|\mathbf{u}_h - \mathbf{u}_e\|_{H^1}$	$\|p_h - p_e\|_{L^2}$	Convergence rates		
				r($\mathbf{u}_{L^2}$)	r($\mathbf{u}_{H^1}$)	r(p_{L^2})
8	8.4e-02	1.5	5.4e-01			
16	2.3e-02	7.3e-01	2.7e-01	1.86	1.05	0.98
32	5.9e-03	3.5e-01	1.3e-01	1.95	1.02	0.99
64	1.5e-03	1.8e-01	6.8e-02	1.98	1.00	0.99
128	3.0e-04	8.9e-01	3.4e-02	1.99	1.00	0.99
256	9.4e-05	5.4e-02	1.7e-02	1.99	1.00	0.99

Table 6.7: Convergence rates and errors for the velocity $\mathbf{u}$ and the pressure p for Stokes flow with $\mu = 1.0$ and $\beta_s = 2.0$. Discretized with $BDM_1 \times DG_0$ elements.

n	$\|\mathbf{u}_h - \mathbf{u}_e\|_{L^2}$	$\|\mathbf{u}_h - \mathbf{u}_e\|_{H^1}$	$\|p_h - p_e\|_{L^2}$	Convergence rates		
				r($\mathbf{u}_{L^2}$)	r($\mathbf{u}_{H^1}$)	r(p_{L^2})
8	8.4e-02	1.5	3.9e-01			
16	2.3e-02	7.3e-01	1.8e-01	1.86	1.05	0.99
32	5.9e-03	3.5e-01	9.2e-02	1.95	1.02	0.99
64	1.5e-03	1.7e-01	4.6e-02	1.98	1.00	0.99
128	3.0e-04	8.6e-02	2.3e-02	1.99	1.00	0.99
256	9.4e-05	1.4e-02	1.1e-02	1.99	1.00	0.99

Table 6.8: Convergence rates and errors for the velocity $\mathbf{u}$ and the pressure p for Stokes flow with $\mu = 10^{-3}$ and $\beta_s = 2.0$. Discretized with $BDM_1 \times DG_0$ elements.

n	$\|\mathbf{u}_h - \mathbf{u}_e\|_{L^2}$	$\|\mathbf{u}_h - \mathbf{u}_e\|_{H(\mathrm{div})}$	$\|p_h - p_e\|_{L^2}$	Convergence rates		
				r($\mathbf{u}_{L^2}$)	r($\mathbf{u}_{H(\mathrm{div})}$)	r(p_{L^2})
8	4.6e-02	4.6e-02	3.6e-01			
16	1.1e-02	1.1e-02	1.8e-01	1.98	1.98	0.99
32	2.9e-03	2.9e-03	9.2e-02	1.99	1.99	0.99
64	7.0e-04	7.0e-04	4.6e-02	1.99	1.99	0.99
128	1.0e-04	1.0e-04	2.3e-02	1.99	1.99	0.99
256	4.6e-05	4.6e-05	1.1e-02	1.99	1.99	0.99

Table 6.9: Convergence rates and errors for the velocity $\mathbf{u}$ and the pressure p for Darcy flow with $\mu = K = 1.0$. Discretized with $BDM_1 \times DG_0$ elements.

n	$\|\mathbf{u}_h - \mathbf{u}_e\|_{L^2}$	$\|\mathbf{u}_h - \mathbf{u}_e\|_{H(\mathrm{div})}$	$\|p_h - p_e\|_{L^2}$	Convergence rates		
				$\mathrm{r}(\mathbf{u}_{L^2})$	$\mathrm{r}(\mathbf{u}_{H(\mathrm{div})})$	$\mathrm{r}(p_{L^2})$
8	4.6e-02	4.6e-02	3.2603			
16	1.1e-02	1.1e-02	8.3e-01	1.98	1.98	1.95
32	2.9e-03	2.9e-03	2.2e-01	1.99	1.99	1.89
64	7.0e-04	7.0e-04	6.9e-02	1.99	1.99	1.70
128	1.0e-04	1.0e-04	2.6e-02	1.99	1.99	1.38
256	4.6e-05	4.6e-05	1.1e-02	1.99	1.99	1.14

Table 6.10: Convergence rates and errors for the velocity $\mathbf{u}$ and the pressure p for Darcy flow with $\mu = 10^{-3}$, $K = 10^{-6}$. Discretized with $BDM_1 \times DG_0$ elements.

n	$\|\mathbf{u}_h - \mathbf{u}_e\|_{L^2}$	$\|\mathbf{u}_h - \mathbf{u}_e\|_{H(\mathrm{div})}$	$\|p_h - p_e\|_{L^2}$	Convergence rates		
				$\mathrm{r}(\mathbf{u}_{L^2})$	$\mathrm{r}(\mathbf{u}_{H(\mathrm{div})})$	$\mathrm{r}(p_{L^2})$
8	7.4e-02	9.0e-02	4.4e-01			
16	2.0e-02	2.2e-02	2.2e-01	1.84	2.00	0.96
32	5.4e-03	5.6e-03	1.1e-01	1.94	1.98	0.97
64	1.3e-03	1.4e-03	5.8e-02	1.97	1.99	0.98
128	3.0e-04	3.0e-04	2.9e-02	1.99	1.99	0.99
256	8.6e-05	8.9e-05	1.4e-02	1.99	1.99	0.99

Table 6.11: Convergence rates and errors for the velocity $\mathbf{u}$ and the pressure p for coupled Darcy–Stokes flow with $\mu = K = 1.0$ and $\beta_s = 2.0$. Discretized with $BDM_1 \times DG_0$ elements.

n	$\|\mathbf{u}_h - \mathbf{u}_e\|_{L^2}$	$\|\mathbf{u}_h - \mathbf{u}_e\|_{H(\mathrm{div})}$	$\|p_h - p_e\|_{L^2}$	Convergence rates		
				$\mathrm{r}(\mathbf{u}_{L^2})$	$\mathrm{r}(\mathbf{u}_{H(\mathrm{div})})$	$\mathrm{r}(p_{L^2})$
8	6.6e-02	1.0e-01	7.3e-01			
16	1.6e-03	2.6e-02	2.4e-01	2.01	2.01	1.57
32	4.1e-03	6.6e-03	1.0e-01	2.00	1.99	1.28
64	1.0e-03	1.6e-03	4.7e-02	1.99	1.99	1.09
128	2.0e-04	4.0e-04	2.3e-02	1.99	1.99	1.02
256	6.4e-05	1.0e-04	1.1e-02	1.99	1.99	1.00

Table 6.12: Convergence rates and errors for the velocity $\mathbf{u}$ and the pressure p for coupled Darcy–Stokes flow with $\mu = 10^{-3}, K = 10^{-6}$ and $\beta_s = 2.0$. Discretized with $BDM_1 \times DG_0$ elements.

n	$\|\mathbf{u}_h - \mathbf{u}_e\|_{L^2}$	$\|\mathbf{u}_h - \mathbf{u}_e\|_{H(\mathrm{div})}$	$\|p_h - p_e\|_{L^2}$	Convergence rates		
				r($\mathbf{u}_{L^2}$)	r($\mathbf{u}_{H(\mathrm{div})}$)	r(p_{L^2})
8	0.93	0.87	5.04			
16	0.90	0.89	5.39	0.03	-0.00	-0.09
32	0.91	0.90	5.64	-0.00	-0.02	-0.06
64	0.92	0.91	5.80	-0.01	-0.01	-0.04
128	0.92	0.92	5.89	-0.00	-0.00	-0.23
256	0.92	0.92	5.95	-0.00	-0.00	-0.01

Table 6.13: Convergence rates and errors for the velocity $\mathbf{u}$ and the pressure p for coupled Darcy–Stokes flow with $\mu = K = 1.0$, $\beta_s = 2.0$. Discretized with $RT_0 \times DG_0$.

n	$\|\mathbf{u}_h - \mathbf{u}_e\|_{L^2}$	$\|\mathbf{u}_h - \mathbf{u}_e\|_{H(\mathrm{div})}$	$\|p_h - p_e\|_{L^2}$	Convergence rates		
				r($\mathbf{u}_{L^2}$)	r($\mathbf{u}_{H(\mathrm{div})}$)	r(p_{L^2})
8	7.7e-02	7.6e-02	0.45			
16	2.1e-02	2.1e-02	0.25	1.86	1.86	0.82
32	5.4e-03	5.4e-03	0.13	1.95	1.95	0.92
64	1.3e-03	1.3e-03	6.8e-02	1.98	1.98	0.97
128	3.4e-04	3.4e-04	3.4e-02	1.99	1.99	0.98
256	8.7e-05	8.7e-05	1.7e-02	1.99	1.99	0.99

Table 6.14: Convergence rates and errors for the velocity $\mathbf{u}$ and the pressure p for coupled Darcy–Stokes flow with $\mu = K = 1.0$, $\beta_s = 2.0$. Discretized with $RT_1 \times DG_1$.

6.4 Preconditioning the L^2-formulation

In this section, the preconditioners $\mathcal{P}_I^{-1}$ and $\mathcal{P}_{II}^{-1}$ applied to the Darcy–Stokes system arising from the L^2-formulation will be tested numerically. To this end, the operators $\mathcal{A}$, $\mathcal{P}_I^{-1}$ and $\mathcal{P}_{II}^{-1}$ must be transformed into discrete operators $\mathcal{A}_h$, $\mathcal{P}_{I,h}^{-1}$ and $\mathcal{P}_{II,h}^{-1}$. The operator $\mathcal{A}$ is discretized using the L^2-formulation presented in Section 4.1, and $\mathcal{P}_I$ and $\mathcal{P}_{II}$ are discretized in a similar manner.

Inverting $\mathcal{P}_{I,h}$ and $\mathcal{P}_{II,h}$ directly is not an option, as this will require infeasible computation resources. Instead of finding the exact inverse, we seek spectrally equivalent operators $\tilde{\mathcal{P}}_{I,h}^{-1} \approx \mathcal{P}_{I,h}^{-1}$ and $\tilde{\mathcal{P}}_{II,h}^{-1} \approx \mathcal{P}_{II,h}^{-1}$. The preconditioner is approximated using algebraic multigrid [60], a generalized

multilevel method. The main idea behind a multilevel method is to use an iterative method, like Gauss–Seidel or Richardson, to smooth the error of the approximation. Then the error can be interpolated into a coarser mesh, without any essential loss of information. This is done multiple times, until the mesh is coarse enough to solve the system directly. Algebraic multigrid is based on the same idea, but the levels of hierarchy are constructed from the matrix, without any geometric interpretation.

6.4.1 Condition number

In order to determine how well the preconditioners perform and to check if they are optimal, the condition numbers of the Darcy–Stokes system preconditioned with $\mathcal{P}_{I,h}^{-1}$ and $\mathcal{P}_{II,h}^{-1}$ are calculated. Recall that for MinRes, a high condition number will result in slow convergence, whereas a low condition number will result in fast convergence.

Table 6.15 displays the exact condition numbers of the preconditioned systems $\mathcal{P}_{I,h}^{-1}\mathcal{A}_h$ and $\mathcal{P}_{II,h}^{-1}\mathcal{A}_h$, both with unity parameters and the physical parameter values suggested in Section 6.1. Both preconditioners have a condition number bounded independently of the discretization parameter h. The results indicate that using physical parameter values gives a condition number that is about twice as big as when using unity parameter values. Note that the condition numbers decrease slightly as n increases when using physical model parameters. It is clear that the coupled preconditioner $\mathcal{P}_{II,h}^{-1}$ improves the condition number to a greater extent than the decoupled preconditioner $\mathcal{P}_{I,h}^{-1}$. In addition, Table 6.15 shows that the condition number of $\mathcal{A}_h$ grows rapidly as the h decreases.

$\mu = K = 1.0$			
n	$\kappa(\mathcal{A}_h)$	$\kappa(\mathcal{P}_{I,h}^{-1}\mathcal{A}_h)$	$\kappa(\mathcal{P}_{II,h}^{-1}\mathcal{A}_h)$
8	3.9e+03	13.15	6.40
16	1.6e+04	13.28	6.55
32	6.8e+04	13.36	6.64
64	—	13.40	6.68
128	—	13.42	6.70
256	—	13.44	6.71

$\mu = 10^{-3}$, $K = 10^{-6}$			
n	$\kappa(\mathcal{A}_h)$	$\kappa(\mathcal{P}_{I,h}^{-1}\mathcal{A}_h)$	$\kappa(\mathcal{P}_{II,h}^{-1}\mathcal{A}_h)$
8	5.8e+05	31.40	15.00
16	8.6e+05	30.79	15.00
32	3.2e+06	28.47	14.47
64	—	22.63	12.83
128	—	16.24	10.59
256	—	15.96	10.36

Table 6.15: Condition numbers κ of the preconditioned Darcy–Stokes systems $\mathcal{P}_{I,h}^{-1}\mathcal{A}_h$ and $\mathcal{P}_{II,h}^{-1}\mathcal{A}_h$ discretized with Taylor–Hood elements. In addition, the condition number of the original system $\mathcal{A}_h$ is displayed.

6.4.2 Number of iterations

To check how well the algebraic multigrid algorithm works, i.e. to check if $\tilde{\mathcal{P}}_{I,h}^{-1}$ and $\tilde{\mathcal{P}}_{II,h}^{-1}$ indeed are spectrally equivalent to $\mathcal{P}_{I,h}^{-1}$ and $\mathcal{P}_{II,h}^{-1}$, respectively, the number of iterations before MinRes converges are counted. As before, the preconditioners are tested with unity parameters and with some of the more physical parameter values presented in Section 6.1. Recall that the tolerance is set to 10^{-7} and the initial guess in random.

Table 6.16 displays the number of iterations before MinRes converges with different model parameters. Applying the preconditioner $\tilde{\mathcal{P}}_{II,h}^{-1}$ results in fewer iterations than using $\tilde{\mathcal{P}}_{I,h}^{-1}$, just as expected from the eigenvalue estimates in Table 6.15. How much the coupling term in the preconditioner effects the number of iterations, seems to vary with the parameter values. The number of iterations using $\tilde{\mathcal{P}}_{I,h}^{-1}$ is about twice as big as with $\tilde{\mathcal{P}}_{II,h}^{-1}$ when $\mu = 10^{-3}$ and $K = 10^{-6}$, but when $\mu = 10^{-3}$ and $K = 10^{-12}$ the number of iterations using the two different preconditioners only differs with about $1 - 5$ iterations. For the sake of completeness, the number of iterations before convergence for solving the preconditioned Stokes system $\mathcal{B}_{s,h}^{-1}\mathcal{A}_{s,h}$ and the preconditioned Darcy system $\mathcal{B}_{d,I,h}^{-1}\mathcal{A}_{d,h}$ are presented. The results are displayed in Table 6.17.

In Table 6.18 the condition number and the number of iterations before MinRes convergences for the preconditioner system $\tilde{\mathcal{P}}_{II,h}^{-1}\mathcal{A}_h$ in 3D is displayed. For simplicity, the experiments are run on the unit cube. From theory the preconditioner should be generic with respect to dimension, consequently the results are expected to be similar to the 2D-results. Due to limited computational resources, the 3D-experiments are run on coarser meshes than the experiments in 2D. The results indicate that the preconditioner $\mathcal{P}_{II,h}^{-1}$ is optimal in 3D, as the condition number and the number of iterations are low and bounded independently of h, both when using unity and physical model parameters.

$\mu = K = 1.0$		
n	$N(\tilde{\mathcal{P}}_{I,h}^{-1}\mathcal{A}_h)$	$N(\tilde{\mathcal{P}}_{II,h}^{-1}\mathcal{A}_h)$
8	41	37
16	43	39
32	45	41
64	45	41
128	45	43
256	47	43

$\mu = 10^{-3}$, $K = 10^{-6}$		
n	$N(\tilde{\mathcal{P}}_{I,h}^{-1}\mathcal{A}_h)$	$N(\tilde{\mathcal{P}}_{II,h}^{-1}\mathcal{A}_h)$
8	80	42
16	84	42
32	86	43
64	85	42
128	84	38
256	96	36

$\mu = 10^{-3}$, $K = 10^{-12}$		
n	$N(\tilde{\mathcal{P}}_{I,h}^{-1}\mathcal{A}_h)$	$N(\tilde{\mathcal{P}}_{II,h}^{-1}\mathcal{A}_h)$
8	47	46
16	51	49
32	53	52
64	54	50
128	55	52
256	57	52

$\mu = 10^{-6}$, $K = 10^{-12}$		
n	$N(\tilde{\mathcal{P}}_{I,h}^{-1}\mathcal{A}_h)$	$N(\tilde{\mathcal{P}}_{II,h}^{-1}\mathcal{A}_h)$
8	65	62
16	68	66
32	68	67
64	67	65
128	66	63
256	62	61

Table 6.16: Number of iterations N for solving the preconditioned Darcy–Stokes systems $\tilde{\mathcal{P}}_{I,h}^{-1}\mathcal{A}_h$ and $\tilde{\mathcal{P}}_{II,h}^{-1}\mathcal{A}_h$. Discretized with Taylor–Hood elements.

$\mu = K = 1.0$		
n	$N(\tilde{\mathcal{B}}_{s,h}^{-1}\mathcal{A}_{s,h})$	$N(\tilde{\mathcal{B}}_{d,h}^{-1}\mathcal{A}_{d,h})$
8	34	18
16	36	18
32	36	18
64	37	18
128	37	18
256	37	18

$\mu = 10^{-3}$, $K = 10^{-6}$		
n	$N(\tilde{\mathcal{B}}_{s,h}^{-1}\mathcal{A}_{s,h})$	$N(\tilde{\mathcal{B}}_{d,h}^{-1}\mathcal{A}_{d,h})$
8	35	23
16	37	23
32	37	26
64	35	26
128	32	29
256	28	29

Table 6.17: Number of iterations N for solving the preconditioned Darcy system $\mathcal{B}_{d,I,h}^{-1}\mathcal{A}_{d,h}$ and the preconditioned Stokes system $\mathcal{B}_{s,h}^{-1}\mathcal{A}_{s,h}$. Discretized with Taylor–Hood elements.

$\mu = K = 1.0$		
n	$\kappa(\mathcal{P}_{II,h}^{-1}\mathcal{A}_h)$	$N(\tilde{\mathcal{P}}_{II,h}^{-1}\mathcal{A}_h)$
4	18.30	72
8	20.25	88
16	20.89	93
32	—	97

$\mu = 10^{-3}, K = 10^{-6}$		
n	$\kappa(\mathcal{P}_{II,h}^{-1}\mathcal{A}_h)$	$N(\tilde{\mathcal{P}}_{II,h}^{-1}\mathcal{A}_h)$
4	38.03	79
8	37.06	72
16	36.75	64
32	—	62

Table 6.18: Condition number κ and number of iterations N for solving the preconditioned Darcy–Stokes system $\mathcal{P}_{II,h}^{-1}\mathcal{A}_h$, discretized with Taylor–Hood elements in 3D.

6.5 Preconditioning the $H(\mathrm{div})$-formulation

In this section the preconditioners $\mathcal{Q}_I^{-1}$, $\mathcal{Q}_{II}^{-1}$, $\mathcal{P}_I^{-1}$ and $\mathcal{P}_{II}^{-1}$ discretized with $BDM_1 \times DG_0$ elements will be tested numerically. The operator $\mathcal{A}$ is discretized using the $H(\mathrm{div})$-formulation presented in Section 4.2, while the operators $\mathcal{P}_I$, $\mathcal{P}_{II}$, $\mathcal{Q}_I$ and $\mathcal{Q}_{II}$ are discretized as explained in Section 5.2.1 and 5.2.2.

Inverting the discrete preconditioners directly is not an option, as this will require infeasible computation resources. Instead of finding the exact inverse, we seek spectrally equivalent operators $\tilde{\mathcal{P}}_{I,h}^{-1} \approx \mathcal{P}_{I,h}^{-1}$, $\tilde{\mathcal{P}}_{II,h}^{-1} \approx \mathcal{P}_{II,h}^{-1}$, $\tilde{\mathcal{Q}}_{I,h}^{-1} \approx \mathcal{Q}_{I,h}^{-1}$ and $\tilde{\mathcal{Q}}_{II,h}^{-1} \approx \mathcal{Q}_{II,h}^{-1}$. The preconditioners are approximated using algebraic multigrid [60], a generalized multilevel method. The main idea behind a multilevel method is to use an iterative method, like Gauss–Seidel or Richardson, to smooth the error of the approximation. Then the error can be interpolated into a coarser mesh, without any essential loss of information. This is done multiple times, until the mesh is coarse enough to solve the system directly. Algebraic multigrid is based on the same idea, but the levels of hierarchy are constructed from the matrix, without any geometric interpretation.

6.5.1 Condition number

The exact condition numbers of the preconditioned systems are calculated for decreasing mesh parameters h, to see if the preconditioners are optimal. For the sake of comparison, the exact condition number of the original Darcy–Stokes system $\mathcal{A}_h$ is displayed in Table 6.19. As expected, the condition number increases rapidly as n increases.

$\mu = K = 1.0$	
n	$\kappa(\mathcal{A}_h)$
4	7.6e+03
8	1.4e+05
16	2.3e+06
32	3.7e+07

$\mu = 10^{-3}, K = 10^{-6}$	
n	$\kappa(\mathcal{A}_h)$
4	1.9e+06
8	7.9e+06
16	3.2e+07
32	1.3e+08

Table 6.19: Condition number κ of the original Darcy–Stokes system $\mathcal{A}_h$.

$\mu = K = 1.0$		
n	$\kappa(\mathcal{P}_{I,h}^{-1}\mathcal{A}_h)$	$\kappa(\mathcal{P}_{II,h}^{-1}\mathcal{A}_h)$
8	20.68	20.66
16	20.84	20.83
32	21.78	21.77
64	22.34	22.33
128	22.59	22.57
256	22.72	22.71

$\mu = 10^{-3}$, $K = 10^{-6}$		
n	$\kappa(\mathcal{P}_{I,h}^{-1}\mathcal{A}_h)$	$\kappa(\mathcal{P}_{II,h}^{-1}\mathcal{A}_h)$
8	4411	27.09
16	4345	35.57
32	4258	47.18
64	4250	62.75
128	—	76.87
256	—	92.32

Table 6.20: Condition number κ of the preconditioned Darcy–Stokes systems $\mathcal{P}_{I,h}^{-1}\mathcal{A}_h$ and $\mathcal{P}_{II,h}^{-1}\mathcal{A}_h$, with $\beta_s = 2.0$ and $\beta_d = 1.0$. Discretized with $BDM_1 \times DG_0$ elements.

$\mu = K = 1.0$		
n	$\kappa(\mathcal{Q}_{I,h}^{-1}\mathcal{A}_h)$	$\kappa(\mathcal{Q}_{II,h}^{-1}\mathcal{A}_h)$
8	8.10	6.56
16	8.35	6.74
32	8.73	7.04
64	8.92	7.19
128	9.00	7.25
256	9.04	7.28

$\mu = 10^{-3} K = 10^{-6}$		
n	$\kappa(\mathcal{Q}_{I,h}^{-1}\mathcal{A}_h)$	$\kappa(\mathcal{Q}_{II,h}^{-1}\mathcal{A}_h)$
8	4401	11.68
16	4445	11.67
32	4358	11.48
64	4210	11.13
128	—	11.04
256	—	10.98

Table 6.21: Condition number κ of the preconditioned coupled Darcy–Stokes systems $\mathcal{Q}_{II,h}^{-1}\mathcal{A}_h$ and $\mathcal{Q}_{II}^{-1}\mathcal{A}_h$ with $\beta_s = 2.0$. Discretized with $BDM_1 \times DG_0$ elements.

Table 6.20 displays the condition numbers of the preconditioned coupled Darcy–Stokes systems $\mathcal{P}_{I,h}^{-1}\mathcal{A}_h$ and $\mathcal{P}_{II,h}^{-1}\mathcal{A}_h$. When using unity parameters, both the decoupled preconditioner $\mathcal{P}_{I,h}^{-1}$ and the coupled preconditioner $\mathcal{P}_{II,h}^{-1}$ are optimal. Changing the model parameters to more physical values has an impact on the preconditioners. The coupled preconditioner $\mathcal{P}_{II,h}^{-1}$ gives a system where the condition number increases slightly as n increases. Hence, the preconditioner is not optimal when using physical model parameters. However, in comparison with the condition number of the original system, cf. Table 6.19, the condition number is indeed low. The decoupled preconditioner $\mathcal{P}_{I,h}^{-1}$ is not optimal and has a larger condition number. This indicates that when discretizing with $BDM_1 \times DG_0$ elements, the coupling operator has a great impact on the performance of the preconditioner.

From Table 6.21, we observe that the preconditioned systems $\mathcal{Q}_{I,h}^{-1}\mathcal{A}_h$ and $\mathcal{Q}_{II,h}^{-1}\mathcal{A}_h$ have condition numbers that are bounded independently of h when using unity model parameters. Setting the parameter values to more physical values yields good results when using the coupled preconditioner $\mathcal{Q}_{II,h}^{-1}$, whereas the decoupled preconditioner $\mathcal{Q}_{I,h}^{-1}$ is neither optimal nor gives low eigenvalues.

6.5.2 Number of iterations

To check how well the algebraic multigrid algorithm works, i.e. to check if the approximation of the preconditioners indeed are spectrally equivalent to the exact preconditioners, the number of iterations before MinRes convergences is counted. The preconditioners are tested with all model parameters set equal to one and with more physical parameter values. Recall that the tolerance is set to 10^{-7} and that the initial guess is random.

$\mu = K = 1.0$		
n	$N(\tilde{\mathcal{P}}_{I,h}^{-1}\mathcal{A}_h)$	$N(\tilde{\mathcal{P}}_{II,h}^{-1}\mathcal{A}_h)$
8	109	108
16	240	236
32	562	557
64	1393	1376
128	—	—
256	—	—

$\mu = 10^{-3}, K = 10^{-6}$		
n	$N(\tilde{\mathcal{P}}_{I,h}^{-1}\mathcal{A}_h)$	$N(\tilde{\mathcal{P}}_{II,h}^{-1}\mathcal{A}_h)$
8	422	227
16	935	416
32	2063	1037
64	—	2891
128	—	—
256	—	—

Table 6.22: Number of iterations N for solving the preconditioned coupled Darcy–Stokes systems $\tilde{\mathcal{P}}_{I,h}^{-1}\mathcal{A}_h$ and $\tilde{\mathcal{P}}_{II,h}^{-1}\mathcal{A}_h$. Discretized with $BDM_1 \times DG_0$ elements.

$\mu = K = 1.0$		
n	$N(\tilde{\mathcal{Q}}_{I,h}^{-1}\mathcal{A}_h)$	$N(\tilde{\mathcal{Q}}_{II,h}^{-1}\mathcal{A}_h)$
8	227	225
16	534	538
32	1256	1256
64	3077	3069
128	7354	7295
256	—	—

$\mu = K = 1.0^{-3}$		
n	$N(\tilde{\mathcal{Q}}_{I,h}^{-1}\mathcal{A}_h)$	$N(\tilde{\mathcal{Q}}_{II,h}^{-1}\mathcal{A}_h)$
8	245	141
16	431	238
32	1269	677
64	2609	1612
128	—	4065
256	—	8997

Table 6.23: Number of iterations N for solving the preconditioned coupled Darcy–Stokes systems $\tilde{\mathcal{Q}}_{I,h}^{-1}\mathcal{A}_h$ and $\tilde{\mathcal{Q}}_{II,h}^{-1}\mathcal{A}_h$. Discretized with $BDM_1 \times DG_0$ elements.

Table 6.22 displays the number of iterations when the Darcy–Stokes system is preconditioned with $\tilde{\mathcal{P}}_{I,h}^{-1}$ and $\tilde{\mathcal{P}}_{II,h}^{-1}$. Although the systems $\mathcal{P}_{I,h}^{-1}\mathcal{A}_{d,h}$ and $\mathcal{P}_{II,h}^{-1}\mathcal{A}_{d,h}$ have condition numbers that are bounded independently of n, cf. Table 6.20, the number of iterations increases as n increases.

In Table 6.23 the number of iterations when preconditioning the Darcy–Stokes system $\mathcal{A}_h$ with $\mathcal{Q}_{I,h}^{-1}$ and $\mathcal{Q}_{II,h}^{-1}$ are displayed. We see the same behaviour here, the number of iterations increases rapidly as n increases, even though the condition numbers are bounded, cf. Table 6.21.

This will be further discussed in Section 6.5.3.

6.5.3 Investigation

In this section we will investigate why the preconditioners $\mathcal{P}_{II}^{-1}$ and $\mathcal{Q}_{II}^{-1}$ are not approximated well by algebraic multigrid. To this end, we look at how the Darcy preconditioners $\mathcal{B}_{d,I}^{-1}$ and $\mathcal{B}_{d,II}^{-1}$ and the Stokes preconditioner $\mathcal{B}_s^{-1}$ occurring in $\mathcal{P}_{II}^{-1}$ and $\mathcal{Q}_{II}^{-1}$ behaves separately.

Table 6.24 displays the condition number and the number of iterations before convergence for the preconditioned Stokes system $\mathcal{B}_{s,h}^{-1}\mathcal{A}_{s,h}$. The condition number is bounded independently of h, but the number of iterations increases as h decreases. It seems as if as algebraic multigrid does not manage to produce a spectrally equivalent operator $\tilde{\mathcal{B}}_{s,h}^{-1} \approx \mathcal{B}_{s,h}^{-1}$.

In Table 6.25 the condition number and the number of iterations before convergence for the preconditioned system $\mathcal{B}_{d,I,h}^{-1}\mathcal{A}_{d,h}$ are displayed. The

$\mu = 1.0$		
N	$\kappa(\mathcal{B}_{s,h}^{-1}A_{s,h})$	$N(\tilde{\mathcal{B}}_{s,h}^{-1}A_{s,h})$
8	6.35	71
16	6.39	154
32	6.39	347
64	6.39	788
128	6.34	2148
256	6.39	—

$\mu = 10^{-3}$		
N	$\kappa(\mathcal{B}_{s,h}^{-1}A_{s,h})$	$N(\tilde{\mathcal{B}}_{s,h}^{-1}A_{s,h})$
8	6.39	78
16	6.41	161
32	6.41	335
64	6.41	803
128	6.42	2196
256	6.44	—

Table 6.24: Condition number κ and number of iterations N for solving the preconditioned Stokes system $\mathcal{B}_{s,h}^{-1}A_{s,h}$, with $\beta_s = 2.0$. Discretized with $BDM_1 \times DG_0$ elements.

$\mu = K = 1.0$		
n	$\kappa(\mathcal{B}_{d,I,h}^{-1}\mathcal{A}_{d,h})$	$N(\tilde{\mathcal{B}}_{d,I,h}^{-1}\mathcal{A}_{d,h})$
8	9.84	39
16	9.85	43
32	9.86	46
64	9.86	47
128	9.86	46
256	9.86	48

$\mu = 10^{-3}$, $K = 10^{-6}$		
n	$\kappa(\mathcal{B}_{d,I,h}^{-1}\mathcal{A}_{d,h})$	$N(\tilde{\mathcal{B}}_{d,I,h}^{-1}\mathcal{A}_{d,h})$
8	9.82	32
16	9.83	33
32	9.83	34
64	9.83	35
128	9.84	33
256	9.84	31

Table 6.25: Condition number κ and number of iterations N for solving the preconditioned Darcy system $\mathcal{B}_{d,I,h}^{-1}\mathcal{A}_{d,h}$, with $\beta_d = 1.0$. Discretized with $BDM_1 \times DG_0$ elements.

preconditioner $\mathcal{B}_{d,I,h}^{-1}$ is optimal in the sense that the condition number of the preconditioned system is bounded independently of h. Algebraic multigrid also works optimal, the number of iterations before MinRes converges is bounded independently of h.

In Table 6.26 the condition number and the number of iterations for the preconditioned system $\mathcal{B}_{d,II,h}^{-1}\mathcal{A}_{d,h}$ are displayed. The preconditioner $\mathcal{B}_{d,II,h}^{-1}$ is optimal in the sense that the condition number is bounded independently of h. However, the number of iterations increases rapidly as n increases. This indicates that the algebraic multigrid algorithm does not manage to produce a spectrally equivalent operator $\tilde{\mathcal{B}}_{d,II,h}^{-1}$.

$\mu = K = 1.0$		
n	$\kappa(\mathcal{B}_{d,II,h}^{-1}\mathcal{A}_{d,h})$	$N(\tilde{\mathcal{B}}_{d,II,h}^{-1}\mathcal{A}_{d,h})$
8	1.40	186
16	1.40	395
32	1.40	822
64	1.40	1700
128	1.40	3387
256	1.40	—

$\mu = 10^{-3}$, $K = 10^{-6}$		
n	$\kappa(\mathcal{B}_{d,II,h}^{-1}\mathcal{A}_{d,h})$	$N(\tilde{\mathcal{B}}_{d,II,h}^{-1}\mathcal{A}_{d,h})$
8	1.40	173
16	1.40	390
32	1.40	817
64	1.40	1690
128	1.40	3297
256	1.40	—

Table 6.26: Condition number κ and number of iterations N for solving the preconditioned Darcy system $\mathcal{B}_{d,II,h}^{-1}\mathcal{A}_{d,h}$. Discretized with $BDM_1 \times DG_0$ elements.

6.5.4 Auxiliary space preconditioning

Algebraic multigrid does not manage to produce spectrally equivalent operators $\tilde{\mathcal{B}}_{s,h}^{-1} \approx \mathcal{B}_{s,h}^{-1}$ and $\tilde{\mathcal{B}}_{d,II,h}^{-1} \approx \mathcal{B}_{d,II,h}^{-1}$, cf. Table 6.24 and 6.26. Hiptmair et al. [13] propose an auxiliary space preconditioning technique to solve the problem. The technique links the vector fields in $H(\mathrm{div})$ with functions in H^1, and the preconditioning in $H(\mathrm{div})$ reduces to second order elliptic operators in H^1. Hence, the standard algebraic multigrid algorithm for the H^1 equations can be applied. More precisely, the matrices corresponding to the operators $(-\Delta)^{-1}$ and $(I - \mathrm{grad}\,\mathrm{div})^{-1}$ in $\mathcal{B}_{s,h}^{-1}$ and $\mathcal{B}_{d,I,h}^{-1}$, respectively, are approximated in an auxiliary space of Lagrange elements W_h, where algebraic multigrid methods are optimal. Then, the operators are projected into the original solution space $\mathbf{V}_h$. The discrete preconditioners $\mathcal{B}_{d,II,h}^{-1}$ and $\mathcal{B}_{s,h}^{-1}$ can be written on block form as,

$$\mathcal{B}_{s,h}^{-1} = \begin{bmatrix} -\Delta_h^{-1} & 0 \\ 0 & I_h^{-1} \end{bmatrix} = \begin{bmatrix} N_s^{-1} & 0 \\ 0 & M_s^{-1} \end{bmatrix} \tag{6.9}$$

$$\mathcal{B}_{d,II,h}^{-1} = \begin{bmatrix} (I_h - \mathrm{grad}\,\mathrm{div}_h)^{-1} & 0 \\ 0 & I_h^{-1} \end{bmatrix} = \begin{bmatrix} N_d^{-1} & 0 \\ 0 & M_d^{-1} \end{bmatrix} \tag{6.10}$$

Our aim is to provide a matrices $\tilde{N}_s$ and $\tilde{N}_d$ where the inverse can be approximated by algebraic multigrid in a sufficiently good way. In addition, $\tilde{N}_s$ and $\tilde{N}_d$ should be spectrally equivalent to N_s and N_d, respectively.

We follow the procedure of Márquez et al. [12]. Denote W_h by the standard space of continuous piecewise polynomials. Let L be the matrix realisation of $-\Delta_h$ in W_h. Let C be the matrix corresponding to the *curl* operator mapping W_h onto $\mathbf{V}_h$. Let Π_d denote the interpolation operator from W_h

onto $\mathbf{V}_h$, and let I_d be the matrix realization of the mapping Π_d. The matrix $N_{a,s}$ is the operator N_s discretized in W_h.

$$\tilde{N_s}^{-1} = S^{-1} + I_d N_{a,s}^{-1} I_d^T + CL^{-1}C^T \tag{6.11}$$

where S is the diagonal of N_s. Similarly, by letting $N_{a,d}$ be the operator N_d discretized in W_h.

$$\tilde{N_d}^{-1} = S^{-1} + I_d N_{a,d}^{-1} I_d^T + CL^{-1}C^T \tag{6.12}$$

where S is the diagonal of N_d. However, we did not have any luck using this technique. We tried using both P_{q+1} and DG_q elements for the auxiliary space W_h for $q = 0, 1, 2$. The auxiliary space was set to be a scalar space and a vector space. We also attempted to use different auxiliary spaces to yield the discrete the matrix L and the preconditioners $N_{a,d}$ and $N_{a,s}$. The interpolation matrix I_d was set to be the mass matrix, and a mass matrix including interior and the exterior facets. In addition, we attempted to implement the $H(\text{div})$ auxiliary preconditioner B_{div} [13, (7.7)], suggested by Hiptmair et al. [13]. Unfortunately, neither of these attempts where successful. As we eventually ran out of time, we suggest this as further work.

Chapter 7

Summary and discussion

In this thesis we have studied preconditioning of unified mixed discretizations of the couped Darcy–Stokes problem. The Darcy velocities have at least two natural solution spaces, giving rise to two different solutions spaces for the coupled Darcy–Stokes problem, namely

$$X = (\mathbf{L}^2(\Omega) \cap \mathbf{H}^1(\Omega_s)) \times (L_0^2(\Omega) \cap H^1(\Omega_d))$$
$$Y = (\mathbf{H}_0(\mathrm{div}, \Omega) \cap \mathbf{H}^1(\Omega_s)) \times L_0^2(\Omega)$$

We have derived and tested the two variational formulations suggested by Karper et al. [6], that is, the L^2-formulation and the $H(\mathrm{div})$-formulation. In the L^2-formulation, the coupled Darcy–Stokes problem is posed in the space X, and the formulation is discretized with the uniformly stable Taylor–Hood elements. In the $H(\mathrm{div})$-formulation the coupled Darcy–Stokes problem is posed in the space Y, and it is discretized with Brezzi–Douglas–Marini elements along with an interior penalty method to ensure stability of the scheme, as suggested by Kanschat et al. [9]. In addition, we checked the errors and convergence rate for the $H(\mathrm{div})$-formulation discretized with lower order Raviart–Thomas elements. We have explored decoupled and coupled preconditioners for both discretizations. The approach taken has been to use robust preconditioners for the Stokes and the Darcy problem and combine them.

7.1 Convergence rates

Taylor–Hood elements, the L^2-formulation

For pure Stokes flow, using unity model parameters yields the convergence rates we expected from *a priori* estimate 4.2, that is, an L^2-rate of third order for the velocity, an H^1-rate of second order for the velocity and an L^2-rate of second order for the pressure. When using physical parameter

values for pure Stokes flow, tendencies to super convergence is observed for the velocity, cf. Table 6.2. One possible explanation to this, is that for small viscosities μ the pressure is large in comparison to the velocity, causing the pressure error to influence the velocities.

For pure Darcy flow with both unity and physical parameter values, we expected an L^2-rate of at least first order for the velocity. The numerical results indicate that the scheme converges at an L^2-velocity rate of an order of one and a half, cf. Table 6.3. When using both unity and physical model parameters, the H^1-pressure rate is of first order, just as expected from the *a priori* estimate 4.3. We also observe that the L^2-pressure rate is of second order, both using unity and physical model parameters.

We could not find an *a priori* estimate for the Darcy–Stokes equations discretized with Taylor Hood elements. Instead, we have made an assumption based on the *a priori* error estimate for the problem discretized with the Mini element presented by Karper et al. [6]. They expect both the L^2-rate of the velocity and the L^2-rate of the pressure to be of at least first order. As the Taylor–Hood elements approximate the velocities in a space of one degree higher polynomials than the Mini element, we made the assumption that the velocity error rate would be of one order higher. Thus we expected an L^2-velocity rate of at least second order and a L^2-pressure rate of at least first order. However, we observed an L^2-rate for the velocity of one and a half order and an L^2-pressure rate of second order when using both unity and physical model parameters, cf. Table 6.5 and 6.6.

Karper et al. [6] present observed convergence rates for the Darcy–Stokes problem discretized with the Mini element, and they observe almost second order convergence for the L^2-error in the pressure and first order convergence for the L^2-error in the velocity, cf. [6, Table 4].

Brezzi–Douglas–Marini elements, the $H(\mathrm{div})$-formulation

For pure Stokes flow, using both unity and physical model parameters yields the convergence rates we expected from *a priori* estimate 4.4, that is, fist order convergence for both the H^1-error in velocity and the L^2-error in the pressure. In addition, we observe an L^2-rate of second order for the velocity. The results can be found in Table 6.7 and 6.8.

For pure Darcy flow, using both unity and physical model parameters yields an L^2-rate and a $H(\mathrm{div})$-rate for the velocity of second order. The pressure L^2-rate is of first order when using unity model parameters and just above first order when using more physical parameter values, cf. Table 6.9 and 6.10.

For coupled Darcy–Stokes flow, using both unity and physical model parameters yields an L^2-rate and a $H(\mathrm{div})$-rate for the velocity of second order. The pressure L^2-rate is of first order. The results can be found in Table 6.11 and 6.12.

Raviart–Thomas elements, the $H(\mathrm{div})$-formulation

Within this work, we have not presented any *a priori* error estimates for the Raviart-Thomas elements. However, we have made some observations. Discretizing the coupled Darcy–Stokes problem with lowest order Raviart–Thomas elements for the velocity and DG_0 elements for the pressure did not give good results. The errors do not decrease when the mesh is refined, but is approximately 0.9 for the velocity and 5.8 for the pressure for all mesh parameters h, cf. Table 6.13. The problem might be that the RT_0 elements does not have sufficiently many degrees of freedom. When discretizing the coupled Darcy–Stokes problem with $RT_1 \times DG_1$ elements the errors decrease as the mesh is refined. We observe that the L^2-rate of the velocity error is of second order, while the L^2-rate of the pressure is of first order. The results can be found in Table 6.14.

Kanschat et al. [9] present numerical convergence rates for the coupled Darcy–Stokes problem discretized with $RT_1 \times DG_1$ elements. They observe that both the L^2-error in the velocity and the L^2-error in the pressure convergences at a rate of second order, cf. [9, Table 2].

7.2 The IP method

If the finite element space in which to search for an approximate solution is not in H^1, gradients are not well defined. Within this work, the IP method is used to remedy this by penalizing the jumps of the numerical approximations across interior facets. More precisely, the IP method is used to discretize second-order Laplace operators with Brezzi–Douglas–Marini, Raviart–Thomas or discontinuous Galerkin elements, as neither of the spaces consisting of these elements are in H^1.

In the $H(\mathrm{div})$-formulation, there is a second-order operator acting on the velocities in the Stokes part of the domain. When discretizing with BDM or RT elements we follow Kanschat et al. [9] and apply the IP method. The same approach is taken when discretizing the second order operator acting on the velocities in the Stokes preconditioner $\mathcal{B}_{s,h}^{-1}$ with BDM elements. The penalty term arising from the IP method introduces a penalty parameter β_s that has to be determined. Kanschat et al. [9] point out that β_s has an effect on the condition number, in the sense that the condition number increases

as β_s increases. The behavior is illustrated in Table 6.2. Therefore, finding a lower bound for β_s is of interest. From Table 6.2 we observe a large velocity error oscillating rapidly when $\beta_s \leq 1.6$. The error stabilizes at $6.0 \cdot 10^{-3}$ for $\beta_s \geq 1.6$. For the preconditioned Stokes problem, we see from Table 6.3 that the condition number "flattens out" for $\beta_s \geq 1.6$. These results indicate that the preconditioner stabilizes the system with respect to large β_s values, in terms of a mesh independent bound on the condition number. Theoretical estimates of the lower bound can also be obtained, cf. [35].

The IP method is also applied to discretize the second-order operator acting on the pressure in the Darcy preconditioner $\mathcal{B}_{d,I,h}^{-1}$ with DG elements, as suggested by Winther et al. [43]. The penalty term arising from the IP method introduces a penalty parameter β_d that has to be determined. To find an optimal value for the penalty parameter β_d, the condition numbers of the preconditioned system $\mathcal{B}_{d,I,h}^{-1}\mathcal{A}_{d,h}$ are calculated. The results are displayed in Figure 6.4. When β_d tends to zero, the condition number grows larger. The condition numbers are bounded independently of h for approximately $\beta_d \leq 3.8$. However, the figure only displays condition number for $n = 4, 8, 16$. It is reason to believe that when n increases, the condition number will not be bounded independently of an arbitrary mesh parameter h unless β_d is set to a very small value. In our numerical experiments the finest grid has $n = 256$ number of elements, and the experiments indicate that the preconditioner is optimal for $\beta_d = 1.0$ up to at least this refinement, cf. Table 6.25. Winther et al. [43] set the parameter $\beta_d = 1.0$, with no further discussion.

7.3 Preconditioning the L^2-formulation

We have explored two preconditioners for the L^2-formulation, the decoupled preconditioner $\mathcal{P}_I^{-1}$ and the coupled preconditioner $\mathcal{P}_{II}^{-1}$. We have shown that the two preconditioners indeed are isomorphisms mapping X onto X^*. In addition, the preconditioners are tested numerically by calculating the exact condition numbers and count the number of iterations it takes to solve the preconditioned systems using the minimal residual method.

Both the preconditioners are optimal when using unity parameters, in the sense that the condition number is bounded independently of the discretization parameter h, cf. Table 6.15. Whit unity model parameters the preconditioned system $\mathcal{P}_{I,h}^{-1}\mathcal{A}_h$ has a condition number $\kappa \approx 13$, while the system $\mathcal{P}_{II,h}^{-1}\mathcal{A}_h$ has a condition number $\kappa \approx 6$. In addition, both the preconditioners are optimal when using more physical parameter values, cf. Table 6.15. The condition numbers are slightly higher with physical model parameters than with unity model parameters. Moreover, the condition numbers de-

crease slightly as n increases when using more physical parameter values.

Applying algebraic multigrid to approximate the preconditioners $\mathcal{P}_I^{-1}$ and $\mathcal{P}_{II}^{-1}$ gives good results. The number of iterations are bounded independently of the mesh size. MinRes uses about 40 iterations to converge for the preconditioned systems with unity model parameters, both when using the coupled and the decoupled preconditioner. Changing the model parameters to have more physical values gives good results in terms of fast convergence that is independent of h, cf. Table 6.16.

We have also tested how the preconditioner $\mathcal{P}_{II}^{-1}$ performs in 3D. The results are displayed in Table 6.18, and indicates that the coupled preconditioner $\mathcal{P}_{II,h}^{-1}$ is optimal in 3D. The condition number is bounded independently of h, and so is the number of iterations before MinRes convergences.

7.4 Preconditioning the $H(\mathrm{div})$-formulation

We have tested four preconditioners for the $H(\mathrm{div})$-formulation, the decoupled preconditioners $\mathcal{P}_I^{-1}$ and $\mathcal{Q}_I^{-1}$ and the coupled preconditioners $\mathcal{P}_{II}^{-1}$ and $\mathcal{Q}_{II}^{-1}$. In our numerical experiments, the $H(\mathrm{div})$-formulation is discretized using $BDM_1 \times DG_0$ elements. The preconditioners have been tested numerically by calculating the exact condition numbers and count the number of iterations it takes to solve the preconditioned systems using the minimal residual method.

When using unity model parameters, both $\mathcal{Q}_I^{-1}$ and $\mathcal{Q}_{II}^{-1}$ are optimal in the sense that the condition number is bounded independently of the discretization parameter h. The preconditioned system $\mathcal{Q}_{I,h}^{-1}\mathcal{A}_h$ has a condition number $\kappa \approx 8$, while the system $\mathcal{Q}_{II,h}^{-1}\mathcal{A}_h$ has a condition number $\kappa \approx 7$. Hence, the coupling term does not seem to have a significant impact on the performance of the preconditioner. When using more physical model parameters, the coupled preconditioner $\mathcal{Q}_{II,h}^{-1}$ is optimal, whereas the decoupled preconditioner $\mathcal{Q}_{I,h}^{-1}$ is neither optimal nor gives a low condition number. From Table 6.21 we observe that $\kappa(\mathcal{Q}_{I,h}^{-1}\mathcal{A}_h)$ is in the range $4200 - 4400$, while $\kappa(\mathcal{Q}_{II,h}^{-1}\mathcal{A}_h) \approx 11$. This indicates that when using more physical model parameters the coupling term seems to have greater impact on the performance of the preconditioners.

Using unity parameters, both $\mathcal{P}_I^{-1}$ and $\mathcal{P}_{II}^{-1}$ are robust to refinement of the mesh. They both have a condition number $\kappa \approx 21$. That is, the coupling term does not seem to have a great impact on the condition number. The coupled preconditioner $\mathcal{P}_{II,h}^{-1}$ is however not completely robust to changes

in the model parameters. There is a slight increase in the condition numbers as h decreases, cf. Table 6.20. However, the condition numbers are low in comparison with condition number of the original system, cf. Table 6.19. Applying the decoupled preconditioner $\mathcal{P}_{I,h}^{-1}$ with physical model parameters gives a large condition number that increases as the mesh is refined.

The number of iterations for the coupled Darcy–Stokes system preconditioned with $\mathcal{P}_{I}^{-1}$, $\mathcal{P}_{II}^{-1}$, $\mathcal{Q}_{I}^{-1}$ and $\mathcal{Q}_{II}^{-1}$ are displayed in Table 6.22 and Table 6.23. The results indicate that the preconditioners are nowhere near optimal. The number of iterations increase rapidly as h decreases. In Section 6.5.3, we found out that this is due to the fact that the Stokes preconditioner $B_{s,h}^{-1}$ and the Darcy preconditioner $\mathcal{B}_{d,II,h}^{-1}$ are not approximated well with algebraic multigrid, cf. Table 6.24 and 6.26.

Hiptmair et al. [13] suggest to use an auxiliary space preconditioning technique to avoid the problem with algebraic multigrid when discretizing preconditioners with $H(\mathrm{div})$ conforming elements, such as the lower order Brezzi-Douglas-Marini elements. We made numerous attempts to apply the technique, some of them are presented in Section 6.5.4. Unfortunately, we did not get good results in terms of neither condition number nor number of iterations. If one can remedy the problem with algebraic multigrid by applying an auxiliary preconditioning technique on $\mathcal{B}_{s,h}^{-1}$ and $\mathcal{B}_{d,II,h}^{-1}$, there is reason to believe that this will also remedy the problem with the preconditioners for the coupled Darcy–Stokes problem.

7.5 Conclusions

The L^2-formulation discretized with Taylor–Hood elements is easy to implement. Creating and applying preconditioners is also fairly easy, and algebraic multigrid works optimally. A disadvantage with this discretization is that it cannot represent the physical pressure jump at the interface. In addition, the scheme is not locally mass conserving.

The $H(\mathrm{div})$-formulation discretized with Brezzi–Douglas–Marini or Raviart–Thomas elements is better suited to represent the physical properties of the solution, in terms of the pressure jump at the interface Γ. In addition, the scheme is locally mass conserving. As the gradients in the weak form of the Stokes equations are not well defined using BDM or RT elements, the IP method must be applied to penalize the jumps across interior facets. The scheme is therefore a bit more extensive to implement.

Preconditioning the $H(\mathrm{div})$-formulation discretized with $BDM_1 \times DG_0$ ele-

ments has proven to be challenging, as algebraic multigrid does not manage to produce spectrally equivalent operators. One remedy for this could be the auxiliary space preconditioning technique suggested by Hiptmair et al. [13]. However, we have experienced that the implementation is not trivial, and we did not succeed.

The technique of combining optimal preconditioners for the Stokes problem and the Darcy problem seems to be efficient for creating robust preconditioners for the coupled Darcy–Stokes problem. Including the coupling term improves the preconditioners in all our test cases. A possible explanation to this, is that the coupled preconditioners are closer to the inverse of $\mathcal{A}$ then the decoupled preconditioners.

7.6 Further work

We have tried to apply an auxiliary space preconditioning technique to remedy that algebraic multigrid does not work as expected for the Stokes preconditioner $\mathcal{B}_{s,h}^{-1}$ and the Darcy preconditioner $\mathcal{B}_{d,II,h}^{-1}$ discretized with $BDM_1 \times DG_0$ elements. However, the attempts where not successful. Based on the works of Hiptmair et al. [13] and Márquez et al. [12], we still believe the technique can remedy the problem, and suggest this as further work.

The preconditioner $\mathcal{P}_{II,h}^{-1}$ is robust when using unity parameters, but there is a slight increase in the condition number as h decreases when using physical parameter values. In order to have a generic preconditioner that can be used in physical applications, finding a cure for this is of interest. Cai et al. [11] suggest adding a parameter to scale certain parts of the preconditioner to remedy similar phenomenas. Due to lack of time, we have however not tested the technique.

We have run experiments with different model parameters, in order to determine how well the preconditioners perform for realistic applications of the coupled Darcy–Stokes model. However, we only ran the experiments on the unit square and the unit cube. For practical reasons, it would be useful to test the preconditioners on more complicated, physical geometries.

Finally, we believe that a natural next step is to extend the preconditioners such that they can be applied to the Darcy–Navier–Stokes model.

Bibliography

[1] Kent Andre Mardal, Xue-Cheng Tai, and Ragnar Winther. A robust finite element method for darcy–stokes flow. *SIAM Journal on Numerical Analysis*, 40(5):1605–1631, 2002.

[2] Santiago Badia and Ramon Codina. Unified stabilized finite element formulations for the Stokes and the Darcy problems. *SIAM journal on Numerical Analysis*, 47(3):1971–2000, 2009.

[3] Erik Burman and Peter Hansbo. A unified stabilized method for Stokes' and Darcy's equations. *Journal of Computational and Applied Mathematics*, 198(1):35–51, 2007.

[4] Hongxing Rui and Ran Zhang. A unified stabilized mixed finite element method for coupling Stokes and Darcy flows. *Computer Methods in Applied Mechanics and Engineering*, 198(33):2692–2699, 2009.

[5] Xiaoping Xie, Jinchao Xu, and Guangri Xue. Uniformly-stable finite element methods for Darcy–Stokes–Brinkman models. *JOURNAL OF COMPUTATIONAL MATHEMATICS-INTERNATIONAL EDITION-*, 26(3):437, 2008.

[6] Trygve Karper, Kent-Andre Mardal, and Ragnar Winther. Unified finite element discretizations of coupled Darcy–Stokes flow. *Numerical Methods for Partial Differential Equations*, 25(2):311–326, 2009.

[7] Cedric Taylor and P Hood. A numerical solution of the Navier–Stokes equations using the finite element technique. *Computers & Fluids*, 1(1):73–100, 1973.

[8] Franco Brezzi, Jim Douglas Jr, and L Donatella Marini. Two families of mixed finite elements for second order elliptic problems. *Numerische Mathematik*, 47(2):217–235, 1985.

[9] Guido Kanschat and Béatrice Rivière. A strongly conservative finite element method for the coupling of Stokes and Darcy flow. *Journal of Computational Physics*, 229(17):5933–5943, 2010.

[10] Carlo D'Angelo and Paolo Zunino. Robust numerical approximation of coupled Stokes' and Darcy's flows applied to vascular hemodynamics and biochemical transport. *ESAIM: Mathematical Modelling and Numerical Analysis*, 45(03):447–476, 2011.

[11] Mingchao Cai, Mo Mu, and Jinchao Xu. Preconditioning techniques for a mixed Stokes/Darcy model in porous media applications. *Journal of computational and applied mathematics*, 233(2):346–355, 2009.

[12] Antonio Márquez, Salim Meddahi, and Francisco-Javier Sayas. A decoupled preconditioning technique for a mixed Stokes–Darcy model. *Journal of Scientific Computing*, 57(1):174–192, 2013.

[13] Ralf Hiptmair and Jinchao Xu. Nodal auxiliary space preconditioning in h (curl) and h (div) spaces. *SIAM Journal on Numerical Analysis*, 45(6):2483–2509, 2007.

[14] Anders Logg, Kent-Andre Mardal, and Garth Wells. *Automated solution of differential equations by the finite element method: The FEniCS book*, volume 84. Springer Science & Business Media, 2012.

[15] Frank M White and Isla Corfield. *Viscous fluid flow*, volume 3. McGraw-Hill New York, 2006.

[16] Shlomo P Neuman. Theoretical derivation of Darcy's law. *Acta Mechanica*, 25(3-4):153–170, 1977.

[17] Marco Discacciati and Alfio Quarteroni. Navier-Stokes/Darcy coupling: modeling, analysis, and numerical approximation. *Revista Matemática Complutense*, 22(2):315–426, 2009.

[18] Gordon S Beavers and Daniel D Joseph. Boundary conditions at a naturally permeable wall. *Journal of fluid mechanics*, 30(01):197–207, 1967.

[19] P.G. Saffmann. Boundary condition at surface of a porous medium. *Studies in applied mathematics*, 50(2):0–93, 1971.

[20] Dietrich Braess. *Finite elements: Theory, fast solvers, and applications in solid mechanics*. Cambridge University Press, 2007.

[21] Howard C Elman, David Silvester, and Andy Wathen. *Finite elements and fast iterative solvers*. Oxford Science Publications, 2006.

[22] Mika Juntunen and Rolf Stenberg. Nitsche's method for general boundary conditions. *Mathematics of computation*, 78(267):1353–1374, 2009.

[23] Douglas N Arnold, Franco Brezzi, Bernardo Cockburn, and L Donatella Marini. Unified analysis of discontinuous Galerkin methods for elliptic problems. *SIAM journal on numerical analysis*, 39(5):1749–1779, 2002.

[24] Béatrice Rivière. *Discontinuous Galerkin methods for solving elliptic and parabolic equations: theory and implementation.* Society for Industrial and Applied Mathematics, 2008.

[25] Lawrence Evans. Partial differential equations. 1998.

[26] Susanne C Brenner. Poincaré–Friedrichs inequalities for piecewise H1 functions. *SIAM Journal on Numerical Analysis*, 41(1):306–324, 2003.

[27] Pierre-Arnaud Raviart and Jean-Marie Thomas. A mixed finite element method for 2-nd order elliptic problems. In *Mathematical aspects of finite element methods*, pages 292–315. Springer, 1977.

[28] Susanne C Brenner and Ridgway Scott. *The mathematical theory of finite element methods*, volume 15. Springer Science & Business Media, 2008.

[29] J Nitsche. Über ein variationsprinzip zur lösung von Dirichlet-problemen bei verwendung von teilräumen, die keinen randbedingungen unterworfen sind. In *Abhandlungen aus dem mathematischen Seminar der Universität Hamburg*, volume 36, pages 9–15. Springer, 1971.

[30] Wm H Reed and TR Hill. Triangularmesh methodsfor the neutron-transportequation. *Los Alamos Report LA-UR-73-479*, 1973.

[31] Douglas N Arnold. An interior penalty finite element method with discontinuous elements. *SIAM journal on numerical analysis*, 19(4):742–760, 1982.

[32] Garth A Baker. Finite element methods for elliptic equations using nonconforming elements. *Mathematics of Computation*, 31(137):45–59, 1977.

[33] Jim Douglas and Todd Dupont. Interior penalty procedures for elliptic and parabolic Galerkin methods. In *Computing methods in applied sciences*, pages 207–216. Springer, 1976.

[34] Douglas N Arnold, Franco Brezzi, Bernardo Cockburn, and Donatella Marini. Discontinuous galerkin methods for elliptic problems. In *Discontinuous Galerkin Methods*, pages 89–101. Springer, 2000.

[35] Yekaterina Epshteyn and Béatrice Rivière. Estimation of penalty parameters for symmetric interior penalty Galerkin methods. *Journal of Computational and Applied Mathematics*, 206(2):843–872, 2007.

[36] Kent-Andre Mardal and Ragnar Winther. Preconditioning discretizations of systems of partial differential equations. *Numerical Linear Algebra with Applications*, 18(1):1–40, 2011.

[37] Michel Fortin and Franco Brezzi. *Mixed and hybrid finite element methods*. New York: Springer-Verlag, 1991.

[38] Hans Petter Langtangen and Aslak Tveito. *Advanced topics in computational partial differential equations: numerical methods and diffpack programming*, volume 33. Springer Science & Business Media, 2003.

[39] Vivette Girault, Guido Kanschat, and Béatrice Rivière. Error analysis for a monolithic discretization of coupled darcy and stokes problems. *Journal of Numerical Mathematics*, 22(2):109–142, 2014.

[40] Yousef Saad. *Iterative methods for sparse linear systems*. Siam, 2003.

[41] Kent-Andre Mardal and Ragnar Winther. Preconditioning discretizations of systems of partial differential equations. *Numerical Linear Algebra with Applications*, 18(1):1–40, 2011.

[42] Grégoire Allaire, Sidi Mahmoud Kaber, and Karim Trabelsi. *Numerical linear algebra*, volume 55. Springer, 2008.

[43] Torgeir Rusten, Panayot Vassilevski, and Ragnar Winther. Interior penalty preconditioners for mixed finite element approximations of elliptic problems. *Mathematics of Computation of the American Mathematical Society*, 65(214):447–466, 1996.

[44] Todd Arbogast and Dana S Brunson. A computational method for approximating a Darcy–Stokes system governing a vuggy porous medium. *Computational geosciences*, 11(3):207–218, 2007.

[45] MATLAB. *version R2014b*. The MathWorks Inc., Natick, Massachusetts, 2014.

[46] John R Lister and Paul J Dellar. Solidification of pressure-driven flow in a finite rigid channel with application to volcanic eruptions. *Journal of Fluid Mechanics*, 323:267–283, 1996.

[47] Rustem F Ismagilov, David Rosmarin, Paul JA Kenis, Daniel T Chiu, Wendy Zhang, Howard A Stone, and George M Whitesides. Pressure-driven laminar flow in tangential microchannels: an elastomeric microfluidic switch. *Analytical chemistry*, 73(19):4682–4687, 2001.

[48] Rustem F Ismagilov, David Rosmarin, Paul JA Kenis, Daniel T Chiu, Wendy Zhang, Howard A Stone, and George M Whitesides. Pressure-driven laminar flow in tangential microchannels: an elastomeric microfluidic switch. *Analytical chemistry*, 73(19):4682–4687, 2001.

[49] Brian S Hardy, Kawika Uechi, Janet Zhen, and H Pirouz Kavehpour. The deformation of flexible pdms microchannels under a pressure driven flow. *Lab on a Chip*, 9(7):935–938, 2009.

[50] Ulrich Tallarek, Erdmann Rapp, Tom Scheenen, Ernst Bayer, and Henk Van As. Electroosmotic and pressure-driven flow in open and packed capillaries: velocity distributions and fluid dispersion. *Analytical chemistry*, 72(10):2292–2301, 2000.

[51] M Mamun Molla and MC Paul. Les of non-newtonian physiological blood flow in a model of arterial stenosis. *Medical engineering & physics*, 34(8):1079–1087, 2012.

[52] Qingshu Yang, Yan Li, Jinfeng Zhou, Xiaoxi Xie, and Su. Modelling of benzene distribution in the subsurface of an abandoned gas plant site after a long term of groundwater table fluctuation. *Hydrological Processes*, 27(22):3217–3226, 2013.

[53] DJ Hart and HF Wang. A single test method for determination of poroelastic constants and flow parameters in rocks with low hydraulic conductivities. *International Journal of Rock Mechanics and Mining Sciences*, 38(4):577–583, 2001.

[54] Maxime Lion, Frédéric Skoczylas, and Béatrice Ledésert. Determination of the main hydraulic and poro-elastic properties of a limestone from Bourgogne, France. *International Journal of Rock Mechanics and Mining Sciences*, 41(6):915–925, 2004.

[55] Jacob Bear. *Hydraulics of groundwater*. Courier Corporation, 2012.

[56] Patrick J Roache. *Verification and validation in computational science and engineering*. Hermosa, 1998.

[57] Patrick J Roache. Code verification by the method of manufactured solutions. *Journal of Fluids Engineering*, 124(1):4–10, 2002.

[58] William L Oberkampf, Timothy G Trucano, and Charles Hirsch. Verification, validation, and predictive capability in computational engineering and physics. *Applied Mechanics Reviews*, 57(5):345–384, 2004.

[59] Patrick Knupp and Kambiz Salari. *Verification of computer codes in computational science and engineering*. CRC Press, 2002.

[60] JW Ruge and Klaus Stüben. Algebraic multigrid. *Multigrid methods*, 3:73–130, 1987.